XXXIII INTERNATIONAL SCIENTIFIC SYMPOSIUM

METROLOGY AND METROLOGY ASSURANCE 2023

PROCEEDINGS

September 7-11, 2023, Sozopol, Bulgaria

https://metrology-bg.org/

TECHNICAL UNIVERSITY OF SOFIA

8 Blvd Kl. Ohridski, 1797, Sofia, Bulgaria

MFACULTY OF MECHANICAL ENGINEERING

Department of
PRECISION ENGINEERING AND MEASURING INSTRUMENTS

Prof. Dimitar Diakov, PhD

Phone: (+359) 2 965 3056

Mobile: (+359) 889 531 258

E-mail: diakov@tu-sofia.bg

metrology@tu-sofia.bg

FACULTY OF AUTOMATICS

Department of
ELECTRICAL MEASUREMENTS

assoc. prof. Ivan Kodjabashev

Phone: (+359) 2 965 2896

Mobile: (+359) 887 516 765

E-mail: kodjabashev@tu-sofia.bg

assoc. prof. Georgi Milushev

Phone: (+359) 2 965 2380

Mobile: (+359) 888 501 235

E-mail: gm@tu-sofia.bg

metrology@tu-sofia.bg

Technical University of Sofia

Bulgarian Institute of Metrology

Union of Metrologists in Bulgaria

Bulgarian Academical Association of Metrology

Kozloduy Nuclear Power Plant

33RD INTERNATIONAL SCIENTIFIC SYMPOSIUM

METROLOGY AND METROLOGY ASSURANCE 2023

PROCEEDINGS

7-11 September 2023

Sozopol, Bulgaria

ORGANISED BY

Technical University of Sofia

- ***Department of Electrical Measurements***
- ***Department of Precision Engineering and Measuring Instruments***

Institute of Electrical and Electronics Engineers, Bulgaria Section

WITH THE ATTENDANCE OF

Bulgarian Institute of Metrology

Union of Metrologists in Bulgaria

Bulgarian Academical Association of Metrology

Kozloduy Nuclear Power Plant

WITH THE SUPPORT OF

RESEARCH AND DEVELOPMENT SECTOR BY THE TU-SOFIA

SOFTTRADE **NIK 47 Ltd** **R&DL "CMME"**

NATIONAL ORGANIZING COMMITTEE

Co-Chairmen

Assoc. Prof. Ivan Kodjabashev, PhD	*TU-Sofia*
Prof. Dimitar Diakov, DSc	*TU-Sofia*

Vice Chairmen

Snejana Spasova, MEng	*BIM*
Vessela Konstantinova, PhD	*UMB*
Prof. Branko Sotirov, PhD	*BAAM*
Emilyan Edrev, MEng	*NPP*

Scientific Secretary

Prof. Georgi Djukendjiev, PhD	*TU-Sofia*

Members

Kiril Banev, MEng	*Kozloduy NPP*
Assoc. Prof. Vassil Bogev, PhD	*TU-Sofia*
Milko Djambazov, PhD	*TU-Sofia*
Assist. Prof. Krasimir Galabov, PhD	*TU-Sofia*
Assoc. Prof. Ivanka Kalimanova, PhD	*TU-Sofia*
Assoc. Prof. Valentina Markova, PhD	*IEEE Bulgarian Section*
Nikola Panchev, MEng	*NIK 47*
Assoc. Prof. Nikolay Stoyanov, PhD	*TU-Sofia*
Prof. Plamen Tzvetkov, PhD	*NBU*
Assoc. Prof. Velizar Vassilev, PhD	*TU-Sofia*
Antoaneta Yovcheva, PhD	*BIM NCM*

Secretariat

Assist. Prof. Ivailo Blagov, PhD	*TU-Sofia*
Assist. Prof. Bozhidar Dzhudzhev, PhD	*TU-Sofia*
Nikolay Gurov, MEng	*TU-Sofia*
Sen. Res. Fel. Momchil Hardalov, PhD	*TU-Sofia*
Assoc. Prof. Hristiana Nikolova, PhD	*TU-Sofia*
Assoc. Prof. Rositza Miteva, PhD	*TU-Sofia*
Assist. Prof. Antonia Pandelova, PhD	*TU-Sofia*

INTERNATIONAL PROGRAMME COMMITTEE

Chairman

Assoc. Prof. George Milushev, PhD	*TU-Sofia*

Members

Assoc. Prof. Kiril Aleksiev, PhD	*BAS, IEEE, Bulgaria*
Prof. Konstantionos Athanasiadis	*EMI, Greece*
Anna Chunovkina, DSc	*VNIIM, Russia*
Prof. Dimitar Dichev, DSc	*TU-Gabrovo, Bulgaria*
Prof. Vladimir Dmitriev, DSc	*TsAGI, Russia*
Dr. Manus Henry	*University of Oxford, England*
Prof. Dietrich Hofmann, PhD	*ICC Spectronet, Germany*
Assoc. Prof. Kiril Kirov, PhD	*TU-Varna, Bulgaria*
Assoc. Prof. Ivan Kodjabashev, PhD	*TU-Sofia, Bulgaria*
Prof. Ivan Kralov, DSc	*TU-Sofia, Bulgaria*
Prof. Peter Lauda, DSc	*TU-Liberec, Czech Republic*
Prof. Ignacio Lira, DSc	*PUCC, Chile*
Prof. Valeri Mladenov, DSc	*TU-Sofia, Bulgaria*
Prof. Zvezditza Nenova, PhD	*TU-Gabrovo, Bulgaria*
Assoc. Prof. Elmo Pettai, PhD	*TUT, Estonia*
Prof. Georgii Rannev, DSc	*IIT, Russia*
Acad. Chavdar Rumenin, DSc	*BAS, Bulgaria*
Prof. Alexandru Salceanu, DSc	*TU Gheorghe Asachi, Romania*
Assoc. Prof. Nikolay Serov, PhD	*NRU MPEI, Russia*
Prof. Alexandr Shestakov, DSc	*SUSU NRU, Russia*
Prof. Branko Sotirov, PhD	*RU Angel Kanchev, Bulgaria*
Jiri Šurán	*CMI, Czech Republic*
Roald Taymanov, DSc	*VNIIM, Russia*
Assoc. Prof. Danko Tonev, PhD	*RU Angel Kanchev, Bulgaria*
Assoc. Prof. Stanimir Valchev, PhD	*NOVA, Portugal*
Prof. Evgeniy Volodarsky, DSc	*NTUU KPI, Ukraine*
Prof. Wiesław Winiecki, DSc	*WUT, Poland*
Prof. Ighor Zaharov, DSc	*NURE, Ukraine*
Prof. Ilia Zhelezarov, PhD	*TU-Gabrovo, Bulgaria*

All papers published in the Proceedings of the 33rd International Scientific Symposium "Metrology and Metrology Assurance 2023" are reviewed by the International Programme Committee.

METROLOGY AND METROLOGY ASSURANCE 2023

7-11 September 2023

Sozopol, Bulgaria

PROCEEDINGS

Technical University of Sofia

Technical University of Sofia Publishing House

ISSN 2603-3194

CONTENT

PLENARY SESSION

Section I GENERAL ASPECTS OF METROLOGY. MEASUREMENT METHODS. UNITY AND ACCURACY OF MEASUREMENTS

Section II SENSORS, TRANSDUCERS AND DEVICES FOR MEASUREMENT OF PHYSICAL QUANTITIES

Section III MEASUREMENT AND INFORMATION SYSTEMS AND TECHNOLOGIES

SECTION III
MEASUREMENT AND INFORMATION SYSTEMS AND TECHNOLOGIES

Research and Modelling of Compared Cartographic Objects in Ukraine

Vira Golian
Department of Software Engineering
Kharkiv National University of Radio Electronics
Kharkiv, Ukraine
0000-0001-5981-4760

Nataliia Golian
Department of Software Engineering
Kharkiv National University of Radio Electronics
Kharkiv, Ukraine
0000-0002-1390-3116

Kyrylo Halchenko
Department of Informatics
Kharkiv National University of Radio Electronics
Kharkiv, Ukraine
0000-0001-9418-1399

Zoia Dudar
Department of Software Engineering
Kharkiv National University of Radio Electronics
Kharkiv, Ukraine
0000-0001-5728-9253

Valentyna Kyriy
Department of Software Engineering
Kharkiv National University of Radio Electronics
Kharkiv, Ukraine
0000-0002-2537-264X

***Abstract*— The analysis of the cartographic object comparison in Ukraine was carried out. In order to correctly read and analyze the map, it is necessary to clearly imagine the depicted area using conventional signs. The algorithms for working with the map are studied in this paper: the digitization algorithm and the graph construction algorithm.**

Keywords—map data, digital algorithm, graph construction algorithm, cartographic elements, library opencv

I. INTRODUCTION

Deep learning methods have recently allowed researchers to successfully solve the problems of processing large amounts of data. In the area of learning improvement, this has led to the ability to design nodes that can learn to act on high-dimensional input spaces. In particular, deep neural networks were used to analyze map data and replace the work of thousands of people who viewed and systematized it. In order to correctly read and analyze the map, it is necessary to clearly imagine the depicted area using conventional signs. At the moment, the most common algorithms for working with the map are the digitization algorithm and the graph construction algorithm.

II. ANALYSIS OF THE SUBJECT DOMAIN

TABLE I. WEB-GIS COMPARSION

Criteria	2GIS	Google Maps
Coverage	Average, which is worse than competitors demonstrate	Best coverage in the world
Detailing	One of the best detailing	Good detailing
Display options	Map	Map, satellite, bikemap, transport

At the moment, the most successful companies working with maps are Googlemaps, 2GIS [1]. These companies are the most represented on the Ukrainian market. A comparison table will be presented in Table 1. Therefore, these cartographic services use the digitization of satellite images and the construction of cartographic elements based on them: straight lines, curves, polygons, and object points.

III. ANALYSIS OF EXISTING ALGORITHMS

A. Digitization Algorithm

The digitization algorithm is used to obtain map objects based on a picture taken by a satellite, such as: streets, houses, squares, etc. To implement this algorithm, it is necessary to process all the data coming to the developed system. During the functioning of robotic systems, a stream of images is produced, which contains a large amount of data about the surrounding world [2]. The following steps are used to initially process this data:

- Conversion of a color four-channel image into a black-and-white one-channel image;
- Digital correction of camera lens aberrations;
- Image filtering.

The general sequence of actions looks like this:

- Pre-processing of the image, i.e., processes of smoothing, noise filtering, contrast enhancement;
- Image binarization and selection of object contours;
- Initial filtering of contours by perimeter, area, shape factor;
- Bringing contours to a single length;
- Sorting through all found contours, searching for a template that is as similar to this contour as possible. Fig. 1 shows the data digitization algorithm

979-8-3503-3810-2/23/$31.00 ©2023 IEEE

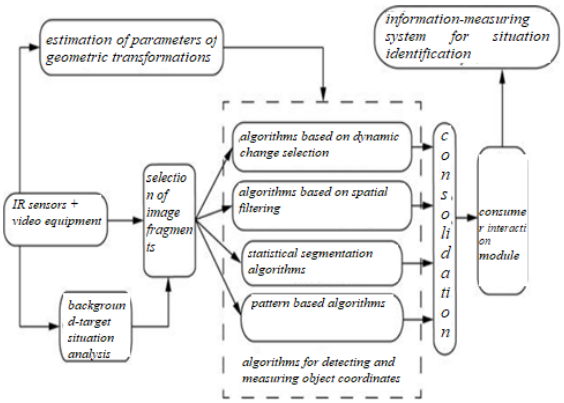

Fig. 1. Structure of software and algorithm support.

At the moment, the OpenCV library is used to implement this algorithm.

OpenCV is a library consisting of functions and algorithms for image processing, computer vision and numerical algorithms with open-source code [3]. This library provides tools for image processing, content analysis, including object recognition, object motion tracking, image transformation, machine learning, and detection of common elements in various images.

The library contains more than 2,500 optimized algorithms, including a full set of both classical and practical machine learning and computer vision algorithms. OpenCV algorithms are used in the following areas:

- Image analysis and processing
- Facial recognition systems
- Identification of objects
- Combining images together to create high-resolution images of the entire scene
- Human-computer interaction system
- Search for similar images from the database
- Identification of objects
- Image segmentation

For example, to convert a color image into a black-and-white single-channel image, if there is a limitation in computing resources, the required image size in pixels is selected. For storage in memory, it is necessary to organize a data structure that would provide quick access to the image and convenient work with it [2]. To do this, the OpenCV library has a special data type – the IplImage structure. In essence, this matrix is interpreted as an image.

The problem of obstacle detection and pattern recognition requires the presence of an undistorted image. OpenCV provides us with a ready-to-use distortion correction algorithm that takes raw images and distortion coefficients from cvCalibrateCamera2 and creates a corrected image.

Using the cvFindContours() function, the OpenCV library helps the developer to recognize objects in the image and extract from them contours for further work. The function cvFindContours() searches for the contours of a monochrome image and returns the number of contours found. Then these contours can be drawn into the image using the cvDrawContours() function. You can use the cvApproxPoly() function to smooth and obtain more accurate contours. The result of the algorithm is shown in Fig. 2.

Fig. 2. The result of the algorithm using OpenCV.

OpenCV is now used in many areas. Here are some interesting examples:

- Google:
  - Googleself-drivingcar in self-driving cars, GoogleOpenCV is used to develop a prototype for recognizing the surrounding environment;
  - GoogleGlass – in these glasses, 3D image reconstruction is built on OpenCV;
  - Google Mobile;
- Robotics and Arduino;
- Industrial production – sometimes some factories use OpenCV to develop a part counting system.
- The Bosch company was engaged in the development of the necessary sensors and cameras for parking, as well as the creation of devices in cars that receive a signal determining whether there are obstacles near the car or not.

B. Algorithm of Graph Theory for Working with Map Objects as with Graph Vertices.

Graph theory is a branch of mathematics that studies the properties of graphs. Visually, a graph can be imagined as a geometric configuration consisting of points (vertices) connected by lines (edges). In the strict definition, a graph is a pair of sets G = (V, E), where V is a subset of any countable set, and E is a subset of V × V.

The definition of a graph is so general that this term can be used to describe many events and objects of everyday life. A high level of abstraction and generalization allows the use of typical algorithms of graph theory to solve externally dissimilar problems in transport and computer networks.

Graph theory is used, for example, in geographic information systems (GIS). Existing or planned buildings, structures, blocks, etc. are considered as vertices, and their connecting roads, utilities, power lines, etc. are considered as edges. The application of various calculations made on such a graph allows, for example, to find the shortest detour or the nearest grocery store, to plan the optimal route.

Dijkstra's algorithm is used to work and find the shortest path between the graph vertices. Dijkstra's algorithm is a graph algorithm discovered by Dijkstra. It finds the shortest path from one vertex of the graph to all other vertices.

Dijkstra's classical algorithm works only for graphs without cycles of negative length.

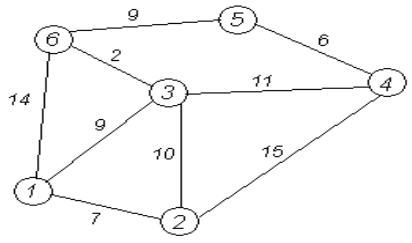

Fig. 3. Graph

The sequence of the algorithm operation for the graph shown in Fig. 3:

1. Initialization. The distance to all vertices of the graph V =∞. The distance to a = 0. No vertex of the graph has yet been processed.

2. We find such a vertex (from those not yet processed) to which the current shortest distance is minimal. In our case, this is vertex 1. We investigate all its neighbours and, if the path to the neighbouring vertex through 1 is less than the current minimum path to this neighbouring vertex, then we remember this new, shorter path as the current shortest path to the neighbour.

3. The first neighbour of the 1st vertex is the 2nd vertex. The path to it via the 1st vertex is the shortest distance to the 1st vertex + the length of the arc between the 1st and 2nd vertex, i.e., 0 + 7 = 7. This is less than the current shortest path to the 2nd vertex, so the shortest path to the 2nd vertex is equal to 7.

4. We perform a similar operation with the other two neighbours of the 1st vertex, i.e., the 3rd and 6th.

5. All the neighbours of vertex 1 are checked. The current minimum distance to vertex 1 is considered final and non-negotiable (Dijkstra first proved that this is indeed the case). Therefore, we will delete it from the graph to mark this fact.

6. Practically there is a return to step 2. We find again the "nearest" unprocessed (undrawn) vertex. This is vertex 2 with the current shortest distance to it = 7. And we try again to reduce the distance to all the neighbours of the 2nd vertex, trying to get to them through the 2nd one. The neighbours of the 2nd vertex are 1, 3, 4.

7. The first (in order) neighbour of vertex No. 2 is the 1st vertex. But it is already processed (or crossed out - see step 6). Therefore, we do not do anything with the 1st vertex.

8. Another neighbor of vertex 2 is vertex 3. If you go to it through the 2nd, the path will be = 7 + 10 = 17. But 17 is bigger than the distance that has already been remembered earlier to vertex No. 3 and is equal to 9, therefore, we do not change the current distance to the 3rd peak.

9. All the neighbours of vertex 2 are reviewed, we freeze the distance to it and cross it out from the graph.

10. According to the already "worked out" scheme, we repeat steps 2 - 6. Now the "closest" vertex is No. 3. After "processing" it, we will get the following results:

11. We do the same with the remaining vertices (No. in order: 6, 4 and 5).

12. The algorithm ends when all the vertices are crossed out. The result of his work can be seen in the last picture: the shortest path from the 1st vertex to the 2nd one is 7, to the 3rd one it is 9, to the 4th one it is 20, to the 5th one it is 20, to the 6th one it is 11 conditional units.

13. The simplest implementation of Dijkstra's algorithm requires O(V^2) operations. It uses an array of distances and an array of marks. At the beginning of the algorithm, the distances are filled with a large positive number (greater than the maximum possible path in the graph), and the array of marks is filled with zeros. Then the distance for the initial vertex is assumed to be zero and the main loop is started.

14. At each step of the cycle, we search for the vertex with a minimum distance and the flag equal to zero. Then we set the mark 1 in it and check all the vertices adjacent to it. If the distance in it is greater than the sum of the distance to the current vertex and the length of the edge, then we reduce it. The cycle ends when the marks of all vertices become equal to 1.

15. These algorithms allow you to build a model of the map and cartographic objects on it. The main components of the map are stored in the free Open Street Map (OSM)[4]. The attractiveness of OSM is the ability to use high-quality cartographic information absolutely legally.

16. Data structure in OSM maps. The basic element of the OSM data structure is a node with geographic coordinates – a latitude and a longitude. The height of the point above the sea level is currently not specified.

17. A point can be an independent object (a traffic light, a kiosk, a spring) and, without restrictions, it can be a part of other objects (lines and relations). Large objects, such as countries, cities and even continents with a set of appropriate tags, can be marked with points.

18. Fig. 4 shows "dot" tag structure

```
<node id="231477" lat="52.2600355" lon="0.0172928" version="2" timestamp="2011-02-27T
02:33:27Z" changeset="7406582" uid="39894" user="markpeers"/>

<node id="231478" lat="52.2552032" lon="0.0281442" version="4" timestamp="2011-02-27T
02:33:25Z" changeset="7406582" uid="39894" user="markpeers">
  <tag k="exit_to" v="Bar Hill B1050; Longstanton"/>
  <tag k="fixme" v="What is with all the layer=3s around this junction?"/>
  <tag k="highway" v="motorway_junction"/>
  <tag k="layer" v="3"/>
  <tag k="name" v="Bar Hill"/>
  <tag k="ref" v="29"/>
</node>
```

Fig. 4. "Dot" data structure

A line is a sequence of dots. You can change the sequence. Logically, several lines can represent one object. For example, a long road consists of several lines. The lines of one road are connected into a single entity under condition that the end point of one line strictly corresponds to the starting point of another line or several lines (in the case of a branching road or exit to another one). Such integrity for the lines is well complied in OSM.

A polygon is a closed line in which the first and last dots coincide. A polygon is not an independent element of OSM. For large polygons (borders of states, coastlines), which consist of a set of open lines, rules are defined. For example, when determining coastlines, land will be on the left in the

course of movement, water will be on the right. For administrative borders, it is clearly indicated who is on the left in the direction of movement, who is on the right.

```
<way id="9933583" version="18" timestamp="2013-01-06T20:59:432" changeset="14555667"
uid="30525" user="The Maarssen Mapper">
  <nd ref="2098832234"/>
  <nd ref="81448050"/>
  <nd ref="1263117830"/>
  <nd ref="1263117982"/>
  <nd ref="81448052"/>
  <nd ref="81448053"/>
  <nd ref="81448054"/>
  <nd ref="1297466013"/>
  <nd ref="81448063"/>
  <tag k="admin_level" v="6"/>
  <tag k="boundary" v="administrative"/>
  <tag k="left:county" v="Cambridgeshire"/>
  <tag k="right:county" v="Essex"/>
  <tag k="source" v="OS_OpenData_Boundary-Line"/>
</way>
```

Fig. 5. Structure of the line object.

C. *Architecture Description*

A relation is a logical combination of points, lines and other relations into a single object. Despite high functionality, relations in OSM are not widely used, although there are attempts to apply relations to various objects. For example, such a purely point object as a bus stop, according to OSM internal statistics (statistics is kept for most objects), is represented by: 1,572,243 points, 2,479 lines, and 1,140 relations.

An object is an element (point, line, attitude) with keywords (attributes). A tag is defined as k = "key" v = "value". If the element does not have tags, then it is not an object, but is a part of other objects (tags can also be included). The object does not have mandatory tags. There are no mandatory requirements for the number, content and order of tags. The one who enters data into OSM determines the composition and content of tags himself.

In different countries or regions, the same objects may differ significantly in the composition and content of tags. For example, a city can be marked with a point or a line (polygon).

Accurate geographic measurements are quite difficult. It is necessary to take into account the following: the Earth is not a perfect sphere, the height above the sea level, the relief, various projection models for displaying the spherical Earth on a plane.

Internet maps use the EPSG: 4326 - WGS-84 projection, which is based on the latitude and longitude of GPS satellite navigation. Degrees are indicated in the decimal form: latitude (lat = 52.2600355), longitude (lon = 0.0172928).

The disadvantage of storing map objects in the OSM data structure is a very large file or database to store all the objects, so reading and parsing, decomposition into objects take a very long time. For node objects, the OSM file must be read once, and for way objects – 2 times.

The need for double reading is caused by the fact that in the XML file node-objects come first, and way-objects follow them. In this case, double reading simply simplifies the algorithm by avoiding the use of intermediate structures for storing the latitude and longitude of points.

In order not to create duplicate objects and to reduce the time of determining the latitude and longitude of the points included in the way, a single mechanism based on the use of index arrays is used. This approach allows you to significantly increase the speed of processing due to the optimization of search operations.

OpenStreetMap is not a project for tracing (drawing) satellite images. The basis of the project is GPS tracks recorded by users, and the images are used as an aid in mapping. You should not move objects created by other users, relying only on photos from the space, because they are often distorted and shifted relative to the real location of the objects.

Bing, IRS and Landsat are available as a substrate. All of them can be used when displaying, but it should be remembered that each substrate has its own offset.

Where does it come from? At first, there is only a photograph and satellite coordinates. Then a special program automatically calculates the coordinates of the corners of each photo. The higher their resolution, the more precisely the coordinates must be calculated. But there are thousands of pictures, and the Earth's surface is not a perfect ellipsoid, so a person cannot check the accuracy of the reference of each picture, and the coordinates turn out to be slightly incorrect. Because of this, in the best case, the picture will be shifted – often by a meter or two, but sometimes by hundreds – and it may even be non-linearly distorted, for example, in the mountains (however, the distortion may be on hills).

The coordinates of objects in OpenStreetMap are measured through GPS data. Of course, in other places the navigator can give incorrect readings (for example, due to reflections from tall buildings, weather, obstacles), but the accuracy of qualitatively collected tracks usually exceeds the accuracy of anchoring available in commercial satellite images, so they are considered the main source of the most reliable data on the location of objects. Therefore, the roads must be circled along the tracks, no matter how the line on the satellite photo twists. The latter must be moved before use so that the network of tracks-roads overlaps the same network in the picture.

CONCLUSIONS

Having considered these algorithms, we can draw the following general conclusion that the problem of constructing cartographic objects is inaccurate aerial photographs, or photographs with low resolution, as well as processing algorithms. Each of the mapping systems has its advantages and disadvantages. The biggest disadvantage is that the mapping systems with the highest accuracy are commercial and paid to use. The main advantage of OSM maps is that they are free, but since they are created by Internet users, they require initial processing before use.

REFERENCES

[1] Kukitz, “Web-GIS Comparsion,” Habr, 30-Oct-2014. [Online]. Available: https://habrahabr.ru/post/242015/. [Accessed: 28-Apr-2023].

[2] R. C. Gonzalez and R. E. Woods, Digital Image Processing. New York: Pearson, 2018.

[3] G. Bradski and A. Kaehler, Learning opencv. Sebastopol (CA): O'Reilly, 2008.

[4] “UK:Main Page,” Uk:Main Page - OpenStreetMap Wiki. [Online]. Available: https://wiki.openstreetmap.org/wiki/Uk:Main_Page. [Accessed: 28-Apr-2023].

Measurment procedure for metrological verification of the measuring channels of the automated process control system for monitoring the turbine generator parameters (СТК-ЕР-М)

1 Krassimir Bossilkov
Metrology Support
Kozloduy NPP EAD Kozloduy,
Bulgaria
kkbosilkov@npp.bg

2 Tsvetelin Georgiev
Metrology Support
Kozloduy NPP EAD Kozloduy,
Bulgaria
ccgeorgiev@npp.bg

3 Elena Nikolova
Metrology Support
Kozloduy NPP EAD Kozloduy,
Bulgaria
enikolova2@npp.bg

4 Maya Radulova
Metrology Support
Kozloduy NPP EAD Kozloduy,
Bulgaria
miradulova@npp.bg

5 Tetiana Chunikhina
Department "information and
Measuring Technologies and Systems"
National Technical University
"Kharkiv Polytechnic Institute"
Tetiana.Chunikhina@khpi.edu.ua

Summary: The report presents the methods for metrological verification of the measuring channels of the automated process control system for monitoring of the turbine generator parameters at Units 5 and 6 at of Kozloduy NPP.

Keywords: Metrological verification, measuring channels, automated process control system

I. INTRODUCTION

At the "Kozloduy" NPP the contact methods of the temperature measurements in the different technological processes, realized with using the resistance and thermoelectrical transducers, are widely applied.

The main metrological characteristic of the resistance and thermoelectrical transducers is the function of conversation, called nominal static characteristic [1, 2].

The feature of the thermoelectrical transducers' exploitation is the variation during the time of the exploitation on the object their nominal static characteristics due to the irreversible physical and chemical processes in the thermoelectrods of the thermocouples. This causes to appearance the error of the temperature measurement.

The main purpose of the modern measuring instruments (measuring channels) is to perform accurate and reliable measurements to obtain complete and reliable measuring information [3].

Verification is the operation, that aims to achieve this purpose [4, 5].

The primary measuring transducers supply the main contribution to the total measurement error of the measuring channels.

Metrological verification of 156 input analog signals for the temperature formed by the resistive transducers in the four-wire circuit is performed during the plant annual outage. The input analog signals are divided into two lists, 78 signals each, from the СТК-ЭР-М automated process control system developed on the basis of the СТК-ЭР-М automated process control system for monitoring of the turbine generator parameters at Units 5 and 6 of Kozloduy NPP.

II. PURPOSE

The ПТК СТК-ЭР-М automated process control system provides for a continuous automated process control of the turbine generator parameters, visualization, and signal formation for deviation of the process parameters from the set values.

The automated process control system consists of:

- ШСТК (5(6)GT01J05) cabinet – a computer cabinet;
- ШСКВ (5(6)GT01J04) cabinet – a transducer cabinet;
- ШКВЗ (5(6)GT01J03) cabinet – a transducer cabinet.

The purpose of the report is to present the newly developed measurement procedure for metrological verification of the measuring channels from the PTK for technological monitoring parameters of the turbogenerator 82.MO.00.MT.1910/00.

III.STRUCTURAL DIAGRAM

The SIEMENS SIMATIC S7–300 programmable logic controller (PLC) located in the СТК-ЭР-М automated process control system cabinet (ШСТК) is the core of every ПТК СТК-ЭР-М automated process control system. The functions of the routine control station (RCS) are performed by the in-built computer (A6) located on the internal side of the ШСТК cabinet door. The panel monitor (PM) A1 on the internal side of the ШСТК cabinet door is used for visualization.

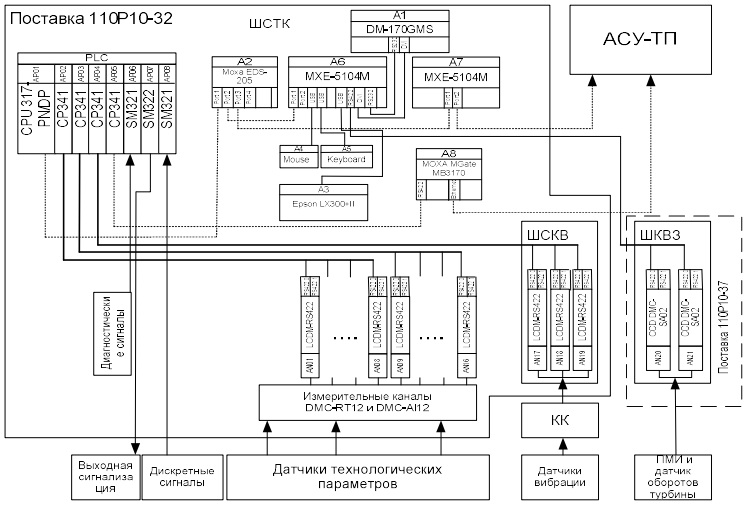

Fig. 1 Structural diagram of the СТК-ЭР-М automated process control system

- ШСТК (5(6)GT01J05):

To provide a continuous power supply in the ШСТК cabinet, a switchover diagram between the two 220 V inputs, the source of uninterruptable power supply (UPS) Eaton 9310 and the source of power supply Mean Well, is used.

To receive the 4-20 mA input signals, a data acquisition system (DAS) consisting of LCDM-RS422 concentrators and digital transducers for normalized CCD DMC-AI12 signals is used.

To receive the input signals from the resistance thermometers with a sampling cycle of 2 s signals, a data acquisition system (DAS) consisting of LCDM-RS422 concentrators and digital transducers for normalized CCD DMC-RT12 signals is used. An Epson LX-300+II printer is installed in the ШСТК cabinet

The input and output signals are galvanically separated by a G2RV type relay made by OMRON.

For connection with the OVATION I&C system via the Modbus TCP protocol, a MOXA MGate MB3170 gate which converts Modbus RTU into Modbus TCP was installed in the СТК-ЭР-М automated process control system cabinet.

IV. Application software for the ПТК СТК-ЭР-М automated process control system

The interface of the СТК-ЭР-М automated process control system has a multi-window structure. It is designed for receiving current information about the generator process parameters which are controlled by the СТК-ЭР-М automated process control system, information on all events and failures recorded by the СТК-ЭР-М automated process control system, review the achieved data in the graph and table formats.

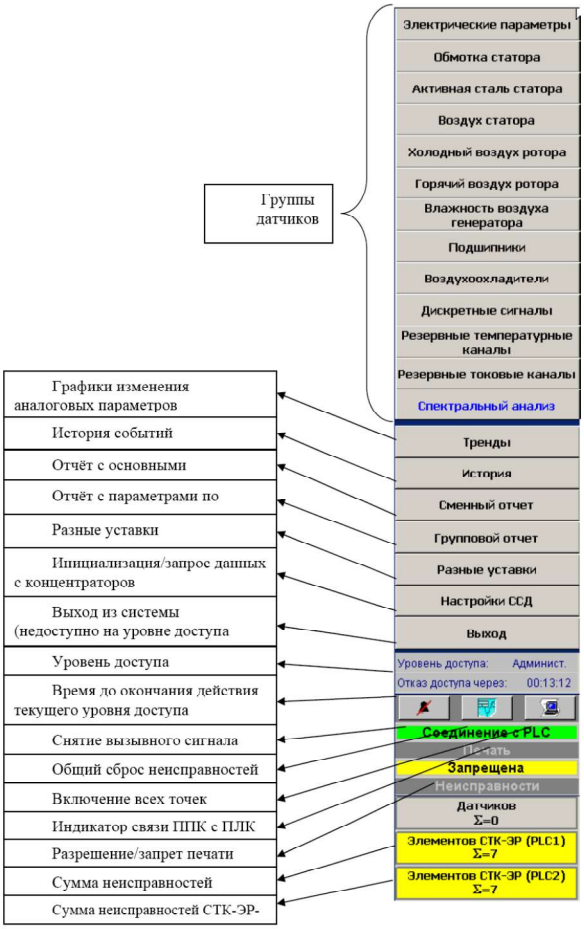

Fig. 2 Main menu

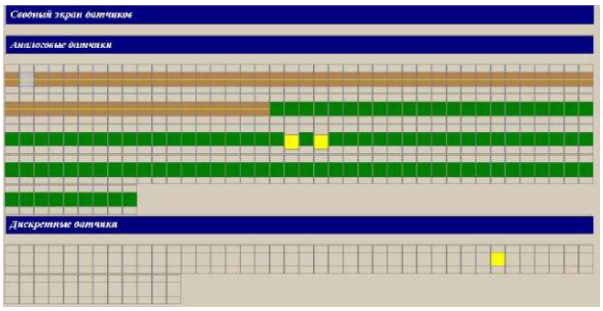

Fig. 3 Sensor display

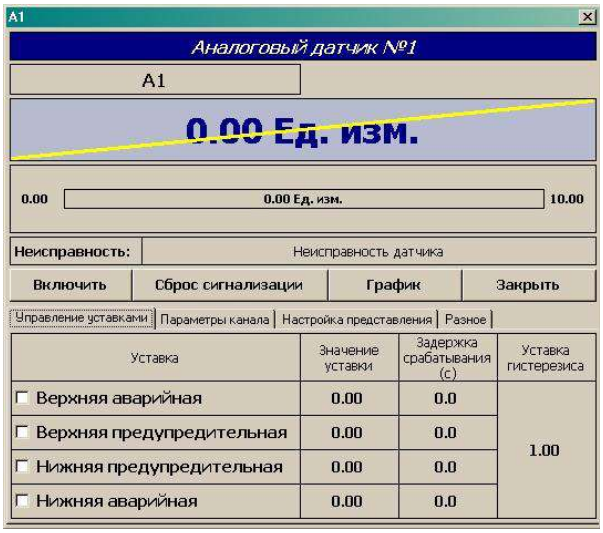

Fig. 4 Analog sensor window (Setting management).

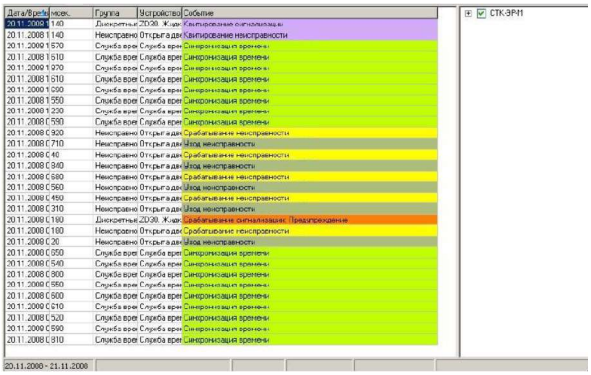

Fig. 5. Event history

V. SOFTWARE CHECK PTK STK-ER-M SYSTEM

Before starting the metrological check of the PTK STK-ER-M system, a software check is performed. The purpose of this check is to establish the compliance of the checksum of the system's software (software security), which is a guarantee that no unauthorized access to the system has taken place after the previous metrological check.

Activities are carried out in the following sequence:

1) An automated comparison of the checksums of the original STK-ER-M software and the current working version of the STK_et_s.zip system is performed with the MD5 File Checker software product.

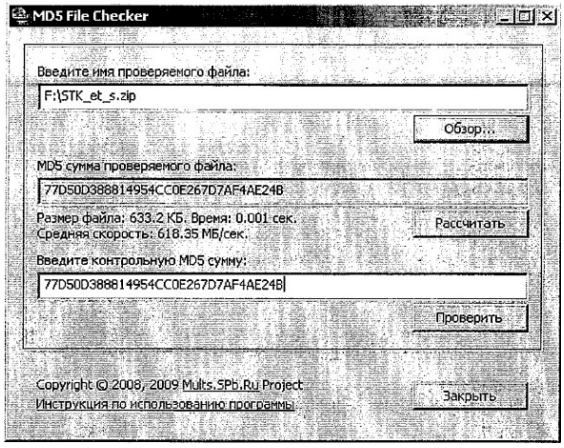

fig.6 MD5 File Checker user screen

Enter the checksum provided by the manufacturer in the "Enter MD5 checksum" field. If there is a match, an automatic message is generated.

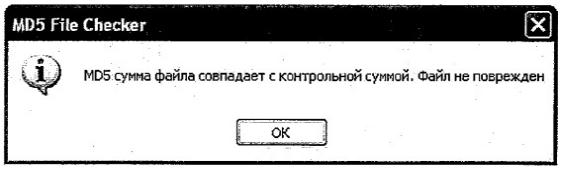

fig.7 Checksum Matching Message

2) When the checksums match, the metrological check of the system is carried out. If the checksums do not match, a message is generated

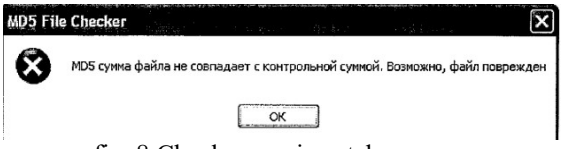

fig. 8 Checksum mismatch message

It goes on to check the software uploaded to the SIMATIC S7-300 programmable logic controller.

1) STK_et_s.zip file is unzipped

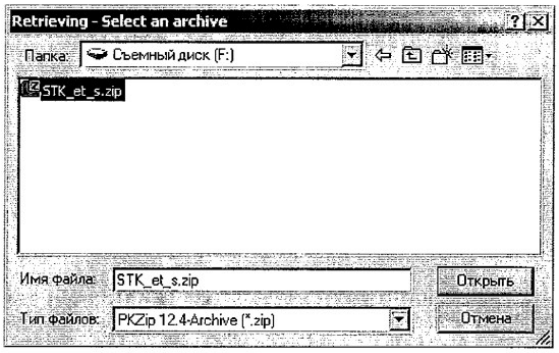

fig.9 Archive

Select the directory marked in fig.10 from the unzipped file

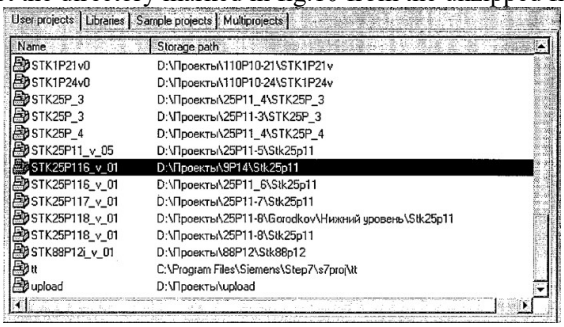

fig.10 Contents of the archive

2) The SIMATIC Manager software is started and the specified directory containing the user program uploaded to the controller is opened.

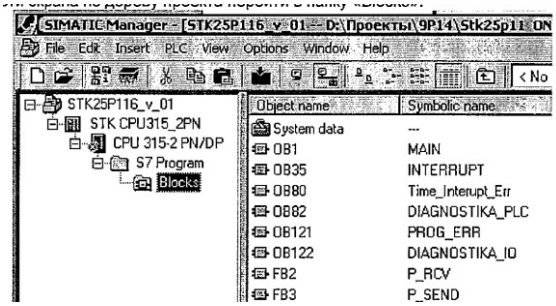

fig.11 User screen of the SIMATIC Manager editor

The compare blocks function compares the user program loaded in the SIMATIC Manager editor with the program loaded in the controller.

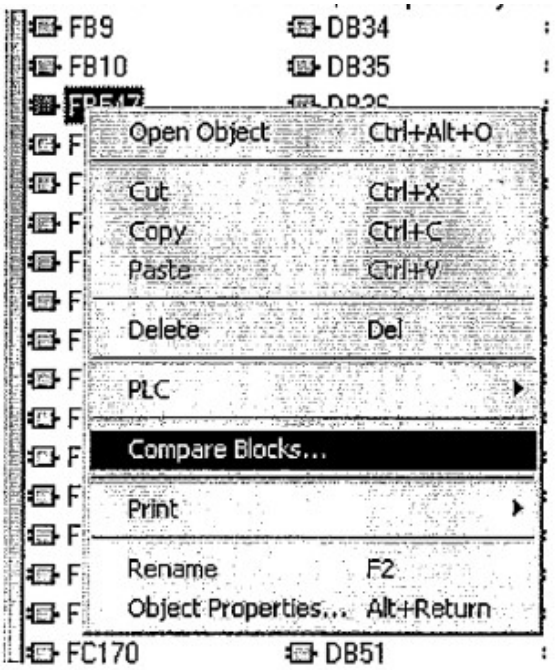

fig. 12 Starting the program block comparison function

When the program blocks do not match, a message is generated with the number of the block in which there is a difference.

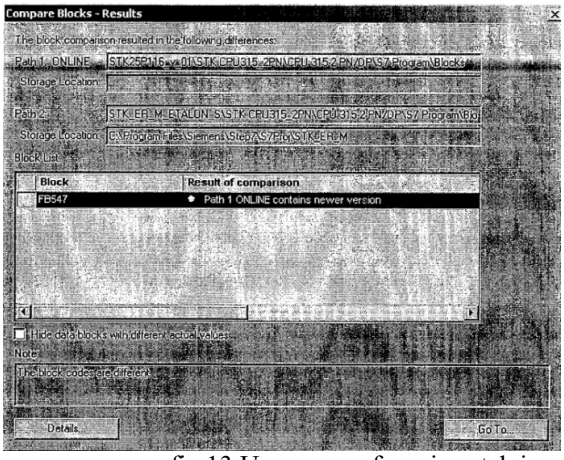

fig.13 User screen for mismatch in program blocks

Remove the difference in the blocks using the SIMATIC Manager editor and repeat the previous step. After generating a message:

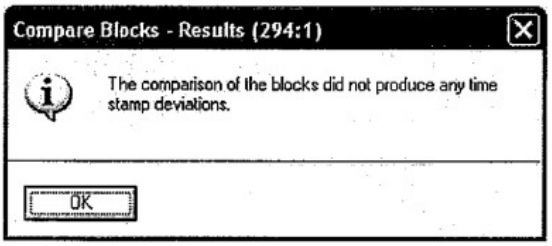

fig.14 Data matching message in program blocks.

3) When the program matches the one uploaded to the controller, the metrological check of the system is carried out.

VI. METROLOGICAL VERIFICATION

According to the requiments of measurement procedure the verification of the measuring channels of temperature must be performed in reference conditions. For the influence quantities the following ranges were established.:

- The temperature of the surrounding air: $(20 \pm 5)^0 C$
- The atmosphere pressure: (84,0-106,7) kPa; (750±30) mm.merc.col.

The relative humidity of the air: (65±15) %.

Therefore, only the intrinsic error of measurement was in measurement results (the complementary errors were absent).

For reducing the random measurement error the measurements with repeated observations can be performed by system (the number of multiple measurements is equal $n = 10$).

The nominal static characteristics of the platinum resistance transducers are approximated by polynomial functions of different degrees in dependence of the temperature range [2].

Administrative verification

The administrative verification by visual inspection should check for:

– Availability of inscriptions and designations;

– Mechanical damage of the CTK-EP-M components and connection cable;

– Completeness in compliance with the technical documentation.

- Technical verification

The technical verification is aimed at validating the functionality of the measuring channel of the automated process control system by sending the electric signal by the relevant reference standard.

A reference standard is connected to the input of the measuring channel to be verified and the upstream circuit is disconnected.

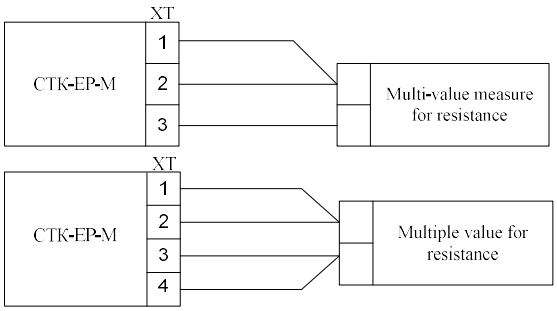

fig.15 Connection diagrams

The upstream components should not affect the readings.

The limit values of the electric signal (min. and max. of the measuring range) are mapped, and the relevant limit readings for the range of the physical quantity should be visualized on the display of the CTK-EP-M automated process control system.

When the readings of the measuring channel correspond to the sent reference signals for the lower and upper limits of the measuring range, the measuring channel is considered functional.

The basic absolute error for the measuring channel for temperature with a primary resistance transducer is determined by metrological verification.

The basic absolute error is determined in at least five values of the measured quantity values evenly distributed in the measuring range. The recommended values are 0%, 20%, 40%, 60%, 80% and 100% of the measuring range and permissible values of the basic percentage error of a measuring channel for temperature of the CTK-EP-M automated process control system.

A multi-value resistance standard or calibrator for electrical quantities is connected to the input of the CTK-EP-M automated process control system by copper conductors. The resistance values are set by the standard according to the Russian GOST 6651-2009 for resistance transducers with temperature coefficient of $\alpha = 0{,}00385°C^{-1}$, which correspond to the checked points listed in Tables 1 and 2.

Table 1

Measuring range 0÷100 °C	Verified point, °C					
	0	20	40	60	80	100
	Value of the input quantity of Pt100 ($\alpha = 0{,}00385°C^{-1}$), Ω					
	100.00	107.7	115.54	123.24	130.90	138.51

Table 2

Measuring range 0÷50 °C	Verified point, °C					
	0	30	60	90	120	50
	Value of the input quantity of Pt100 ($\alpha = 0{,}00385°C^{-1}$), Ω					
	100.00	111.67	123.24	134.71	146.07	157.33

On the display of the CTK-EP-M automated process control system, the checked measuring channel is selected, and the current measurement values of temperature are observed. The readings for all set points are entered into the OVATION I&C system.

- One reading is made for every value of the standard; however, the operator may increase the number of reading at its discretion.

Determination of the basic absolute error in the i^{th} point in the mearuing range of the measuring channel is calculated by the formula:

$$\Delta_i = \boldsymbol{X}_{i\,measurement} - \boldsymbol{X}_{reference\,standard} \quad (1)$$

whereas:

$X_{\text{imeasurement}}$ - measured value on the display of the OVATION I&C system, °C;

$X_{\text{reference standard}}$ – value of the input signal in the measurement units of the physical quantity, °C.

The highest absolute error received in all points in the measuring range are assigned as an error of the measuring channel.

$$\Delta = \mathbf{max}|\Delta_i| \quad (2)$$

The checked measuring channel will be fit for use if the following condition is fulfilled:

$$\Delta \leq \Delta_{permissible}, \quad (3)$$

whereas:

$$\Delta_{permissible} = \gamma_{permissible} \frac{X_{max} - X_{min}}{100}, \text{ °C} \quad (4)$$

X_{max} *and* X_{min} – upper and lower limit of the measuring range °C.

$\gamma_{permissible}$ - permissible percentage error of a measuring channel.

If the received absolute error is higher than the permissible error, the parameters of the components of the measuring channels will be set up. The set-up is performed by an expert from the unit responsible for the maintenance of the CTK-EP-M automated process control system.

The metrological verification report includes the results received before and after the set-up of the measuring channel.

VII. Documentation of the metrological verification results

The data from the performed verification are included in the report Fig. 16.


Протокол от метрологична проверка
№
Приложение 1
стр. 1 от ....
Техн. позиция
Хардуерен адрес
Входен сигнал
Еталонен ел. сигнал, ел.величина
5.1 Проверка на грешката на измервателен канал
Изход 1:
Изход 2:
Изход 3:
Изход 4:
Изход 5:
Изход 6:
Изчислена ст-т на физ. величина,
Измерена ст-т на физ. величина,
Абсолютна грешка,
Допустима грешка, физ. величина
Допустима грешка, %
ЗАКЛЮЧЕНИЕ: ГОДЕН / НЕГОДЕН
Дата на проверка:
Извършил проверката:

fig. 16 Report form

VIII. Conclusion

This metrological verification of the PTK -STK- ER-M automated process control system provides for the appropriate and optimal performance of the metrological verification activities.

Measuring channels with a primary measuring transducers the resistance transducers (Pt 100) were considered. According to the requirements of measurement procedure the verification of the measuring channels was performed at the six points ((0, 20, 40, 60, 80, 100) % of the two operating measurement ranges). A multi-value resistance standard was applied for forming standard signals at the realization of the verification of the measuring channels.

For each checked temperature measuring channels the absolute maximum error was defined. This absolute maximum error was compared with absolute maximum error, corresponding the given in [metodika pov stk] value of the fiducial error (±0,2 %). On the base of this comparision the confirmation whether the measuring channel is suitable for further exploitation or not was formed.

The collection of data from the metrological verification is enabled.

Reference

[1]. GOST 3044-94. Thermoelectric converters. Nominal static graduation tables. Interstate standard. 226 p.

[2]. GOST 6651-2009 State system for ensuring the uniformity of measurements. Platinum, copper and nickel resistive temperature transducers. General technical requirements and test methods. Interstate standard. 25 p.

[3]. O. Velychko, T. Gordienko. Comparative research of quality indicators measuring instruments: practical aspects. Ukrainian Metrological Journal. 2021. № 3. P. 24-30.

[4]. JCGM 200:2008. International vocabulary of metrology-Basic and general concepts and associated terms (VIM). 3-rd Edition, 2007, 146 p.

[5]. Zakharov I., Neyezhmakov P., Botsiura O. Verification of the indicating measuring instruments taking into account their

instrumental measurement uncertainty // Measurement Science Review, 2017, Volume: 17, Issue: 6, pp.: 269-272.

[6] 30.АСУ.GT.ИЕ.115-0 Operating procedure of the PTK -STK- ER-M automated process control system.

[7] 82.MO.00.MT.1910/00 Methods for metrological verification of the measurement trains of the automated process control system for monitoring the turbine generator parameters.

REACTOR COOLANT PUMP VIBRATION MONITORING AND DIAGNOSTIC SYSTEM AT KOZLODUY NPP EAD (RCP VMDS - 195M)

1st Nadya Pagelska
Metrology Support
Kozloduy NPP EAD Kozloduy, Bulgaria
nkpagelska@npp.bg

2nd Vladimir Bashev
Metrology Support
Kozloduy NPP EAD Kozloduy, Bulgaria
vtbashev@npp.bg

3rd Ivaylo Tsenov
I&C Systems
Kozloduy NPP EAD Kozloduy, Bulgaria
imcenov@npp.bg

Summary: The report describes the implemented RCP vibration monitoring and diagnostic system and verification of measurement variables of the measurement channels for vibration velocity, vibration displacement, angular velocity (turnovers) and verification of the I/O controller KVV-6.

- A short description of the vibration monitoring and diagnostic system (RCP VMDS - 195M) is made.
- The design of the vibration monitoring and diagnostic system (RCP VMDS - 195M), components, system operating modes, system graduation and calibration, and function of the main displays are discussed.

Keywords: RCP VMDS – 195M, vibration monitoring and diagnostics, metrological verification, reference standards, graduation, calibration, software for mathematical processing of the measurement results; The I/O controller -6 is a product equipped with a configurator to perform a target function, control unit, and an analogue signal processor.

I. INTRODUCTION

According to the plant design, there are four 195 M type reactor coolant pumps in operation at Units 5&6 of Kozloduy NPP. In connection with the implementation of the approved design modification of the existing diagnostic systems for the 195 M type reactor coolant pumps, 16 accelerometers and Eddy Current sensors (primary transducers) are installed on every RCP as a part of the measurement channels for vibration velocity, vibration displacement and turnovers. The installed primary transducers and their adjacent measurement transducers incorporated in the relevant measurement channel design provide the required input data by application software for the system to perform the vibration monitoring and diagnostics of the RCP vibration parameters. The systems were supplied in 2021 and installed under the WWER-1000 lifetime extension project.

II. VIBRATION MONITORING AND DIAGNOSTICS SYSTEM (RCP-195M VMDS)

The RCP VMDS is designed or monitoring and diagnostics of the RCP-195M vibration parameters as well as the process parameters of the plant I&C system to provide for the early detection of abnormal conditions of the RCP mechanical and electrical parts.

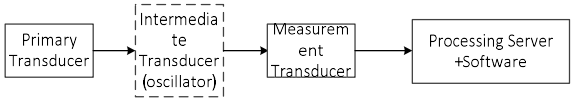

Fig.1 Measurement channel diagram

- PT - Primary Transducer
- IT - Intermediate Transducer (oscillator)
- MT - Measurement Transducer
- CS - Processing Server
- SW - Software
- Visualization of the data for recorded diagnostic events of the RCP VMDS;
- Operation of the RCP VMDS in a remote terminal mode;
- Interactive work with RCP VMDS database;
- Presenting the result of the RCP VMDS functioning;
- Recording, data processing, resolution of diagnostic tasks, interaction with external systems, integrated processing and analysis of the data from the RCP VMDS; visualisation and providing the information to the users of the RCP VMDS; documentation of the data from the RCP VMDS operation and reliable backup of the data.

- I/O controller-6. It consists of two parts: the first (permanent), consisting of a permanent rack with a power supply unit placed in it, and the second (variable) which provides orientation of the I/O controller-6 equipped with a control unit and communication units: analogue signal processor-11 and analogue signal processor-1, up to 12pcs.

III. MEASUREMENT VARIABLES OF THE VIBRATION MONITORING AND DIAGNOSTIC SYSTEM (RCP-195M VMDS).

The implemented system consists of 64 measurement channels for four RCPs per unit. It provides metrological verification of the variables of the measurement channels for monitoring and diagnostics of the RCP-195M vibration parameters (Fig.2):
Measuring range of the measuring channel:

- Vibration velocity – from 0 to 20 mm/s (from 2 to 3,000 Hz), permissible error ± 3%;
- Vibration displacement of the rotor – from 0.8 to 2.8 mm (from 1 to 5,000 Hz), permissible error ± 3%;
- Rotor angular speed – from 0 to 1.500 min^{-1}, permissible error ± 3%;

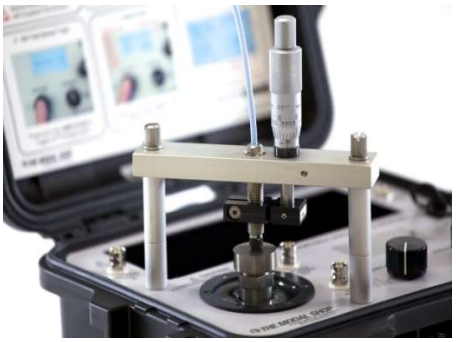

Fig. 2 Shaker table for verification of the measurement variables of accelerometers and Eddy Current sensors

The analog signal processor-11 and analog signal processor-11/1 in the I/O controller-6 have measurement variables. They provide analogue signals from 3 sensors. The analog signal processor-11 for conversion of the DC voltage input signal into a digital code ranges from 0 to -20V, and the analog signal processor 11-1 - alternating voltage from 0 to 0,4V.

The permissible error is ± 1% (for both units).

IV. TOOLS FOR THE VERIFICATION OF MEASUREMENT VARIABLES

The description and characteristics of the instrumentation and equipment used for the verification of measurement variables are given in Table 1:

Table 1 Tools for the verification of measurement variables

Description	Nominal values of the measurement limits	Tolerance
Signal generator: Operating voltage, V Frequency, Hz	 5 10	 ±10 % ±0,05 %
Thermo-hygrometer: Relative humidity, % Temperature, °C Atmospheric pressure, kPa	 40 to 80 15 to 35 86 to 108	 ±5 % ±2 °C ±1 kPa
Portable shaker table: Vibration velocity root mean square, mm/s Vibration displacement (peak-peak value), µm	 0 to 20 0 to 1000	 ±3 %
Calibrator with a range of voltage	0 to 50	±0,2 %
Multimeter: voltage, V	 0 to1000	 ±0,09 %

V. METHODOLOGY FOR THE VERIFICATION OF MEASUREMENT VARIABLES

Before the beginning of every verification of measurement variables of the measurement channel to the VMDS, a visual inspection takes place to check for mechanical damages to the body of the primary transducer of the measurement channel and the connecting cable.

5.1 Verification of the measurement variables of the measurement channel for vibration velocity

5.1.1 Graduation pattern of the measurement channel for vibration velocity:

- Placing the primary transducer of the measurement channel on the platform of the shaker table;
- Starting the shaker table;
- The function for the graduation of the measurement channel for vibration velocity of the relevant primary transducer is enabled in the window of the application software;

The graduation coefficient is entered into the settings of the measurement channel verified for vibration.

5.1.2 Determination of the measurement variables of the measurement channel for vibration velocity

In the window of the application software, the function for the determination of the measurement variables of the measurement channel for vibration velocity is enabled.

- Verification in the amplitude range at the vibration frequency of 100 HZ and root square of vibration velocity of 1, 5, 10, 15 and 20 mm/s;
- Verification in frequency range with root mean square of the vibration velocity of 4 mm/s and vibration frequency of 30, 40, 80, 100, 160, 200, 400 and 500 Hz.

5.2. Verification of the measurement variables of the measurement channel for rotor displacement

5.1.2 Graduation pattern of the measurement channel for vibration displacement:

The measurement results at the frequency of 100 Hz for two values of vibration displacement of 50 and 350 µm;
The graduation coefficients are entered into the settings of the measurement channel which is verified for vibration.

5.1.2 Determination of the measurement variables of the measurement channel for vibration displacement of the rotor

Identification of the signal generator parameters: Signal shape - sinusoidal, generation frequency 10 Hz, voltage room mean square 4V.
The distance from the surface of the site of the shaker table to the surface of the primary transducer of the measurement channel for rotor vibration displacement should be (1,5±0,1) mm.

In the window of the application software, the function for the determination of the measurement variables of the measurement channel for vibration velocity is enabled.

-Verification in the amplitude range at the vibration frequency of 100 Hz and displacement values of vibration displacement of 50, 85, 175, 260 and 350 μm;

- Verification in frequency range with vibration displacement values of 150 μm and vibration frequency of 30, 40, 80, 100, and 150 Hz.

5.3 Verification of the measurement variables of the measurement channel for rotor angular velocity

5.3.1 Determination of the measurement variables of the measurement channel for rotor angular velocity

The distance from the surface of the site of the shaker table to the surface of the primary transducer for rotor angular velocity should be (3,1±0,1) mm.
In the window of the application software, the function for the determination of the measurement variables of the measurement channel for rotor angular velocity is enabled.

- Verification with vibration displacement value of 1000 μm and rotation frequency values of 480, 720, 1020, 1260, 1500 1/min.

5.4 Verification of the measurement variables of the analog signal processor-6.

5.4.1 Determination of the metrological characteristics of analog signal processor-11

- Verification of the main conversion error of the voltage input in digital code for the analog channels of the analog signal processor-11.
The following activities are carried out:
The measurement channels for the analog channels of the analong processor-11 are verified according to the diagram included in the design documentation without a power supply.
- Voltage controlled by a multimeter is supplied to the output of the power supply source.
A single measurement is made for every point.

5.4.2 Determination of the measurement variables of the analog signal processor-11/1

Verification of main conversion error of the voltage input in digital code for the analog channels of the analog signal unit-11/1.
The following activities are carried out:
The measurement channels for the analog channels of the analong processor 11 are verified according to the diagram included in the design documentation without a power supply.
The signal parameters for frequency of 100 Hz and voltage whose values are controlled by a multimeter are set at the generator input. A single measurement is made for every point.

5. 5 Processing of the measurement results

5.4.1. The relative percentage error in the j[th] point of the measuring range of the measurement channel for every *i*[th] measurement is defined according to the formula:

$$\gamma_{ji} = \frac{X_{i\text{изм}} - X_{\text{д}}}{X_{\text{к}}} \cdot 100\ \%$$

5.4.2 The relative percentage error of the n-measurement in the j[th] point of the measurement span, γj %, is defined according to the formula:

$$\gamma_j = \frac{1}{n}\sum_{j=1}^{n} \gamma_{ij}$$

where
n – the number of measurements of the signal in the j[th] in the measurement span;
γij – relative error in the i[th] measurement of signal in the j[th] point in the measurement units of the measured quantity.

5.4.3 The basic percentage error of voltage conversion into digital code, δ_{basic}, %, for analog signal unit-11 and analog signal unit-11/1 is determined according to the formula:

$$\delta_{осн} = \left| \frac{N_{изм}}{32000} - \frac{U_{вх.изм}}{U_{вх.\max}} \right| \cdot 100\ \%$$

N_{modified} – measured room mean square value;
32000 – code value corresponding to 100% of the input signal range;
$U_{\text{input modified}}$– measured value of the input constant voltage, V;
$U_{input\ maximum}$ – maximum range of the input signal, V.

5.4.4 The maximum value of the real values for the error of the measurement channel γ, % obtained at all points of the measurement range is defined according to the formula:

$$\gamma = \max|\gamma_j|$$

Where γ_j is the relative percentage error in the j[th] point in the range of measurement of the measurement channel.

The measurement channels are fit for operation if the maximum value of the obtained values does not exceed the value indicated in the technical documentation of the RCP VMDS - 195M.
After the completion of the operations for verification of measurement variables of the measurement channel, the data is recorded in the verification reports.
Upon a positive result of the verification of the measurement variables of the measurement channel of the RCP VMDS - 195M, a certificate for verification of the measurement variables of the RCP VMDS - 195M is issued.

VI. CONCLUSION

By implementing the RCP VMDS, a full metrological verification of the measurement channels is performed. The system ensures limitation on the subjective error factor when processing the measurement results,

reduction of the time needed for metrological control and timely preparation of final documentation following the activity. The collection of data from the metrological verification is enabled.

This development provides for qualitative and optimal performance of the metrological control activities.

Reference:

[1] 421412.120 И5 Metrology, Vibration Monitoring and Diagnostic System of Reactor Coolant Pumps at Units 5&6 of Ko-zloduy NPP (320 КАЭС RCP type VMDS). Procedure for verification of measurement variables. SRPA “Impulse”–Ukraine.

[2] 421412.120 ИЭ Vibration Monitoring and Diagnostic System of Reactor Coolant Pumps at Units 5&6 of Kozloduy NPP (320 КАЭС RCP type VMDS). Operating procedure. SRPA “Impulse”–Ukraine.

[3] 468332.204 И5-ЛУ Metrology of the КВВ-6 I/O controller. Calibration procedure

RESEARCH APPROACH AND SPECTRUM ALLOCATION ANALYSIS FOR 5G NETWORK DEVELOPMENT

Teodora Pasarelska
Communications Directorate, Ministry of transport and communications
Sofia, Bulgaria
tpasarelska@mtitc.government.bg

Plamen Tzvetkov
Department of Telecomunications
New Bulgarian University
Sofia, Bulgaria
ptsvetkov@nbu.bg

Rosen Pasarelski
Department of Telecomunications
New Bulgarian University
Sofia, Bulgaria
rpasarelski@nbu.bg

***Abstract* - The planning and distribution of the radio frequency spectrum and the trends in the development of electronic communications on a global and European scale take into account the need to manage the radio frequency spectrum according to the provisions of the Radio Regulations of the International Telecommunication Union, the decisions and recommendations of the European Commission and the Committee for Electronic Communications to the European Conference on Posts and Telecommunications.**

In order to achieve the effective management of the radio frequency spectrum, the principles of legality, predictability, transparency, publicity, consultativeness, equality, proportionality should be respected.

The main goal is to ensure the optimal use of the radio frequency spectrum in its management, providing prerequisites for the development of 5G networks in the Republic of Bulgaria. For this purpose, the basic principles in the management and distribution of the radio frequency spectrum, in this case the 700 and 800 MHz radio frequency bands, are studied and analyzed.

The contribution is in the systematization of problems related to the quality operation of the special radio communication systems, together with the public mobile systems.

The expected results are to achieve a harmonized use of the radio frequency spectrum, which is of particular importance for its effective management. The methods used are aimed at ensuring effective and efficient use of the radio frequency resource.

The contribution in the use of this approach will result in satisfying the consumer demand for new quality services and providing a secure investment environment for business, as well as promoting competition and developing the country's economy, and the European single market in the electronic communications sector.

Keywords - 5G, Radio frequency, Spectrum, Base station, Interference, Measurements.

1. Introduction

One of the main tasks is to analyze the circumstances for effective management of the radio frequency spectrum, which is directly related to the growth of consumer demand and the interest of business in its satisfaction.

To achieve this task, it is necessary to create algorithms to reduce the risk, to ensure sufficient radio frequency resource for telecommunications enterprises. For the introduction of more efficient spectrum technologies, it is necessary to enable enterprises by providing an algorithm for investing in the development of telecommunication networks.

The technical conditions for the use of the radio frequency spectrum should be in accordance with both European principles and national characteristics. This is in connection with the rapid development and entry of new generations of mobile telecommunication services in the community, where the demand for free frequency resources for the construction and development of huge telecommunication mobile networks is increasing. To this end, an exploratory approach is needed, with a view to establishing the possibility of working together in radio frequency bands intended for the implementation of 5G technologies and current ground-based radionavigation/radar systems. Some of the most suitable radio frequency bands for deploying 5G networks are 700 MHz and 800 MHz. At these ranges, methods should be provided to determine the mutual influence on the normal operation of radionavigation ground systems and radioelectronic equipment and mobile terminals.

2. Mathematical analysis and interference models in 5G base stations

Analyzing the interference in 5G base stations can be determined by several mathematical concepts and techniques. The paper presents a mathematical analysis of base station interference in 5G, covering topics such as signal propagation, interference modeling, and interference mitigation techniques.

2.1. Signal propagation model

One of the essential factors affecting interference is the signal propagation pattern [1][3]. The most commonly used model is the path loss model, which describes how signal power decreases with distance from the transmitter. The path loss model can be expressed as:

$$PL(d) = PL(d_0) + 10.n.\log10(\frac{d}{d0}) \quad (1)$$

where $PL(d)$ is the path loss at distance d,
$PL(d_0)$ is the path loss at the reference distance d_0,
n is the path loss rate.

2.2. Disturbance modeling

In 5G, multiple base stations can operate in the same area, causing interference to each other's signals. Disturbances can be divided into two main categories:

- Co-Channel Interference (CCI): CCI occurs when multiple base stations use the same frequency channel.
- Adjacent Channel Interference (ACI): ACI occurs when base stations use adjacent frequency channels. Although the interference is relatively weaker compared to CCI, it can still affect performance, especially for users located near the edge of cell coverage.

2.3. Signal to Interference Ratio (SIR)

Signal to interference ratio - SIR is a key metric used to evaluate the quality of a wireless communication link in the presence of interference. It is defined as the ratio of the power of the received signal to the power of interference from other sources. A higher SIR indicates better signal quality and reduced interference. [2]

$$SIR = \frac{\text{Signal Power}}{\text{Interference Power}}$$

2.4. Techniques to reduce interference

Several techniques are used to minimize interference and improve overall network performance:

- Frequency reuse - Base stations are deployed using a specific pattern to allocate non-overlapping frequency channels to nearby cells. This approach minimizes CCI and ACI.
- Interference coordination - Base stations can coordinate with each other to reduce interference by avoiding simultaneous transmission to neighboring cells.
- Beamforming - 5G base stations use advanced beamforming techniques to focus signal energy on specific users, reducing interference to other users.

2.5. Mathematical study with signal propagation model involving multiple base stations and a fading channel

Let's consider a complex example involving multiple base stations and a fading channel. We'll analyze the interference in a 5G network with three base stations located in a suburban area, taking into account Rayleigh fading for a more realistic scenario.

Assumptions:

- Three Base Stations - BS1, BS2, and BS3, operating at different frequencies (f_1, f_2, f_3) with transmit powers (P_{t1}, P_{t2}, P_{t3}) of 30 dBm each.
- Rayleigh Fading - The wireless channel experiences Rayleigh fading, which introduces random variations in signal strength.
- Path Loss Exponent - The path loss exponent 'n' is 2, typical for suburban environments.
- For this example, we'll consider a user located at a distance of 300 meters from each base station. We will calculate the Signal-to-Interference Ratio (SIR) for the user in the presence of Rayleigh fading.

Step 1: Calculations of path loss for all three base stations at 300 meters.

Using the free-space path loss model:

Path loss for BS1 (at f_1):

$$PL_{BS1}(300m) = 20.log_{10}(300) + 20.log_{10}(f_1) + 20.log_{10}(\frac{4\pi}{c}) \quad (2)$$

Path loss for BS2 (at f_2):

$$PL_{BS2}(300m) = 20.log_{10}(300) + 20.log_{10}(f_2) + 20.log_{10}(\frac{4\pi}{c}) \quad (3)$$

Path loss for BS3 (at f_3):

$$PL_{BS3}(300m) = 20.log_{10}(300) + 20.log_{10}(f_3) + 20.log_{10}(\frac{4\pi}{c}) \quad (4)$$

Step 2: Introducing of Rayleigh Fading.

Rayleigh fading introduces random variations to the received signal power. We'll model the fading channel as a complex Gaussian random variable with zero mean and a variance of 1.

Let's assume the fading gains for BS1, BS2, and BS3 as h1, h2, and h3, respectively.

Step 3: Calculations of the received power at the user location (300 meters) for all three base stations.

Received Power (P_r) is given by the formula:

$$P_r = P_t - PL(d) \quad (5)$$

where P_t is the transmit power of the base station.

For Base Station 1 (BS1):

$$P_{r\_BS1} = 30dBm - PL_{BS1}(300m) \quad (6)$$

for the given frequency f1

For Base Station 2 (BS2):

$$P_{r\_BS2} = 30dBm - PL_{BS2}(300m) \quad (7)$$

for the given frequency f2

For Base Station 3 (BS3):

$$P_{r\_BS3} = 30dBm - PL_{BS3}(300m) \quad (8)$$

for the given frequency f3

where:

P_{r_BS1}, P_{r_BS2}, P_{r_BS3} - are received powers at the user location for Base Stations 1, 2, and 3.

P_t - is the transmit power of the base station.

$PL_{BS1}(300m)$, $PL_{BS2}(300m)$ and $PL_{BS3}(300m)$, are path losses for Base Stations 1, 2, and 3 at a distance of 300 meters.

f_1, f_2 and f_3 - are frequencies of the respective base stations.

Step 4: Incorporating Rayleigh Fading in the received power.

The received power with Rayleigh fading for each base station is given by:

$$P_{r\_BS1\_faded} = |h1|^2 \,.\, P_{r\_BS1} \quad (9)$$

$$P_{r\_BS2\_faded} = |h2|^2 \,.\, P_{r\_BS2} \quad (10)$$

$$P_{r\_BS3\_faded} = |h3|^2 \,.\, P_{r\_BS3} \quad (11)$$

where $|h1|^2$, $|h2|^2$, $|h3|^2$ - are the squared magnitudes of the fading gains h1, h2 and h3, respectively.

Step 5: Calculations of the Signal-to-Interference Ratio (SIR) at the user location.

SIR is given by the formula: $SIR = \frac{\text{Signal Power}}{\text{Interference Power}}$

$$SIR = \frac{Pr\_BS1\_faded}{(Pr\_BS2\_faded + Pr\_BS3\_faded)} \quad (12)$$

Let's continue with the calculation of the Signal-to-Interference Ratio (SIR) at the user location, considering Rayleigh fading and the received powers for all three base stations.

Recap of the parameters:

- Base Station 1 (BS1) operates at frequency f1 with a transmit power of 30 dBm.
- Base Station 2 (BS2) operates at frequency f2 with a transmit power of 30 dBm.
- Base Station 3 (BS3) operates at frequency f3 with a transmit power of 30 dBm.
- The path loss exponent 'n' is 2.

We are using the free-space path loss model.

Using the values for frequency (f) and the speed of light (c):

$f_1 = 3.5.10^9$ Hz

$f_2 = 4.2.10^9$ Hz

$f_3 = 4.8.\ 10^9$ Hz

$c = 3.\ 10^8$ m/s

Calculate the path losses:

$PL_{BS1}(300\ m) \approx 46.08$ dB

$PL_{BS2}(300\ m) \approx 46.74$ dB

$PL_{BS3}(300\ m) \approx 47.18$ dB

Introducing of Rayleigh Fading.

Let's assume the fading gains for BS1, BS2, and BS3 as h1, h2, and h3, respectively. The fading gains follow a complex Gaussian distribution with zero mean and a variance of 1.

$$Let\ \ h1 = a_1 + jb_1 \qquad (13)$$

$$Let\ \ h2 = a_2 + jb_2 \qquad (14)$$

$$Let\ \ h3 = a_3 + jb_3 \qquad (15)$$

where a_1, b_1, a_2, b_2, a_3, b_3 are random variables following a standard normal distribution.

Calculations of the received power at the user location (300 meters) for all three base stations.

Received Power (P_r) is given by the formula:

$$P_r = P_t - PL(d)$$

where P_t is the transmit power of the base station.

For Base Station 1 (BS1):

$P_{r\_BS1} = 30dBm - PL_{BS1}(300\ m) \approx 30dBm - 46.08dB \approx -16.08dBm$

For Base Station 2 (BS2):

$P_{r\_BS2} = 30dBm - PL_{BS2}(300\ m) \approx 30dBm - 46.74dB \approx -16.74dBm$

For Base Station 3 (BS3):

$P_{r\_BS3} = 30dBm - PL_{BS3}(300\ m) \approx 30dBm - 47.18dB \approx -17.18dBm$

Incorporating Rayleigh Fading in the received power.

The received power with Rayleigh fading for each base station is given by:

$P_{r\_BS1\_faded} = |h1|^2 \cdot P_{r\_BS1}$

$P_{r\_BS2\_faded} = |h2|^2 \cdot P_{r\_BS2}$

$P_{r\_BS3\_faded} = |h3|^2 \cdot P_{r\_BS3}$

Calculations of the Signal-to-Interference Ratio (SIR) at the user location.

SIR is given by the formula

$$SIR = \frac{\text{Signal Power}}{\text{Interference Power}}$$

$$\text{SIR} = \frac{\text{Pr\_BS1\_faded}}{(\text{Pr\_BS2\_faded} + \text{Pr\_BS3\_faded})}$$

Finally, we interpret the SIR value to determine the level of interference experienced by the user. A higher SIR indicates better signal quality and reduced interference, while a lower SIR indicates a higher level of interference.

Due to the complexity introduced by Rayleigh fading and the randomness of fading gains, the exact numerical result will vary with each simulation run. However, the analysis demonstrates the process of incorporating fading and calculating the SIR in a more realistic 5G network scenario with multiple base stations. [5] [8]

3. Research approach design and planning activities

The research approach is aimed at defining objects separated by functional principle and according to their interconnectedness.

3.1 Intended objects of research

- radio technical system/for close navigation (ground);
- radar system;
- base stations according to specifications;
- equipment for round-trip measurements with a car or a portable backpack (Drive Test equipment);
- end user terminals.

3.2 Determination of territorial points for conducting the research

The research is conducted in a territory with the most significant influence of joint use of a frequency resource, where the radio navigation systems [7] are located and in a sanitary area with a certain test range with a radius of 5 kilometers from the center to the mobile point.

The following methods are used when conducting the research:

- **Method of comparative analysis**

Through this method, conclusions are drawn about the conformity of a certain characteristic (parameter, norm) of a base station, portable handheld terminals and/or its main equipment and software to the set requirements by using the results of successfully performed studies.

- **Method of measurements**

The measurement method is a method using built-in and/or external measuring devices, equipment and tools. The measurements are aimed at assessing the mutual influence on the normal functioning of radionavigation ground systems and radioelectronic equipment of mobile networks.

4. Research approach scenario

4.1 Certain scenarios should be followed when conducting research

- Checking the operational capability of the radar station;
- Submitting a signal to turn on the base stations;
- Measurement and analysis of the presence of disturbances in the form of screen illumination;
- The absence of interference determines the efficiency and quality of conducting conversations with subscriber devices.

A study to verify the operation of a radio-technical system for near-field navigation with included base stations at the designated study points.

Research is conducted under the following scenario:

- Radio technical system for close navigation is switched on.

The operability of the system is checked by:

- Control of supply voltages.
- Device for controlling the operability of the distance channel BK-007. The general operability of the radio jamaica is checked; the creation of an electric azimuth-rangefinder grid on the IKO screen; operation of the ranging and continuous-azimuth transmitter; the "180" signal encoder and decoder, equipment for monitoring the operability of the azimuth channel BK-006.

4.2 The land mobile connection

4.2.1 Monitoring the airwaves for the presence of interference

Monitoring the airwaves for the presence of interference - from the equipment or cross-border interference:

- Collection of statistics from base stations – RTWP statistics (measurement for the Upload DATA part of the provided spectrum at 700 MHz and 800 MHz). [10]
- Measurement of the Download DATA part of the provided spectrum at 700 MHz and 800 MHz, by means of bypass measurements with a portable scanner to the Drive Test equipment.
- Measurement of the entire provided spectrum using a "Spectrum Analyzer" and a directional antenna.

4.2.2 Temporary access for shared use

Temporary access is determined for the joint use of radio frequency bands 703-733 MHz, 758-788 MHz, 791-821 MHz, 832-862 MHz for the study of terrestrial networks enabling the provision of electronic communication services, together with radio equipment of a specialized type. The measurements are carried out with specialized measuring equipment for monitoring the radio frequency spectrum for civil needs. Three mobile stations for monitoring the radio frequency spectrum located at the points determined for the needs of the study with predetermined geographical coordinates participate in the measurements. [9]

5. Standards of accuracy and/or reliability of research results

1) The accuracy of the data and the results of the conducted studies are compared with the requirements of the technical and operational documentation of the equipment and the relevant standards.
2) Deviations from the requirements of the technical and operational documentation of the equipment are not allowed.
3) A comparison of the results of the conducted tests of the equipment with the requirements of the technical and operational documentation is carried out.
4) Accuracy norms and (or) data accuracy indicators and research results of the main apparatus and equipment are laid down in research procedures for each apparatus subject to research.
5) The following protocols are used for the purpose of measurements: ICMP, HTTP, FTP, as well as the currently used Packet Data performance metrics.
6) As a result, statistical data will be collected and analyzed on the interference levels measured by the receiving part of the Base Stations (eNB) and the technical equipment - Drive Test, which will be compared with the periods of operation (beginning and end) of the current radio communication systems.

In table 1 is presented base station baseline power limit.

Table 1

Frequency range	Bandwidth of protected block	Maximum mean EIRP	Measurement bandwidth
Uplink frequencies in the range 698-736 MHz ([4])	≥ 5 MHz	– 50 dBm per cell	5 MHz
	3 MHz	– 52 dBm per cell	3 MHz
	≤ 3 MHz	– 64 dBm per cell	200 kHz
FDD uplink frequencies as defined in Decision 2010/267/EU (i.e. 832-862 MHz)	≥ 5 MHz	– 49 dBm per cell	5 MHz
Downlink frequencies in the range 738-791 MHz	≥ 5 MHz	16 dBm per antenna	5 MHz
	3 MHz	14 dBm per antenna	3 MHz
	< 3 MHz	2 dBm per antenna	200 kHz
FDD downlink frequencies as defined in Decision 2010/267/EU (i.e. 791-821 MHz)	≥ 5 MHz	16 dBm per antenna	5 MHz

6. Conclusions when carrying out the broadcast in the direction from the mobile stations

Base station to mobile devices is from 7% to 100% per sector of one Base Station, by positioning the mobile equipment in front of a specific sector. Mobile devices to a Base Station are defined from 0% to 100% per sector of a Base Station, by positioning the mobile equipment in front of a specific sector.

Due to technical limitations, the continuous load at 100% is limited to about 2 minutes, after which there is a pause of 10 seconds.

Criteria for acceptance of research as successful: (given 10 MHz bandwidth).

In table 2 is presented scanner results and UE / OSS results of signal strength.

Use of certain radio frequencies and radio frequency bands for preparatory spectrum studies in 700 MHz and 800 MHz as follows:

Radio frequency bands of the 700 MHz range:

Table 2

Scanner Results:	
Signal Strength LTE (RSRP) *used to define LTE covered area, where to monitor KPI below:*	> -110 dBm
Signal Quality LTE (RSRQ)	> -9
Signal Quality LTE (SINR)	> -12

UE / OSS results:	
RACH SSR	> 99 %
Call Setup Success Rate	> 98 %
Drop Call Rate	< 0,5 %
Handover Success Rate	> 95%
Overall CSFB SSR	> 96 %
LTE UL NACK Rate	< 10 %
LTE DL NACK Rate	< 10 %
Average UL interference	< -115 dBm
User Avg DL Throughput	> 30 Mbps
User Avg UL Throughput	> 10 Mbps

The research is conducted in the 800 MHz range in frequency bands 791 – 821 MHz (base stations) and 832 – 862 MHz (end devices).

A radar system transmitting and receiving in the 837+/-2.5 MHz radio frequency band is in operation during the ground survey of the current equipment.

- The equipment is configured in the 3 bands in 700 and 800 MHz;
- Measurement of noise of the studied spectrum;
- Conducting conversations with the subscriber devices in the control room and outside;
- Data exchange with the subscriber devices in the device and outside it, by completing the results for Download DATA and Upload DATA;
- Carrying out monitoring measurements for field strength during operation of base stations and subscriber devices.

Results of the electromagnetic compatibility study of the ground systems providing electronic communication services in the 700 MHz and 800 MHz bands and the specialized ground radar and radio navigation equipment are:

- test in the 700 MHz range, test telephones at a distance of up to 100 m and test at a distance of up to 1000 m from the equipment room of the special part;
- test in the 800 MHz range, test telephones at a distance of up to 100 m and test at a distance of up to 1000 m from the equipment room of the special part.

7. Results

The results of the electromagnetic compatibility study of ground systems in the 700 MHz and 800 MHz bands and ground radar equipment consider the impact on current ground specialized radio communication equipment.

When starting the base stations along the entire development of the indicator of the dispatch radar, a solid cone with a width of 5^0 is visualized in azimuths of 30^0 and 62^0 in all scales, which becomes denser (becomes brighter) and reaches a width of 10^0 when data transfer is carried out between a subscriber device (test phone) and the base station.

The research in the 700 MHz range was carried out when the base stations were launched along the entire development of the dispatch radar indicator, visualizing a solid cone with a width of 5^0 in azimuth 62^0 at all scales, which thickens (becomes brighter) and reaches a width of 10^0 when transferring data between a subscriber unit (test phone) and the base station.

The survey in the 800 MHz band was carried out using a base station at a launch location along the entire sweep of the control radar indicator. A dense cone with a width of 5^0 in azimuth 60^0 is visualized at all scales, which thickens (becomes brighter) and reaches a width of 10^0 when transferring data between a subscriber unit (test phone) and the base station.

After detecting interference in the 800 MHz range, the study was carried out using a more distant base station. [11]

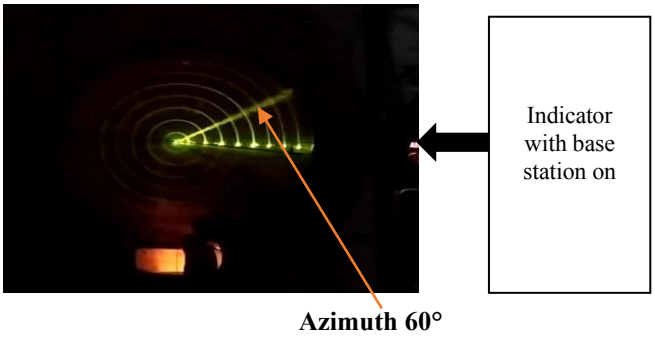

Fig. 1 Indicator of established impact

In Table 3 is given tabular presentation of the results.

Table 3

№	Scope	Frequency band (MHz)	Result	A feature
1.	700 MHz	703-713/758-768	no influence	
		713-723/768-778		
		723-733/778-788		
2.	800 MHz	791-801/832-842	has an impact	Active and SPC modes
		801-811/842-852	has an impact	Active and SPC modes
		1-821/852-862	has an impact	only in SPC mode

The established influences cannot be avoided by the current apparatus by applying organizational-technical measures and/or reconfiguration of systems. [12].

8. Final conclusions

With the research of the parameters and radio technical characteristics of the current based radionavigation and radar systems and the mobile system of the fifth generation - 5G, a complete and clear picture is defined for real research setups, norms and procedures in the research of the radio frequency spectrum.

The scope and possibilities of the effective and efficient use of the radio frequency spectrum are being expanded, which is in connection with the deployment of new radio communication and mobile telecommunication services in the community. A procedure for establishing the possibility of joint work in radio frequency ranges intended for the implementation of 5G technologies [6] and ground-based radio navigation and radar systems is defined.

Prerequisites for future research on the actual use of the radio frequency spectrum in wireless systems:

- Application of adaptive allocation of resources with a proportional rate of the limited resource;
- Adaptive allocation of resources in the radio frequency ranges designated for broadband mobile telecommunication systems;

The overall performance should be optimized. Power distribution must be carefully designed as it includes:

- power distribution between cutting frequency subchannels in different radio frequency bands.

Influence of the imperfect status of the channel information on the adaptive allocation of radio frequency resources.

REFERENCES

[1] Donald E. Kerr - Propagation of short radiowaves", ISBN 0 86341 099 5, Peter Peregrinus Ltd., London, United Kingdom, 1990

[2] Jochen H. Schiller - Mobile Communications, Second Edition, ISBN 0 321 12381 6, Pearson Education Limited, 2003

[3] Constantine A. Balanis - Antenna theory analysis and design, ISBN: 0-471-66782-X, John Wiley&Sons Inc., 2005

[4] Rosen Pasarelski - "Универсални мобилни телекомуникационни системи", ISBN: 978-954-535-770-1, Издателство на Нов Български Университет, 2013.

[5] Rosen Pasarelski - Милиметровият честотен обхват като перспектива за 5G мрежи. Годишник Телекомуникации 2019, том 6, с. 161 - 170, eISSN 2534-854X., 2019.

[6] Rosen Pasarelski, V. Kadrev, T. Pasarelska - Петото поколение (5G) – мобилни системи и технологии за комуникации на бъдещето, ISSN: 1314-2690, Телеком 2018, 2018.

[7] Stefan Biliderov, Rumen Georgiev - Otsenka na statisticheskite harakteristiki na otnositelnoto polozhenie na obekti v sistemata GPS, YUNS na Fakultet "Aviatsionen" s mezhdunarodno uchastie, tom 2, D. Mitropoliya, s. 215-223. ISBN 954-713-65-X (t. 2), 2003

[8] Sadinov, S., Kogias, P., Angelov, K., Malamatoudis, M., Aleksandrov, A. - The Impact of Channel Correlation on the System Performance and Quality of Service in 5G Networks, 2020 7th International Conference on Energy Efficiency and Agricultural Engineering, EE and AE 2020 - Proceedings, 2020, 9278982

[9] Georgi Petrov, A. Stancheva, V.Kadrev - Specialized databases for spectrum management research, analysis and forecasting of the effects of working electromagnetic fields, Godishnik na departament Telekomunikatsii, NBU, ISSN 2534-854X, 2014 g., tom 1, 2014

[10] EU - Commission implementing decision (EU) 2016/687 on the harmonisation of the 694-790 MHz frequency band for terrestrial systems capable of providing wireless broadband electronic communications services and for flexible national use in the Union.

[11] EU - Commission Decision 2010/267 of 6 May 2010 on harmonised technical conditions of use in the 790-862 MHz frequency band for terrestrial systems capable of providing electronic communications services in the EU.

[12] EU - Decision (EU) 2017/899 of the European Parliament and of the Council of 17 May 2017 on the use of the 470-790 MHz frequency band in the Union.

[13] MTC - National plan for allocation of the radio frequency spectrum in the Republic of Bulgaria.

Mobile Station for Collecting Measurement Information

Spasov Ted Spasimir
dept. Electrical Measurement Systems
Technical University of Sofia
Sofia, Bulgaria
email tespasov@tu-sofia.bg

Dzhudzhev Bozhidar Petkov
dept. Electrical Measurement Systems
Technical University of Sofia
Sofia, Bulgaria
b.djudjev@tu-sofia.bg

***Abstract*— In this article, a developed mobile platform with Arduino – microcontroller for monitoring air parameters in a working environment (temperature and relative humidity) is presented. The system is organized in such a way that it is possible to work in real time with remote control and remote reception of the measurement data. The mobile platform can be used to measure the temperature and humidity of the air in a working environment in rooms with harmful working conditions for people.**

Keywords—mobile platform, temperature, humidity, microcontroller

I. INTRODUCTION

Temperature and humidity are two key physical quantities that have a significant impact on the environment and our lives. They play an important role in regulating comfort, climate and the functioning of various ecosystems. Temperature measures the amount of heat in a given space and determines the degree to which objects are heated or cooled. Humidity, on the other hand, expresses the amount of water vapor in the air and affects condensation.

The relationship between temperature and humidity has important implications for human health, comfort and performance. Optimal levels of these parameters in various areas, such as living quarters, workplaces and public buildings, are essential to maintain a healthy and productive environment.

A. Temperature

It is known that the temperature [1, 11, 7, 22] is proportional to the average kinetic energy. The temperature of bodies characterizes the degree of heating, which is determined by the internal kinetic energy of the thermal movement of molecules.

Various temperature measurement methods are described in [2, 8, 11, 7, 22]. Temperature cannot be measured directly. Its measurement is practically possible by the method of comparing the heating of two bodies, in which a certain physical property of the bodies is used.

There are three basic physical principles used in temperature measurements: Measurement of thermal radiation of heated bodies; Determination of the temperature of the environment by measuring some physical characteristics depending on it; By measuring some temperature-dependent physical characteristics of the thermometric bodies placed in the environment and receiving its temperature by means of heat exchange.

B. Humidity

Humidity is one of the main parameters of the environment and a basic characteristic for many gaseous substances.

In literature [15, 7, 22] an overview of moisture parameters and methods for measuring humidity is made.

In many industrial processes there are requirements to control the moisture content. Atmospheric humidity affects the feeling of comfort, and is also an important parameter for ensuring optimal operation of warehouses for food and non-food goods, building materials, etc. The humidity of the products guarantees their long-term storage, which is very important for cereals, fodder, tea, coffee, etc.

Also, in industrial productions related to the use of air and other technical gases, in order for the process to run optimally, it is necessary to control the humidity in accordance with the technological requirements.

In [14, 16, 22] methods for measuring the humidity of the air are described.

In cases where the humidity of the atmospheric air is measured, both characteristics are used. The atmosphere could be thought of as water dissolved in air.

Accordingly, when the saturation of the solution is reached, it starts to rain. In such cases, we speak of 100% relative humidity. As the temperature increases, the ability of air to dissolve water increases.

There are different methods of measuring humidity. As microprocessor technology develops, accuracy increases.

There is a wide variety of devices [4, 7] for temperature monitoring and control in an industrial environment, starting from simple temperature controllers and reaching complex distributed control systems.

II. AIM OF THE STUDY

The purpose of the study is monitoring and control of air temperature and humidity.

There is a wide variety of devices for monitoring and controlling temperature and humidity in industrial environments [3, 12, 4, 8, 21], starting from simple temperature controllers [12] and ending up with complex distributed control systems.

Most often, temperature monitoring and control devices in an industrial environment are either stationary or carried [4] by personnel performing the measurements. However, this is impossible if the measurement of temperature and humidity is to be carried out in places dangerous for the movement of people. In temperature and humidity control in

The present research was funded by the Research Sector of Technical University - Sofia under contract 231ИХЪБ0004-08.

unfavorable human environments, the present project will provide a solution.

The task of the study is to develop a mobile platform for measuring temperature and humidity in hard-to-reach and unfavorable environments.

III. SELECTION OF ELEMENTS

Different temperature and humidity monitoring and control systems may have different elements in their structure, but in most cases they contain a temperature and humidity sensor, a measuring device, a database, software and notification means.

Wireless models are of greatest interest nowadays and allow the measurement information to be sent wirelessly to a base station or gateway and from there to a computer spatially hundreds of kilometers away.

Such wireless systems are used when there are different, distant from each other points at which the temperature and humidity are to be measured, for example in case the measurement information is to be transmitted from a station moving in the measurement process.

Choosing the right type of device among the wide variety of temperature and humidity measurement and control systems is an important issue. Most often, the choice begins with determining the type of measuring transducer (sensor).

There are many types of measurement transducers or sensors [10] that are used to measure temperature. Their action is based on different physical laws.

The created mobile station is a technical solution that uses modern technologies and components, aimed at achieving reliable and complex reporting of environmental parameters. The software generated on Arduino integrates a DHT22 sensor that performs the measurement of humidity and temperature with a high degree of accuracy and precision.

In this way, the station provides comparable and up-to-date data on the microclimatic conditions in the specific location.

An important part of the station is its mobility and control. Driven by DC motors, this mechanism, complete with the appropriate software, allows the system to be placed and directed to different objects and locations in the environment, which enriches the possibilities of observation and measurement. The user can monitor and control the station remotely using the built-in HC-06 communication module. This leads to the expansion of the possibilities of application and usability of the system in various spheres.

The current form can be used in a number of areas. From its role in climate control, through industrial and agricultural applications, to use in scientific research, the proposed system provides valuable data for environmental analysis and management.

A. Hardware

- Arduino Uno Rev.3 Development Board

The Arduino Uno development board is a microcontroller development board built with the ATmega328P. There are 14 digital input-output (I/O) ports, 6 analog inputs, a 16 MHz crystal resonator, four LEDs (one user connected to the 13th digital I/O port and three that indicate board operation: ON, Tx and Rx), USB connector, power connector, reset button and ICSP connector. Six of the digital I/O ports can be used as PWM outputs.

- DC motor

To drive the supporting mobile platform (trolley) we use a constant current electric motor.

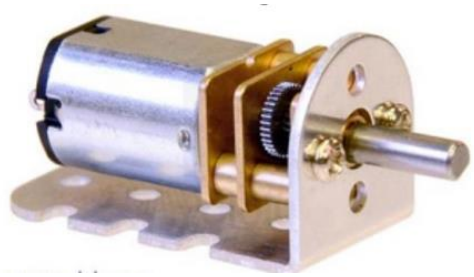

Fig. 1. DC motor with reduction gear

A DC motor with reduction gear (fig.1) was chosen for the project as it is suitable for robots and cars. It is characterized by low weight and high torque, as well as low revolutions. Finely crafted, durable and low power consumption. A wheel can easily be mounted on the motor output shaft. Widely used for mini models, cars, robots, linear motion control, etc. [5, 9, 18]

- L298N electric motor control module

The L298N module allows simultaneous control of two DC motors (or one reversible stepper motor) by controlling the speed and direction of rotation. The module can control motors supplied with a voltage in the range 5V - 35V. A 5V regulator is placed on the board for convenience if the supply voltage is up to 12V.

The direction and speed of rotation of electric motor 1 is controlled by pins IN1 and IN2, and for electric motor 2 by pins IN3 and IN4.

- DHT22 temperature and humidity sensor

The DHT22 module is a humidity and temperature sensor. It is suitable for weather stations. The measurement takes place only after initiating a signal from the controller, during the rest of the time it is in low consumption mode. It uses a one-way protocol with one connection line (not 1-Wire).

The DHT22 sensor is designed to measure humidity and temperature with high accuracy, and the data is transmitted via a 1-Wire interface requiring only one port from the microcontroller.

The DHT22 measures temperature from -40° to 80° C and relative humidity in the range 0% - 99%. It has a pre-calibrated digital output and is characterized by great reliability and stability.

- HC-06 Bluetooth module

The HC-06 module adds to the project the possibility of wireless connection and control. Since the HC-06 uses serial communication, connecting it to Arduino development boards is easy. HC-06 is a Bluetooth module that provides wireless communication between various devices through Bluetooth technology. This module is distinguished by its reliability, easy integration and wide application in various

fields. Its main function is to establish a connection and exchange data between devices such as microcontrollers, smartphones, computers and other peripherals.

B. Softwawre

- Arduino IDE

The open source software (Arduino IDE) for programming the boards allows installing various specific programs [25]. The Arduino Integrated Development Environment (IDE) is a powerful and intuitive software tool designed for programming, developing and managing microcontrollers from the Arduino platform. This integrated development software provides the designer with an environment where they can easily create and run programs that control physical devices and sensors, and thus implement various projects with a significant simplification of the programming process.

- Remote XY

Remote XY is a powerful software tool designed to ease and facilitate the development process of interactive remote control and monitoring applications. This integrated development software enables the creation of user interfaces and visual elements that interface and communicate with various microcontroller platforms. An important quality of RemoteXY is the possibility of wireless communication between the microcontroller platform and smartphones or tablets via Bluetooth or Wi-Fi. This makes it possible to implement remote controls, data monitoring and real-time reactions.

On figure 2 a diagram showing the connections between the elements of measurement and control systems is shown.

On figure 3 a picture of the assembled mobile station is presented.

IV. EXPERIMENTAL STUDIES

The objective of the experimental measurements is to show the usability, the functioning of the developed mobile platform, its remote control, the action of the sensor and the possibilities of obtaining measurement results on a phone.

To demonstrate the capabilities of the mobile platform, measurements of temperature and humidity were made in an apartment (bedroom, corridor and dining room).

The data is transmitted remotely to a smart phone, tablet or computer. The application for working on the mobile platform was developed on the RemoteXY program as shown on figure 4.

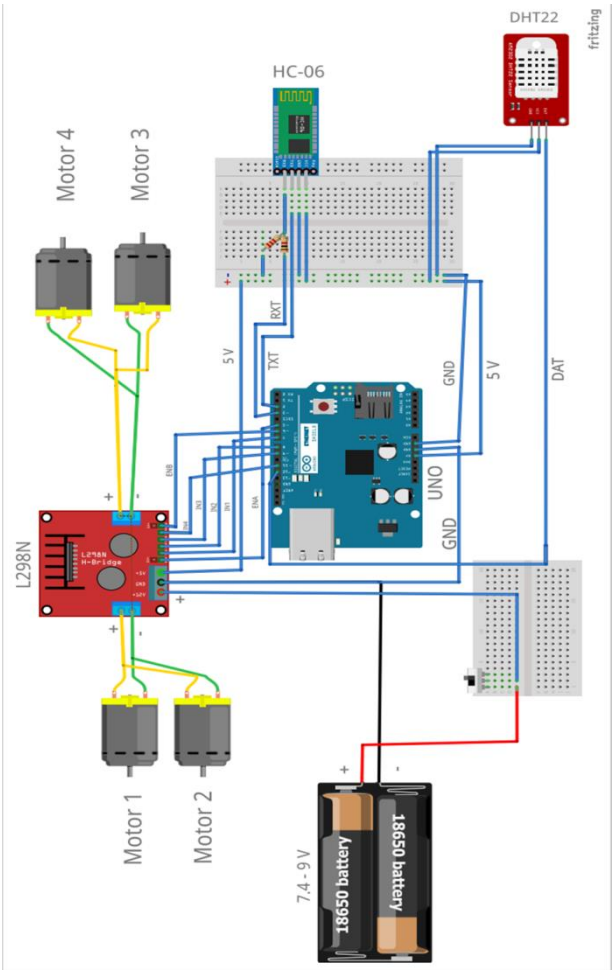

Fig. 2. Connection diagram between the elements

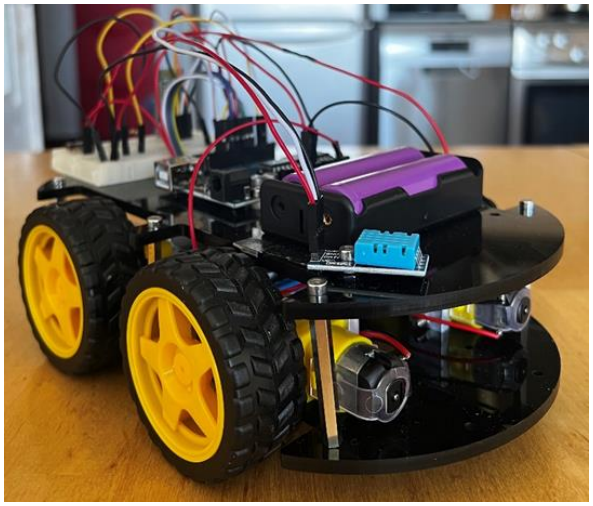

Fig. 3. Mobile station

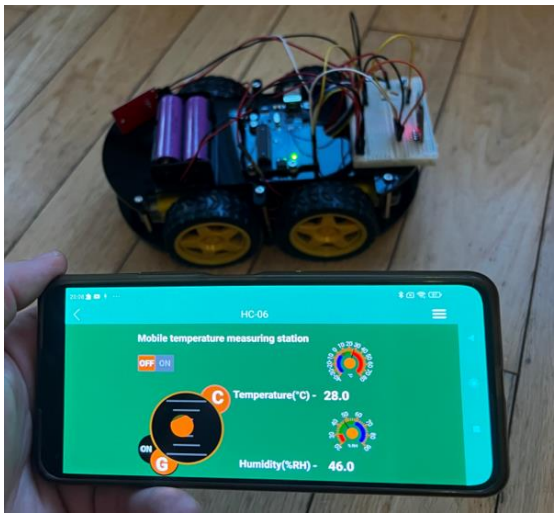

Fig. 4. Mobile platform with the control application

TABLE I. MEASUREMENT RESULTS

place of measurement	Measurement №1		Measurement №2		Measurement №3	
	t, °C	*φ, %*	*t, °C*	*φ, %*	*t, °C*	*φ, %*
bedroom	28	44	28	43	29	43
corridor	29	41	28	43	28	45
dining room	29	42	29	41	30	40

V. CONCLUSIONS

The created mobile station is a technical solution that uses modern technologies and components, aimed at achieving reliable and complex reporting of environmental parameters. The software generated on Arduino integrates a DHT22 sensor that performs the measurement of humidity and temperature with a high degree of accuracy and precision.

In this way, the station provides comparable and up-to-date data on the microclimatic conditions in the specific location.

An important part of the station is its mobility and control. Driven by DC motors, this mechanism, complete with the appropriate software, allows the system to be placed and directed to different objects and locations in the environment, which enriches the possibilities of observation and measurement. The user can monitor and control the station remotely using the built-in HC-06 communication module. This leads to the expansion of the possibilities of application and usability of the system in various spheres.

The current form can be used in a number of areas. From its role in climate control, through industrial and agricultural applications, to use in scientific research, the proposed system provides valuable data for environmental analysis and management.

In future more sensors will be added to the developed mobile platform.

REFERENCES

[1] Измерване на температурата. СП „ИНЖЕНЕРИНГ РЕВЮ“ бр.2, 2010г https://www.engineering-review.bg/

[2] Безконтактно измерване на температура. СП „ИНЖЕНЕРИНГ РЕВЮ“ бр.5, 2011г. https://www.engineering-review.bg/

[3] Измерване параметрите на микроклимата. СП „ИНЖЕНЕРИНГ РЕВЮ“ бр.7, 2012г. https://www.engineering-review.bg/

[4] Продуктова листа на „TESTO

[5] Yonatan Yordanov, Radoslav Deliyski, "DESIGN AND DEVELOPMENT OF A REMOTE CONTROL FOR A SMALL WATERCRAFT", Proceedings of International conference Challenges in Higher Education and Research in the 21st Century (CHER21), 2023, ISSN: 2683-0337, in print

[6] Температурни сензори. https://www.ifm.com/bg/bg/category/200_020_040

[7] https://farbitis.ru/bg/interesting-geography/temperature-measurement-and-temperature-controlsss/

[8] Температура. Измерване и контрол на температурата. Методи и средства за измерване на температурата https://farbitis.ru/bg/interesting-geography/temperature-measurement-and-temperature-controlsss/

[9] Yonatan Yordanov, Radoslav Deliyski, Bojidar Djujev, "APPLICATION OF ARTIFICIAL INTELLIGENCE IN ENGINEERING EDUCATION", Proceedings of International conference Challenges in Higher Education and Research in the 21st Century (CHER21), 2023, ISSN: 2683-0337, in print

[10] Измерване на температура.Датчици и сензори. https://www.ifm.com/bg/bg/category/200_020_040

[11] https://www.meteorologiaenred.com/bg/la-temperatura.html#google_vignette

[12] Каракехайов З. И др.Проектиране на вградени микрокомпютърни системи с микроконтролери. Хардуер и софтуер.PENSOFT София-Москва, 2000 https://books.google.bg/books?id=8gOpXp7K8-QC&pg=PA167&lpg=PA167&dq=%D0%B8%D0%B7%D0%BC%D0%B5%D1%80%D0%B2%D0%B0%D0%BD%D0%B5+%D0%BD%D0%B0+%D1%82%D0%B5%D0%BC%D0%BF%D0%B5%D1%80%D0%B0%D1%82%D1%83%D1%80%D0%B0&source=bl&ots=0d9xnjwDK9&sig=ACfU3U07ay1rM

[13] Как да правим постоянен мониторинг на температура и влажност? HTTPS://WWW.ENGINEERING-REVIEW.BG/BG/KAK-DA-PRAVIM-POSTOYANEN-MONITORING-NA-TEMPERATURA-I-VLAZHNOST-/2/4424/

[14] Измерване на влажност. СП „ИНЖЕНЕРИНГ РЕВЮ“ бр.6, 2010г. и бр. 2, 2012г.

[15] Влажност на въздуха. https://bg.wikipedia.org/wiki/%D0%92%D0%BB%D0%B0%D0%B6%D0%BD%D0%BE%D1%81%D1%82_%D0%BD%D0%B0_%D0%B2%D1%8A%D0%B7%D0%B4%D1%83%D1%85%D0%B0

[16] Методи и средства за измерване на влажност. https://bgkids.hallowedgaming.com/user-51/metodi-i-sredstva-za-izmervane-na-vlazhnost.html

[17] Измерване на влажност на въздуха с психрометър. HTTPS://BIOEVIBUL.COM/NEWS/1129

[18] Antonia L. Pandelova, Svetlin I. Vladov, Nikolay S. Stoyanov, Bozhidar P. Dzhudzhev, System for Monitoring and Analysis of Environmental Data, PROCEEDINGS OF THE TECHNICAL UNIVERSITY OF SOFIA, ISSN: 2738-8549, VOL. 72, NO. 2, YEAR 2022, pp. 38-42

[19] Христов В. Микроконтролерна система за мониторинг на показателите на въздуха и околната среда. Годишник на ТУ Софияя, том 69, книга 3, 2019г.

[20] Програмиране в среда на ARDUINO. Ръководство.

[21] Измерване на температура и влажност. https://farbitis.ru/bg/interesting-geography/temperature-measurement-and-temperature-controlsss/

[22] https://html.alldatasheet.com/html-pdf/1179032/ETC1/HC-06/689/6/HC-06.html

[23] https://www.ardboard.com/index.php?route=product/product&product_id=71

[24] https://remotexy.com/en/help/

[25] Arduino (https://www.arduino.cc/en/Main/Software)

[26] Yonatan Yordanov, Radoslav Deliyski, Bojidar Djujev, "APPLICATION OF ARTIFICIAL INTELLIGENCE IN ENGINEERING EDUCATION", Proceedings of International conference Challenges in Higher Education and Research in the 21st Century (CHER21), 2023, ISSN: 2683-0337, in print

[27] Yonatan Yordanov, Radoslav Deliyski, "DESIGN AND DEVELOPMENT OF A REMOTE CONTROL FOR A SMALL WATERCRAFT", Proceedings of International conference

Virtual Instrument for mass measurements with Arduino Uno

Nikolay Kililov
dept. Electrical Measurement Systems
Technical University of Sofia
Sofia, Bulgaria
kirilov_1994@abv.bg

Dzhudzhev Bozhidar Petkov
dept. Electrical Measurement Systems
Technical University of Sofia
Sofia, Bulgaria
b.djudjev@tu-sofia.bg

Nikolay S. Stoyanov
dept. Electrical Measurement Systems
Technical University of Sofia
Sofia, Bulgaria
n_stoyanov@tu-sofia.bg

Antonia L. Pandelova
dept. Electrical Measurement Systems
Technical University of Sofia
Sofia, Bulgaria
apandelova@tu-sofia.bg

***Abstract*—The paper presents a developed virtual instrument for mass measurements using Arduino Uno Rev3 and software LabVIEW.Experimental test with the virtual instrument are presented and analyzed.**

Keywords—mass, virtual instrument, LabVIEW, Arduino Uno

I. INTRODUCTION

In our time, mass measurements are carried out everywhere. It is one of the most measured parameter.

Mass is a physical quantity - a property of physical bodies that indicates how much matter is in them. It is constant for a body of constant volume and density, it is not changed by the position of the body, movement or change of its shape [1].

According to the International System of Units SI the unit for mass is kilogram (kg).

There are different methods instruments for mass measurements. The simplest instrument for determining mass and weight is the lever scale. It is a beam with support in its middle part. There are dishes at each end of the beam. An object to be measured is placed on one plate and weights of standard dimensions are placed on the other until the system is brought to equilibrium. Such a device has been very popular and has been used for many years in trade and kitchens.

Currently, various methods based on receiving an electrical signal are used to measure mass. In the case of measuring very large masses, such as a heavy vehicle, pneumatic and hydraulic systems are used.

Nowadays the most used instruments for mass measurements are tensor resistors. Under pressure they change their geometrical dimensions which lead to change in the internal resistance. In order to receive an electrical signal Wheatstone bridge is used (fig.1).

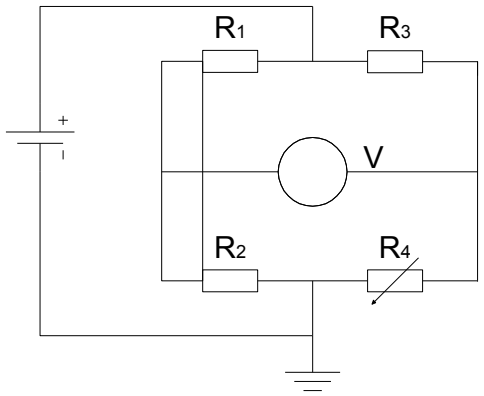

Fig. 1. Wheatstone bridge

In the paper the components for development of a virtual instruments for measuring mass is presented.

II. COMPONENTS FOR DEVELOPING A VIRTUAL INSTRUMENTS FOR MASS MEASUREMENT

The block diagram of the virtual instrument is presented of figure 2.

The object which mass needs to be measured is put on the load cell. The load cell produces electrical signal proportional to the mass of the object. The electrical signal is amplified and send to the input of the Arduino Uno circuit board. There it is digitalized and send to the computer in the software LabVIEW where it will be processed and visualized.

Identify applicable funding agency here. If none, delete this text box.

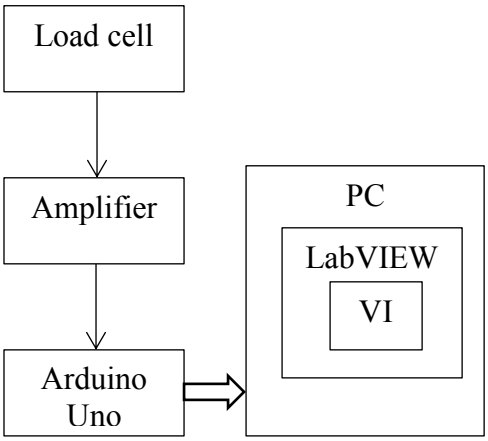

Fig. 2. Block diagram of the virtual instrument for mass measurements

A. Load Cell

The load cell (fig.3) used for the virtual instrument is manufactured in Chine. It has aluminum alloy with weight and pressure sensor. The measuring range is up to 10 kg. The load cell is connected to two platforms - one under and one above it. The platform under the load cell is used for horizontal leveling of the load cell. The one above is where the object which mass is needs to be measured is put on.

When an object is placed on the load cell due to the mass of the object, the cell will produce an electrical signal proportional to the mass.

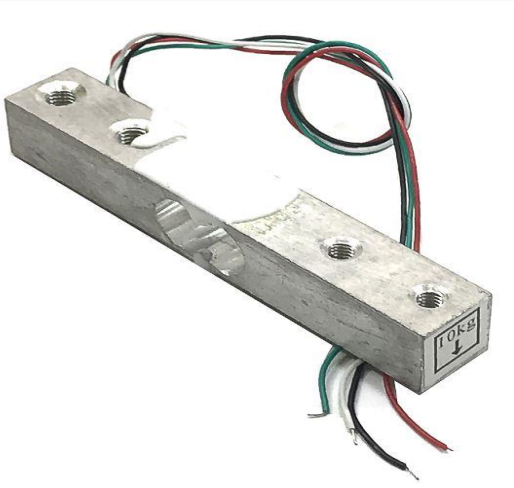

Fig. 3. Load cell

B. Amplifirer model HX711

The signal from the load cell is very small and needs to be amplified. For that purpose an amplifier HX711 is used.

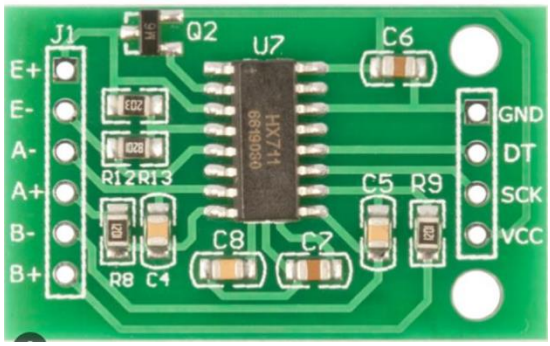

Fig. 4. Amplifirer model HX711

C. Arduino uno Rev3

The Arduino IDE is an integrated development environment that contains a text editor, a message area, a text console, and a toolbar for menu functions and a series of menus. The medium is directly connected to the hardware on the board to communicate with it as well as upload programs.[2,4]

Two programs with different functions have been developed for the system. One of the programs is used when the device needs to be calibrated. The second program is the main one that is used after the calibration is done.[3]

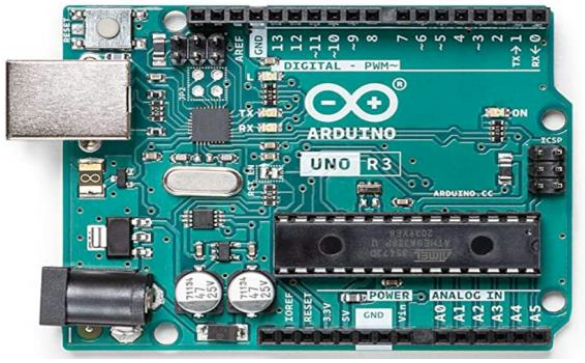

Fig. 5. Arduino Uno Rev3

D. Software LabVIEW

LabVIEW (LV) is an object-oriented programming language that contains a rich set of tools for data collection, analysis, presentation, and storage of data and results, as well as tools to help create programs. LV's main advantage over other development environments is its rich tooling support

E. Virtual Instrument (VI)

Virtual instruments are closely related and developed on the basis of computer-based measurement systems. With them, convenient and easy maintenance during use, implementation of the measurement algorithm and management of hardware measurement resources is achieved. [5]

Three main components are used in the interactive environment LabVIEW for building BI: User Interface, Block Diagram, Icons and Link Window. The front panel is the user interface of the virtual instrument. The means for monitoring and managing the operation of the AI are located on the front panel. It consists of indicators and executive bodies presented on the computer screen. Different types of graphic and signal indicators, arrow and digital displays, tables are used to visualize the results. Control devices

visualize various input quantities and enter their data to the AI block diagram. Indicators simulate external devices and visualize the data that the block diagram has received or generated. Graphical flexibility allows more than a few virtual instruments to fit on the screen. The user works through icons, each corresponding to a real measuring device, and through the computer mouse the controls are acted upon.

Fig. 6. Software of the virtual instrument fot mass measurements

III. EXPERIMENTAL STUDY

Of figure 7 the complete developed virtual instrument for mass measurements is presented. When all the components of the instrument are connected the program is started. Before the measurements start several seconds should be waited for the instrument to get the tare of the upper platform.

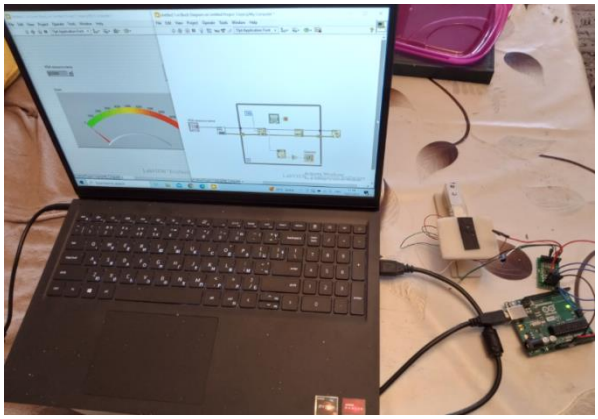

Fig. 7. Virtual instrument for mass measurement

With the developed virtual instrument two types of measurements were performed.

The first is repeatability test. With the virtual instrument fully prepared measurements with different standard masses were done. For every measurement 10 values were taken and mean value was calculated (fig.8). Tests were done in the range of 0.10 to 2 kg. The results are presented in table 1.

From the results it is seen that the error in the whole range is less than 1% and most of the measurements are less than 0.5%.

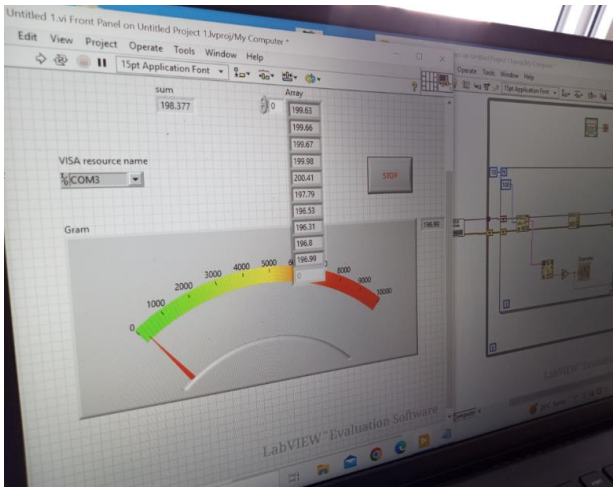

Fig. 8. virtual instrument fot mass measurements with calculation of the mean value of 10 measurement.

TABLE I. EXPERIMENTAL RESULTS FOR REPEATABILITY

Standart mass, kg	Measured mass, kg	Δ, g	δ, %
0.01	0.00996	0,04	0,4
0.02	0.019803	0,197	0,985
0.05	0.049956	0,044	0,088
0.10	0.099993	0,007	0,007
0.20	0.200109	-0,109	-0,0545
0.50	0.500005	-0,005	-0,001
1.00	0.998786	1,214	0,1214
2.00	1.99403	5,97	0,2985

The second type of tests is for reproducibility.

Before every measurement the virtual instrument is disassembled and assembled again. Then measurement with a standard mass is done. The results are presented in table 2

TABLE II. EXPERIMENTAL RESULTS FOR REPRODUCIBILITY

Standart mass, kg	Measured mass, kg	Δ, g	δ, %
0.01	0,008908	1,092	10,92
0.02	0,017715	2,285	11,425
0.05	0,049416	0,584	1,168
0.10	0,099181	0,819	0,819
0.20	0,195406	4,594	2,297
0.50	0,491339	8,661	1,7322
1.00	0,995705	4,295	0,4295
2.00	1,98881	11,19	0,5595

From the results it is seen that the max error almost 11.5%. The errors are bigger in the lower range. It can be seen that in the range of 0.05 to 2 kg the error is less than 2.5%.

IV. CONCLUSIONS

The developed virtual instrument for mass measurements gives satisfactory result in the range of 0.05 to 2 kg for both test – repeatability and reproducibility. In the range under the specified the error jump drastically in some cases up to 10 times. Thus it is recommended that this virtual instrument is used for mass measurement above 0.05 kg.

REFERENCES

[1] John G. Webster, “The Measurement, Instrumentation and Sensors Handbook”, 2018

[2] Yonatan Yordanov, Radoslav Deliyski, Bojidar Djujev, "APPLICATION OF ARTIFICIAL INTELLIGENCE IN ENGINEERING EDUCATION", Proceedings of International conference Challenges in Higher Education and Research in the 21st Century (CHER21), 2023, ISSN: 2683-0337, in print

[3] Програмиране в среда на ARDUINO. Ръководство.

[4] Yonatan Yordanov, Radoslav Deliyski, "DESIGN AND DEVELOPMENT OF A REMOTE CONTROL FOR A SMALL WATERCRAFT", Proceedings of International conference Challenges in Higher Education and Research in the 21st Century (CHER21), 2023, ISSN: 2683-0337, in print

[5] Richard Jennings, Fabiola De la Cueva, “LabVIEW Graphical Programming”, Fifth Edition, 2019

SECTION IV
MEASUREMENTS IN THE INDUSTRY

Reverse Engineering of a Part using 2D Images

1st Mihail Zagorski
TU-Sofia, FIT;
"AI and CAD systems Lab",
R&D&I Consortium, Sofia Tech Park
Sofia, Bulgaria
mihail.zagorski.tu@gmail.com

2nd Radoslav Miltchev
TU-Sofia, FIT;
"AI and CAD systems Lab",
R&D&I Consortium, Sofia Tech Park
Sofia, Bulgaria
rmiltchev@tu-sofia.bg

3rd Todor Gavrilov
TU-Sofia, FIT;
"3D Creativity and RP Lab",
R&D&I Consortium, Sofia Tech Park
Sofia, Bulgaria
todor.gavrilov@gmail.com

4th Nikolay Nikolov
TU-Sofia, FIT;
Dept. "Theory
of Mechanisms and Machines"
Sofia, Bulgaria
nickn@tu-sofia.bg

5th Yavor Sofronov
TU-Sofia, FIT;
"3D Creativity and RP Lab",
R&D&I Consortium, Sofia Tech Park
Sofia, Bulgaria
ysofronov@tu-sofia.bg

***Abstract*—The paper aims to investigate the process of reverse engineering of a part using 2D images. In this example, the geometry of a partially damaged functional part from a shift lever assembly is reconstructed and the element is reproduced using CAD software. Finally, the reconstructed part is 3D printed with a suitable polymer material.**

Keywords—reverse engineering, 3D modeling, reconstruction, 3D printing, rapid prototyping

I. Introduction

Reverse Engineering is a method for creating CAD models of physical parts, the designs of which are not available [1]. The reconstructed CAD model is then used for various purposes – creating new documentation, improving the geometry of the object [2], FEM analysis [3,4], reconstruction of a partially damaged part or one that is not commercially available [5], among others. The traditional approach for obtaining the part's geometry includes its initial 3D scanning with accurate metrology equipment (Coordinate Measuring Machines or precise 3D scanners), converting of the created point-cloud to a mesh and then applying modeling features on it in order to create a solid or a surface model of the element [6]. A diagram of the process is shown on Fig. 1 [7].

One of the main disadvantages of the usage of metrology equipment is its price. There are budget 3D scanners but with limited accuracy, geometry of the part, etc. [8].

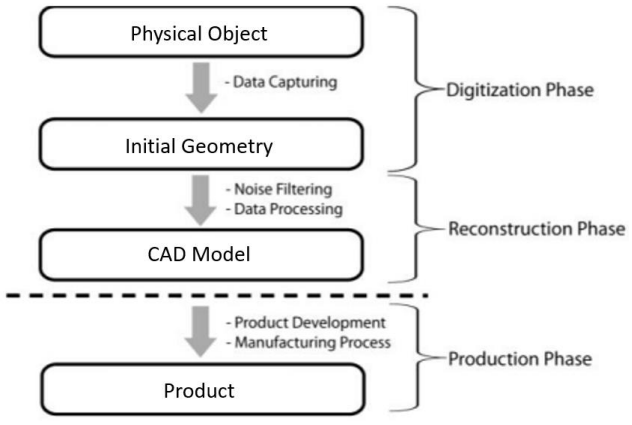

Fig. 1. Diagram of reverse engineering process.

Another option for reconstruction of objects with relatively simple geometry is using a 2D document scanner to obtain the contours of the element. However, this method also has its disadvantages, mainly the requirement for the part to be as flat as possible (for example an engine gasket).

A good alternative of the above described methods is to take several photos of the part and to use them as templates for remodeling in CAD software.

Furthermore, an important aspect of the reverse engineering process is the need for additional work in terms of optimization for the new manufacturing method [9]. Often the component or device needing to be restored is produced using a large-scale manufacturing method (for example casting, injection molding, stamping, etc. [10]). Thus, in case of reproducing the specific part, a different method for small-scale manufacturing should be used (for example milling, turning, 3D printing, etc.), further adding to the workload [11].

This article follows a methodology for the process of reverse engineering, optimization and production of a functional part using 2D camera images for the reconstruction of its geometry. Autodesk Fusion 360 is used as a CAD software for the purposes of the study.

II. Materials and Methods

The object of the study is a damaged functional part from a shift lever assembly for an outboard engine. The part is shown on Fig. 2.

Fig. 2. A damaged part from a shift lever assembly.

As seen on Fig. 2 one of the teeth of the object has been broken, making the part unusable. The missing tooth is thus reconstructed in a virtual model and the whole element is reproduced physically. The original component is produced using injection molding, following common practices for

designing injection-molded parts (drafts, uniform wall thickness, etc.). However, if these elements were reproduced in the 3D printed object too, the overall strength of the part would be weakened. This is the main reason why the process for the part's reconstruction does not only require reverse engineering, but also an optimization of the construction of the object. The whole process can be divided in six main steps. The methodology is shown on Fig. 3.

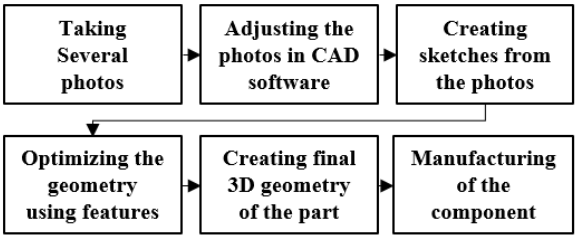

Fig. 3. A depiction of the process.

A. *Taking photographs*

The first step of the process is taking two photos on both sides of the flat surface (top and bottom view). The part should be centered relative to the camera center in order to avoid the perspective view as much as possible. The background should have a contrast color compared to the color of the component because it would be easier to remove automatically afterwards. The two photos used for the reverse engineering process are shown on Fig. 4 and Fig. 5.

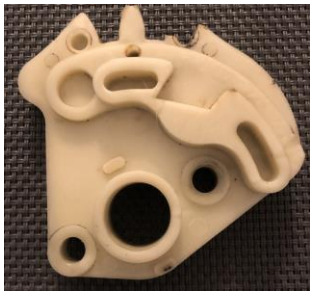

Fig. 4. A top view of the part.

Fig. 5 A bottom view of the part.

B. *Adjusting the images*

First, the background of the photos is removed in a photo editing software and then the images are inserted into the CAD software one by one. Each photo should be rotated and aligned to the two sides of a plane and it should be scaled to the exact dimensions of the real part. For this purpose the overall dimensions of the part are measured accurately with a caliper. The final step of the adjusting process for the bottom view is shown on Fig. 6.

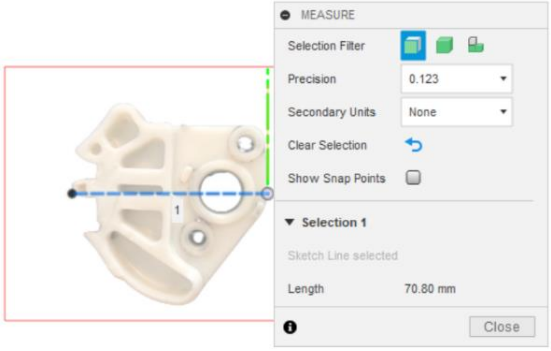

Fig. 6. Adjusting the bottom view image.

C. *Creating sketches*

The adjusted images are used as reference templates for creating 2D sketches, as shown on Fig. 7 and Fig. 8.

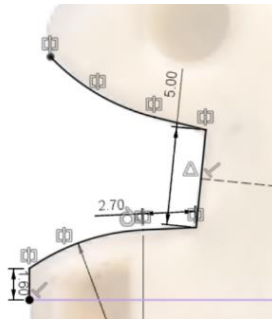

Fig. 7. Sketching the teeth of the part.

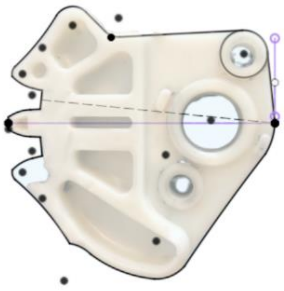

Fig. 8 A completed sketch of the outside contour of the part.

The process continues for the different geometry features which should be included and/or reconstructed in the 3D model – for example, the damaged tooth of the part is fully reconstructed based on the other two teeth. Fully-defined sketches should be created. Double-checking of certain dimensions with a caliper is highly recommended.

D. *Optimizing the geometry*

The geometry should be optimized for the manufacturing method which will be used for the production of the part. The chosen method for the current object is an additive manufacturing technology: Fused Deposition Modeling/Fused Filament Fabrication (FDM/FFF). Thus, the number of cavities and holes which are not related to the functionality of the part should be reduced for two main reasons:

- Producing a part with better mechanical properties;
- Reducing the number of support structures during 3D printing.

As a result of the optimization process, the technological cavities on the bottom of the part are removed in the 3D model, as shown on Fig. 9.

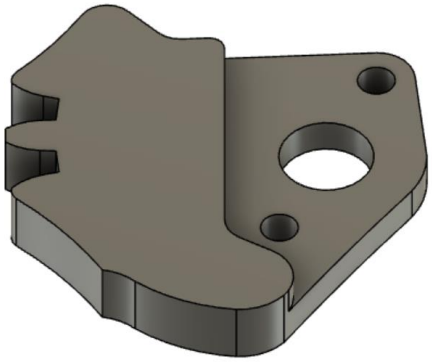

Fig. 9. Bottom view of the unfinished 3D model without cavities.

E. *Creating final geometry of the part*

The process of 3D modeling continues with adding more sketches from the contours of the images (Fig. 10). The completed sketches are used for adding (Fig. 11) or removing of material (Fig. 12) using the Extrude feature. Fillets are added for rounding of sharp edges (Fig. 13).

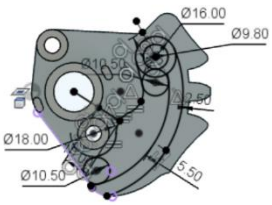

Fig. 10. Defining a sketch.

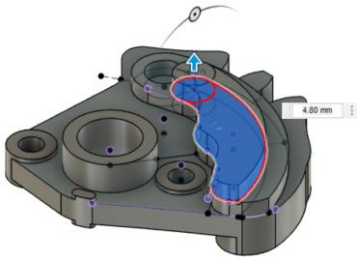

Fig. 11 Adding material.

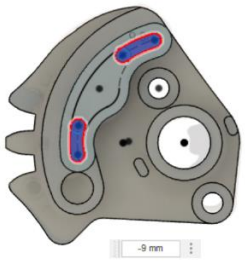

Fig. 12 Removing material.

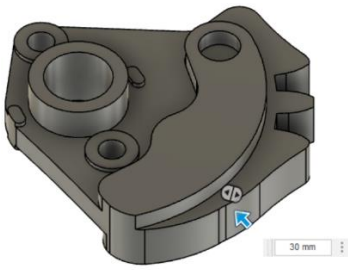

Fig. 13 Adding a fillet.

Some of the cavities on the top of the part are left on purpose because they would not affect the 3D printing process, neither the strength nor the functionality of the reconstructed object, but they would save some polymer material and printing time.

The final geometry of the object's 3D model is shown on Fig. 14 and Fig. 15.

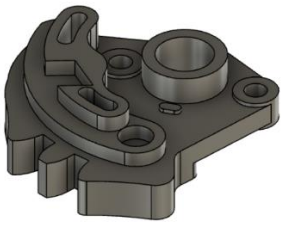

Fig. 14. 3D model of the part – isometry view from the top.

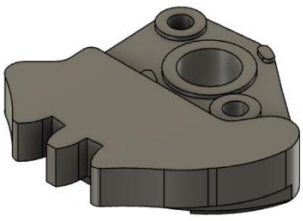

Fig. 15 3D model of the part – isometry view from the bottom.

After the 3D modeling process is finished the geometry is exported to high-density mesh in STL file format for the next step. A preview of the mesh with the export settings is shown on Fig. 16. The resulted mesh has 9902 elements (triangles) and its size is 484 KB.

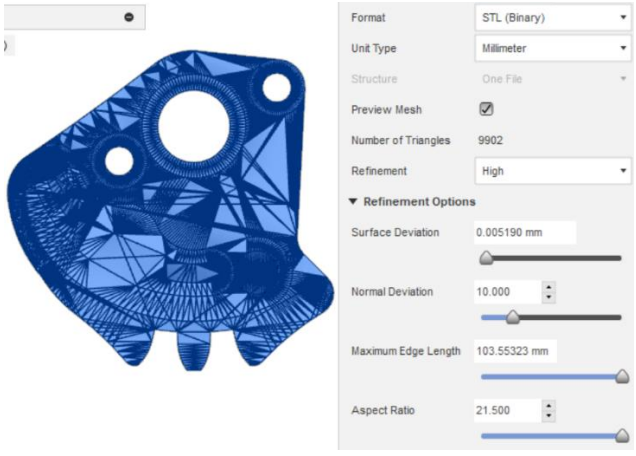

Fig. 16. A preview of the mesh and the export settings.

F. *Manufacturing*

The part is produced with FDM/FFF 3D printing technology. The selected material is PETG (polyethylene terephthalate glycol-modified) due to its high toughness [12]. The component is printed on a Creality Ender-2 Pro 3D printer. The model is sliced with PrusaSlicer software, as shown on Fig. 17.

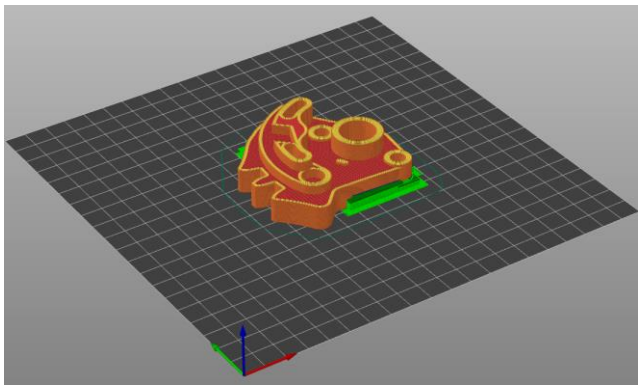

Fig. 17. Orientation of the part in PrusaSlicer.

The basic process parameters are presented in Table 1.

Table 1. Basic parameters of the 3D printing process.

Parameter	***Value***	***Unit***
Layer Height	0.2	mm
Initial Layer Height	0.3	mm
Line Width	0.4	mm
Number of Perimeters	4	-
Number of Top Layers	4	-
Number of Bottom Layers	4	-
Infill Density	80	%
Infill Pattern	Honeycomb	-
Build Plate Temperature	75	°C
Print Speed - Perimeters	30	mm/s
Print Speed - Infill	60	mm/s
Fan Speed	25	%
Retraction Length	5	mm
Retraction Speed	25	mm/s
Build Plate Adhesion Type	Skirt	-
Generate Support Material	Yes	-
Auto Generated Supports	Yes	-
Overhang Threshold	45	°
Estimated Printing Time	356	min
Used Filament	16.38	m

The selected infill pattern is honeycomb because it has the highest combined compression, tensile, and shear strength compared to other types of infill [13].

III. Results and Discussion

The 3D printed part is shown on Fig. 18 and Fig. 19.

Fig. 18. 3D printed part – top view.

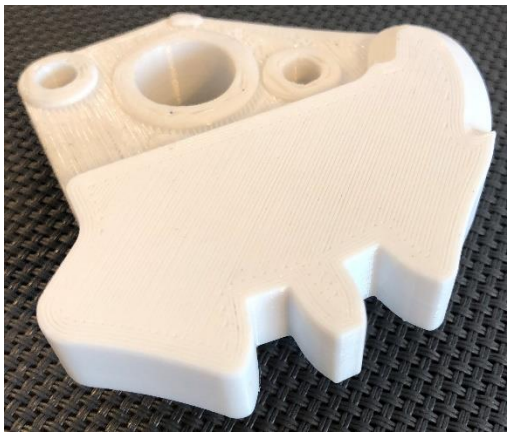

Fig. 19 3D printed part – bottom view.

The proposed methodology is executed step by step. The main advantage is that it allows the reconstruction of specific elements of complex systems which are subjected to intense wear (gears, bearings, bushings, etc.) or elements in which some constructive defects are revealed after prolonged exploitation (especially objects which work in conditions of cycle fatigue). This methodology creates a possibility to repair a larger system which lacks technical support, spare parts or the required documentation for restoring of the damaged components without the need of expensive metrology equipment.

The main disadvantage of the proposed methodology is that its implementation requires a lot of technical knowledge and highly qualified personnel with in-depth experience in the field of CAD software and 3D printing.

Further improvements of the proposed methodology could be made – for example by implementing Finite Element Analysis (CAE) for a more advanced optimization of the geometry of the part without decreasing its mechanical properties.

Acknowledgment

The authors would like to thank the Artificial Intelligence and CAD Systems Laboratory at Research & Development & Innovation Consortium at Sofia Tech Park for supporting of the presented research.

References

[1] K. P. Venuvinod and W. Ma, “Reverse Engineering and CAD Modeling”, Rapid Prototyping, pp. 75–134, Springer, 2004.

[2] K. Mohaghegh, M. Sadeghi, A. Abdullah and R. Boutorabi, “Improvement of reverse-engineered turbine blades using construction geometry”, The International Journal of Advanced Manufacturing Technology, vol. 49, pp. 675–687, November 2010.

[3] M. Endo, “Reverse engineering and CAE”, JSME International Journal Series C, vol. 48, pp. 218–223, June 2005.

[4] S. Sabev and P. Kasabov, “3D Modeling, Simulation and Analysis of Anti-vibration Boring Bar”, ENVIRONMENT. TECHNOLOGIES. RESOURCES. Proceedings of the International Scientific and Practical Conference, vol. 3, pp. 310-313, June 2021.

[5] E. Bagci, “Reverse engineering applications for recovery of broken or worn parts and re-manufacturing: Three case studies”, Advances in Engineering Software, vol. 40, pp. 407–418, June 2009.

[6] A. Hattab, I. Gonsher, D. Moreno and G.Taubin, “Differential 3D Scanning”, IEEE Computer Graphics and Applications, vol. 3. pp.. 43–51, May 2017.

[7] S. Rooppakhun, N. Chantarapanich and K. Sitthiseripratip, “Advanced Medical Imaging and Reverse Engineering Technologies in Craniometric Study”, Forensic Medicine - From Old Problems to New Challenges, September 2011.

[8] A.-B. M. Ebrahim, “3D Laser Scanners' Techniques Overview”, International Journal of Science and Research (IJSR), vol. 4, pp. 323–331, October 2015.

[9] K. Kamberov., B. Zlatev and T. Todorov, “Design development of a car fan shroud based on virtual prototypes”, LNICST 2019, vol. 283, pp. 309 – 317, September 2019.

[10] A. Wilson, “Large-Scale Manufacturing, Standardization, and Trade”, The Oxford Handbook of Engineering and Technology in the Classical World, Oxford University Press , 2008.

[11] J. Salobir, J. Duhovnik and J. Tavcar, “Methods and Principles of Product Design for Small-Scale Production Based on 3D Printing”, Proceedings of the Design Society: International Conference on Engineering Design 2019, vol. 1, pp. 789–798, July 2019.

[12] K. Szykiedans, W. Credo and D. Osiński, “Selected Mechanical Properties of PETG 3-D Prints”, Procedia Engineering, vol. 177. pp. 455–461, December 2017.

[13] M. Fernandez-Vicente, W. Calle, S. Ferrándiz and A. Conejero, “Effect of Infill Parameters on Tensile Mechanical Behavior in Desktop 3D Printing”, 3D Printing and Additive Manufacturing, vol. 3, pp. 183–192, September 2016.

Determination of the Penetration Depth of Laser Marking of Glass Fiber Reinforced Polymers

Ivan Mitev
dep. " Economics"
Technical university-Gabrovo
Gabrovo, Bulgaria
imitev@tugab.bg

Simeon Tsenkulovski
dep. "Mechanical Engineering and Instrumentation"
Technical university-Gabrovo
Gabrovo, Bulgaria
s.tsenkulovski@advanced-technology.eu

Georgi Karlovski
dep. "Mechanical Engineering and Instrumentation"
Technical university-Gabrovo
Gabrovo, Bulgaria
g_karlovski@abv.bg

Abstract – **Due to the need for identification of industrial products, laser marking has been increasingly used in recent years. It is the preferred method for achieving permanent and contrasting surface markings on both metals and a wide variety of non-metallic materials. In the present study, the change in the energy parameters of a laser installation based on Fiber lazer - RFFL-P-502B was tracked.on the penetration depth when marking layered composites based on epoxy resins. Graphical and tabular results are presented of marking with V=50mm/s; f = 50Hz and P = 5÷50W.**

Keywords — non-metallic materials, laser marking, depth of penetration

I. INTRODUCTION

When ensuring the security and efficiency of production processes in order to prevent trade in counterfeit goods, it is imperative to create opportunities in production for the complete identification and tracking of products that leave the company's territory by placing legible and permanent markings [1]. This is particularly important in some industrial sectors (space, aviation, automotive, medical, etc.) where products must meet specific requirements and standards. As a result, product identification must be of the highest quality to ensure traceability, safety and reliable operation. In recent years, emphasis has been placed on product identification through permanent marking without inks or adhesives. Barcode printing and direct marking of parts can be done by a variety of manufacturing processes, such as: punching, micro-dot, writing or electro-pencil. However, laser marking applications are becoming the norm for most manufacturing areas as they offer several advantages, such as [2÷5]:

- contactless work;
- high repeatability;
- high scanning speed;
- width of the marking;
- comparable to the size of the laser spot;
- high flexibility;
- high automation of the process, etc.

Due to the need for identification in the industries described above, laser marking has been increasingly used in recent years [6].

It is the preferred method for achieving permanent and high-contrast surface inscriptions, both on metal [3,4,7,8] and on a wide variety of non-metallic materials ranging from glass [9], ceramics [10÷13], organic materials [14÷19], textiles [20,21], etc. The quality of the resulting marking depends on many factors [3]:

- geometry of the marking;
- expansion of the heat-affected zone;
- presence of microcracks;
- durability under harsh working conditions;
- readability, etc

From the literature [22÷26] it can be seen that the main technological parameters affecting laser marking are:

- average power;
- scanning speed (ie marking speed);
- pulse frequency, etc.

In the present study, the influence of the output power of the laser installation on the depth of the marking obtained on samples of glass fiber reinforced polymers was traced.

II. MATERIALS AND METHODS OF RESEARCH

Reinforced polymer materials "Epoxy glass cloth laminated sheets" with mechanical characteristics according to Standard for test: GB/T 1303.1-1998 - table 1 were tested.

TABLE 1. MECHANICAL CHARACTERISTICS

№	Items	Unit	Standard	Test Value (Average value)
1.	Flexural Strength Perpendicular to Laminations	MPa	≥ 340	353
2.	Dielectric Strength Perpendicular to Laminations in 90ºC Transformer Oil	kV/m	≥ 11.8	15.5
3.	Breakdown Voltage Parallel to laminations in 90ºC Transformer Oil	kV	≥ 35	36,4
4.	Impact Strength	kJ/m^2	≥ 33	48
5.	Permittivity (1MHz)	-	≤ 5.5	4.8
6.	Dissipation Factor (1MHz)	-	≤ 0.04	0.02
7.	Insulation Resistance Immersion in Water (D – 24/23)	Ω	$\geq 5{,}0x10^8$	$7{,}0x10^8$
8.	Water Absorption (D – 24/23)	mg	≤20	11
9.	Density	g/cm^3	1.70÷1.90	1.85

The marking of the samples was done with the help of a laser installation - fig.1, developed on the territory of the Adtech company, based on Fiber lazer - RFFL-P-502B.

Its main technological characteristics are presented in table 2.

Measurement of the depth of the mark was carried out on a measuring microscope - fig.2, using Insize ISD-V150/V250/V300 software.

978-1-6654-8569-2/22/$31.00 ©2022 IEEE

Fig. 1. General appearance of Fiber lazer - RFL - P – 502B

TABLE 2. CHARACTERISTICS OF THE LASER INSTALLATION

№	Items	Unit	Standard Value	Variation Step
1.	Output Power	w	5÷50	5
2.	Frequency	kHz	50÷100	0,001
3.	Marking Speed	mm/s	1÷2000	1
4.	Defocusing	+/- from the focal length, mm		1
5.	Focal spot	µm	37÷42	1

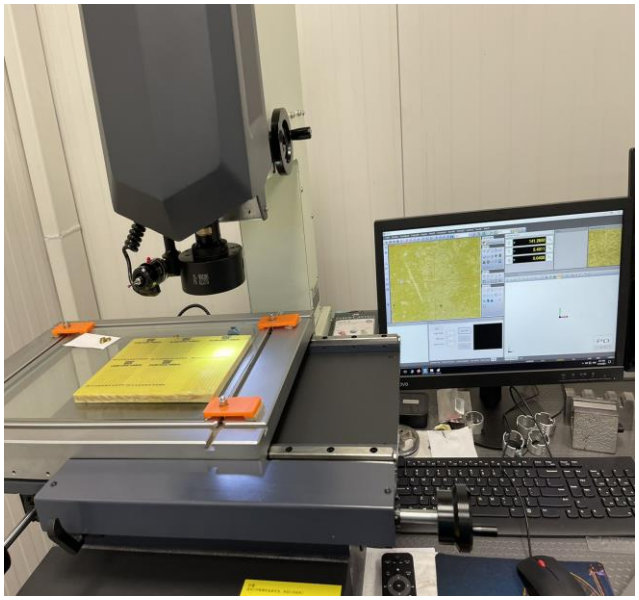

Fig.2. General view of measuring microscope "INSIZE"

Penetration depth was determined by zeroing the Z-axis values of the mark surface and accounting for changes in focus at the bottom of the marked channel. The distance between individual points spaced 10 mm apart is determined by moving the measuring line along the X axis

III. EXPERIMENTAL PART

Specimens of epoxy polymer materials reinforced with glass fibers are marked using the apparatus of Fig. 1,

The power values vary in the range 5÷50 kW, the marking speed is 50mm/s with a focal spot diameter of 40µm and a pulse purity of 50kHz – fig.3.

Fig. 3. General view of the marked samples

The depth of penetration of the laser beam was measured in 5 control points for each investigated power, located along the marked line at a distance of 10 mm. Part of the measurements are presented in Fig.4, and all experimental results are presented in Table 3.

TABLE 3. EXPERIMENTAL DATA

№	P, W	δ, µm						
		p.1	p.2	p.3	p.4	p.5	$p_1 \div p_5 / 5$	δ_{max}, µm
1	2	3	4	5	6	7	8	9
1	5	150	135	205	155	120	153	160
2	10	280	305	300	310	280	295	320
3	15	456	466	485	495	454	471	480
4	20	645	645	595	630	573	618	640
5	25	450	735	765	785	770	701	800
6	30	705	855	720	790	840	782	960
7	35	870	800	850	890	800	842	1120
8	40	745	960	900	1020	890	903	1280
9	45	955	1035	965	980	1045	996	1440
10	50	990	1060	1180	1140	1185	1111	1600

From the photos in Fig.4, it can be seen that the profile of the channel is not uniform along the length of the marking. This is also proven by the experimental results in Table 3,

where the values for δ vary in relatively wide intervals. At an output power of laser radiation up to 20W, the measured values range from 20 to 80μm. When increasing the output power from 20 to 50W, the fluctuations of the experimental results reach limits of 100÷300μm. This is a result of the different vaporization temperature of the reinforcing and matrix phases making up the polymer composite.

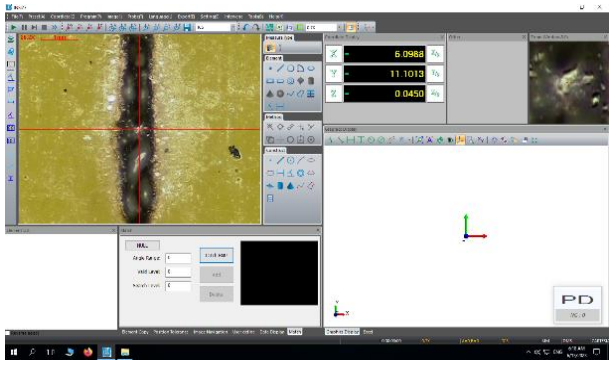

a.

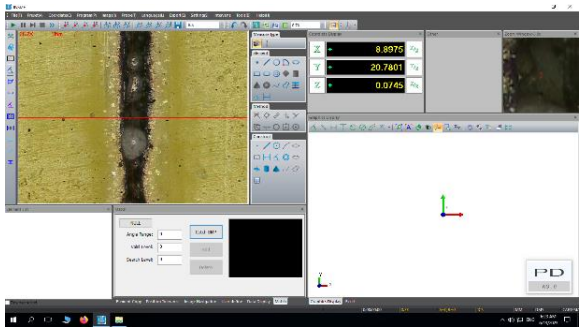

b.

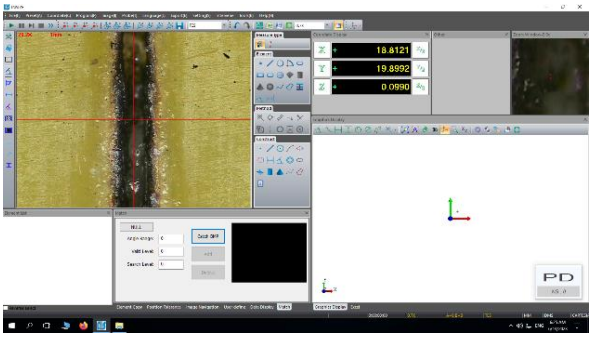

c.

Fig.4. Experimental results at V=50mm/s; f= 50Hz and

a - 25W; b - 40W; c - 50W.

The graphical interpretation of the results of Table 3 is shown in Fig. 4.

Theoretically, for single-component non-metallic materials, the maximum penetration depth of the laser beam – δmax, can be calculated with the expression 1 [27]

$$\delta_{max} = 2P / (\pi.r.\rho.\upsilon\ .\ c.T) \qquad (1)$$

where: P – laser radiation power, W;
r - focal spot radius, μm;
ρ – material density, g/cm3;
υ – marking speed, mm/s;
c – heat capacity of the material, J/kg.ºC;
T – evaporation temperature, ºC.

Using the data from tables 1 and 2, as well as reference data [28], the maximum theoretical values of the penetration depth during laser marking of the studied materials were calculated. (column 9 of Table 3)

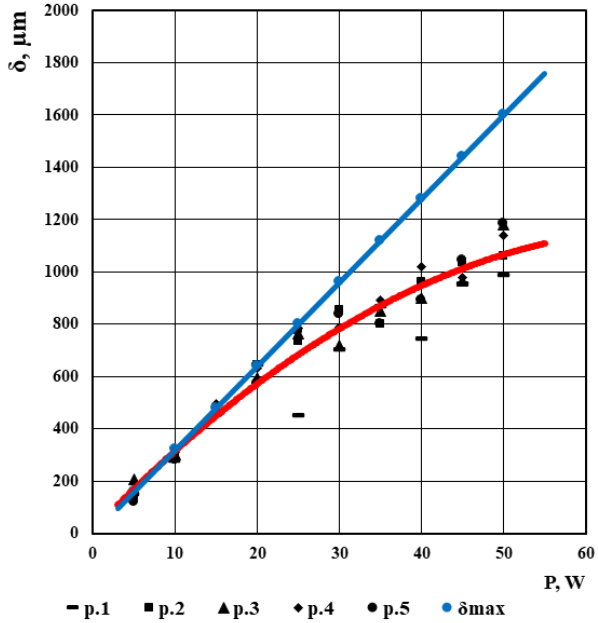

Fig.4. Penetration depth of the mark at P = 5÷50W , V = 50 mm/s, f= 50Hz.

Comparing the theoretical and experimental results, it can be seen that, according to formula 1, the penetration depth is linearly dependent on the power of the laser radiation. The obtained experimental results show that this is valid only for small marking powers – up to 20W. In them, the experimental results differ from the theoretical ones by less than 10% (table 4)

TABLE 4. EXPERIMENTAL DATA

№	P, W	(Σp1÷p5 / 5) .100/ δmax, %	№	P, W	(Σp1÷p5 / 5) .100/ δmax, %
1	5	4,375	6	30	18,542
2	10	7,819	7	35	26,607
3	15	1,875	8	40	29,453
4	20	3,438	9	45	30,833
5	25	12,375	10	50	30,563

As the power increases above 20W, the marking depth decreases by 20÷30% compared to the theoretical one. This can be explained both by the difference in the evaporation temperature of the matrix and reinforcing phase, and by the increase in power losses due to the absorption of the emitted particles by the aerosol separated in the treated area.

IV. CONCLUSIONS

The following more important conclusions can be drawn from the research conducted and the results obtained:

- Research has been conducted on the change in the depth of laser marking in layer-reinforced composite materials based on epoxy resin.
- It was found that as the output power of the laser beam increased from 5 to 50W at a constant marking speed of 50mm/s and a frequency of 50Hz, the average marking depth increased from 153 to 1111μm.
- It has been proven that, as a result of the different thermophysical characteristics of the matrix and the reinforcing phase in the composite, the measured values vary within relatively wide limits, with an output power of up to 20W, they are up to 100μm, and when the power increases to 50W, they vary between 100÷300μm.
- It has been proven that, unlike single-component non-metallic materials, in layered reinforced composites, the depth of the marked layer does not change in direct proportion to the power. At powers up to 20W, the dependence is directly proportional, but as the output power increases up to 50W, it changes along a parabolic curve. This is a result of the loss of power due to the absorption of some of the radiation in the aerosols released during tagging.

This work was supported by the European Regional Development Fund within the OP "Science and Education for Smart Growth 2014 - 2020", Project CoC "Smart Mechatronic, Eco- and Energy-saving Systems and Technologies", No BG05M2OP001-1.002-0023

REFERENCES

[1] Amara EH, Haïd F, Noukaz A. Experimental investigations on fiber laser color marking of steels. Appl Surf Sci 2015;351:1–12. doi:10.1016/j.apsusc.2015.05.095.

[2] Ready JF, et al. LIA handbook of laser materials processing. New York: Springer Verlag; 2001.

[3] Leone C, Genna S, Caprino G, De Iorio I. AISI 304 stainless steel marking by a Qswitched diode pumped Nd:YAG laser. J Mater Process Technol 2010;210(10):1297– 303. doi:10.1016/j.jmatprotec.2010.03.018.

[4] Astarita A, Genna S, Leone C, Memola Capece Minutolo F, Squillace A, Velotti C. Study of the laser marking process of cold sprayed titanium coatings on aluminium substrates. Opt Laser Technol 2016;83:168–76. doi:10.1016/j.optlastec.2016.04.007

[5] Li J, Lu C, Wang A, Wu Y, Ma Z, Fang X, Tao L. Experimental investigation and mathematical modeling of laser marking two-dimensional barcodes on surfaces of aluminum alloy. J Manuf Process2016;21:141–52. doi:10.1016/j.jmapro.2015.12.007.

[6] Niemenski G. Challenges for the laser job shop. Industrial Laser Solutions; 2014. p. 31–4. January/February.

[7] Wlodarczyk KL, Ardron M, Waddie AJ, Dunn A, Kidd MD, Weston NJ, Hand DP. Laser microsculpting for the generation of robust diffractive security markings on the surface of metals. J Mater Process Technol 2015;222:206–18. doi:10.1016/j. matprotec.2015.03.001.

[8] Wlodarczyk KL, Ardron M, Waddie AJ, Taghizadeh MohammadR, Weston NJ, Hand DP. Tamper-proof markings for the identification and traceability of high-value metal goods. Opt Express 2017;25(13):15216–30. doi:10.1364/OE.25.015216.

[9] Dumont Th, Lippert T, Wokaun A, Leyvraz P. Laser writing of 2D data matrices in glass. Thin Solid Films 2004;453-454:42–5. doi:10.1016/j.tsf.2003.11.148.

[10] Penide J, Quintero F, Riveiro A, Fernández A, del Val J, Comesana R, Lusquinos F, Pou J. High contrast laser marking of alumina. Appl Surf Sci 2015;336:118–28. doi:10.1016/j.apsusc.2014.10.004.

[11] Peter J, Doloi B, Bhattacharyya B. Parametric analysis of Nd: YAG laser marking on ceramics. Int J Manuf Tech Manage 2011;24(1-4):124–38. doi:10.1504/IJMTM.2011.046764

[12] Leone C, Genna S, Tagliaferri F, Palumbo B, Dix M. Experimental investigation on laser milling of aluminium oxide using a 30W Q-switched Yb:YAG fiber laser. Opt Laser Technol 2016;76:127–37. doi:10.1016/j.optlastec.2015.08.005.

[13] Park YW, Kim T, Rhee S. Development of a monitoring system for quality prediction in laser marking using fuzzy theory. J Laser Appl 2007;19(1):55–63. doi:10.2351/1.2402519.

[14] Petutschnigg A, Stöckler M, Steinwendner F, Schnepps J, Gütler H, Blinzer J, Holzer H, Schnabel T. Laser treatment of wood surfaces for ski cores: an experimental parameter study. Adv Mater Sci Eng 2013 art. N°123085. doi:10.1155/2013/123085.

[15] Leone C, Lopresto V, De Iorio I. Wood engraving by Q-switched diodepumped frequency-doubled Nd:YAG green laser. Opt Lasers Eng 2009;47(1):161–8. doi:10.1016/j. optlaseng.2008.06.019.

[16] Zelenska KS, Zelensky SE, Poperenko LV, Kanev K, Mizeikis V, Gnatyuk VA. Opt Laser Technol 2016;76:96–100. doi:10.1016/j.optlastec.2015.07.011.

[17] Shin Y, Kim Y, Park S, Jung B, Lee J, Nelson JS. Pit and rim formation during laser marking of acrylonitrile butadiene styrene plastic. J Laser Appl 2005;17(4):243–6. doi:10.2351/1.2080405

[18] Genna S, Leone C, Lopresto V, Tagliaferri V. An experimental study on the surface mechanisms formation during the laser milling of PMMA. Polym Compos 2015;36(6):1063–71. doi:10.1002/pc.23442.

[19] Chen MF, Hsiao WT, Huang WL, Hu CW, Chen YP. Laser coding on the eggshell using pulsed-laser marking system. J Mater Process Technol 2009;209:737–44. doi:10.1016/j.jmatprotec.2008.02.075.

[20] Stoyanov B., Kr. Drumev, D. Genov, "Fashion design using laser engraving technology", Journal of the Technical university of Gabrovo, Vol.52'2016, page 53-57, ISSN 1310-6686

[21] Stoyanov B., Kr. Drumev, D. Genov, "Microscope analysis of laser treated cotton fabrics", Journal of the Technical university of Gabrovo, Vol.52'2016, page 58-60, ISSN 1310-6686

[22] Li XS, He WP, Lei L, Wang J, Guo GF, Zhang TY, Yue T. Laser direct marking applied to rasterizing miniature Data Matrix Code on aluminum alloy. Opt Laser Technol 2016;77:31–9. doi:10.1016/j.optlastec.2015.08.020.

[23] Mitev, I., Unconventional electrotechnological processes, EKS-PRESS, Gabrovo, 2020, ISBN 978-954-490-698-7

[24] Ready JF, et al. LIA handbook of laser materials processing, New York: Springer Verlag; 2001. ISBN:0912035153.

[25] Han A, Gubencu D. Analysis of the laser marking technologies. Nonconventional Technol. Rev. 2008;4:17–22.

[26] Tuz L. Quality of marks on metals made with the use of the Nd:YAG laser engraving method. Metall Foundry Eng. 2013;39(1):55–64. doi:10.7494/mafe.2013.39.1.55.

[27] Grigoryanets, A., Fundamentals of laser processing of materials, Mechanical Engineering, Moscow, 1999, ISBN 5-217-00432-0

[28] Sendov, S., Heat and Mass Transfer, Technica, Sofia, 1993, ISBN 954-03-0127-0

Selection of coolant and cutting based on statistical measurements when working with quick-change holders

Georgi Karlovski
dept. Mechanical engineering and technology
Technical University of Gabrovo
Gabrovo, Bulgaria
g_karlovski@abv.bg

Kalin Krumov
dept. Mechanical engineering and technology
Technical University of Gabrovo
Gabrovo, Bulgaria
kalin_krasimirov_krumov@abv.bg

Irina Aleksandrova
dept. Mechanical engineering and technology
Technical University of Gabrovo
Gabrovo, Bulgaria
irina@tugab.bg

***Abstract*— The article presents the results of a study of the accuracy of machined surfaces of 42CrMoS4 hardened steel workpieces by turning using a quick-change holder on a Swiss-type CNC lathe, model GOODWAY SW-20. Experiments were conducted using different coolants and cutting speeds. A statistical analysis of the accuracy of the machined surfaces was performed using the "large sample" method. It has been shown that the choice of lubricant-coolant and cutting speed determines the magnitude of the variance of the controlled dimensions, i.e. has a significant impact on the stability of the technological process..**

Keywords*— coolant, cutting speed, hardened steel, quick-change holder, statistical analysis.

I. INTRODUCTION

In modern engineering, it is of particular importance to ensure, on the one hand, the exact dimensions of the machined surfaces and the maintenance of the correct geometric shape of the manufactured parts, and on the other hand, high productivity and flexibility of the technological processes. This is achieved by using CNC machines and tooling (a complex of cutting and auxiliary tools), which ensures a reduction in the loss of time for establishing and changing cutting tools, as well as by choosing optimal working conditions (elements of the cutting mode, type, pressure and method of introducing the lubricating-cooling liquid, etc.).

When machining on CNC lathes, both standard and quick-change holders of various designs are used [6,8]. A number of studies of the quality, technological and technical-economic parameters of the turning process are known, as a result of which the influence of both the working conditions and the used cutting tools was determined, modeled and analyzed [1,4,7,9]. The conducted comparative experimental studies of the roughness of the machined surfaces and the durability of cutting tools when turning 42CrMoS4 alloy steel using a standard holder and an original design quick-change holder and their statistical analysis, reflected in [2], prove the effectiveness of applying the quick-change holder . It has been found that its use leads to an increase in productivity as a result of a reduction in auxiliary time, while guaranteeing a high and stable quality of the treated surfaces. The conducted statistical test of the parametric hypotheses of equality of mathematical expectations and variances proves that comparable values of the average roughness of the processed surfaces are obtained when using a standard and quick-change holder, but when using the quick-change holder the dispersion of roughness is less, respectively the stability of the technological process is greater, the durability of the tools is greater, the time to replace worn metal-ceramic carbide inserts is much less, as well as the time to set up the equipment (approximately 40 times). However, the possibilities of increasing the accuracy of the treated surfaces when turning using quick-change holders by choosing working conditions - cooling medium and elements of the cutting mode - have not been evaluated.

The purpose of the present study is to determine and statistically analyze the accuracy of machined surfaces of hardened steel 42CrMoS4 workpieces using a quick-change holder, different cooling media and cutting speeds.

II. EXPERIMENTAL STUDIES AND STATISTICAL ANALYSIS OF ACCURACY

In the research process, details (Fig. 1) of alloyed steel 42CrMoS4 (1.7227 [5]) with a hardness of 33-35 HRC were processed.

The research was carried out on a CNC lathe (Swiss type), model GOODWAY SW-20, whose magazine is loaded with turning knives with quick-change holders `(Fig. 2).

The statistical analysis of the accuracy was made based on the measurement of the controlled dimensions - diameter D=11.8±0.2 mm and length L=11.6±0.2 mm - (fig. 1a) on lots of 3300 parts..

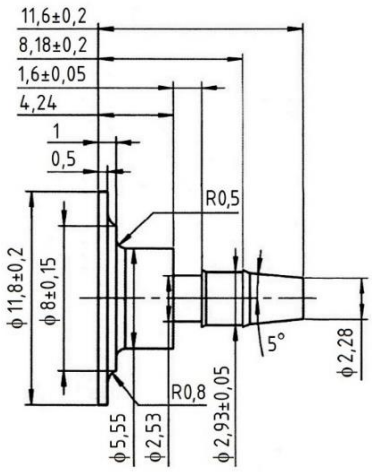

a.

b.

Fig.1. Processed details: a – structural drawing; b - details after turning

a.

b

Fig.2. Work area of GOODWAY SW-20 lathe (a) and tool shop with used turning knives with quick-change holders (b)

Two series of experimental studies were carried out - to study the influence of the type of lubricating-cooling fluids (LUFs) on accuracy and to study the influence of cutting speed. Cutting tools with replaceable metal-ceramic hard alloy plates VCMT 110302 (designation is according to ISO 1832) were used, ensuring a constant geometry of the tools: front angle, back angle, main setting angle, auxiliary setting angle, radius at the tip of the tool mm.

In order to determine the influence of the cooling medium on the accuracy of the processed parts, two lubricating coolant brands were used in the processing process - ECOCOOL MACH 40 and Vasco 6000, the technological characteristics of which are presented in [11,12]. The details of the batches were processed in constant cutting mode: cutting speed Vc = 150 m/min; feed f = 0.05 mm/rev; cutting depth ap = 0.02 mm. These values of Vc, f and ap correspond to those recommended in the literature and provide the tool life requirements, productivity and quality of the processed surfaces of this type of steels during turning [10].

The obtained experimental results for the controlled dimensions using two types of lubricating coolantare presented in table 1, and their graphical interpretation - in fig. 3 and fig. 4.

Comparing the obtained values for the controlled disturbances in table 1, it is found that when using VASCO 6000 coolant, the deviations from the set tolerances are more in number. This necessitates a change in operating modes and a reduction in cutting speed. In this regard, when applying this lubricating coolant, experimental studies were carried out at two cutting speeds - Vc = 150 m/min and Vc = 125 m/min, while the values of the cutting depth and feed were constant - ap = 0.02 mm and f = 0.05 mm/rev. The experimental results are presented in Table 2 and Fig. 5.

In order to compare the results for the accuracy of the controlled dimensions when using two types of lubricating coolant (table 1) and at two different cutting speeds (table 2), a statistical analysis was carried out, which included the verification of two statistical hypotheses - for the equality of the variances of two random variables and for equality of mathematical expectations of two random variables.

The verification of the statistical hypotheses was carried out in accordance with the methodology presented in [3], in the following sequence:

1. The arithmetic mean values of the controlled dimensions were determined when using lubricating coolant, brands ECOCOOL MACH 40 and Vasco 6000 (respectively and ; and) and at cutting speeds Vc = 150 m/min and Vc = 125 m/min and application of lubricating coolant Vasco 6000 (respectively and ; and) (table 3).

2. The statistical estimates of the variances of the dimensions D and L of the treated surfaces for each experiment were determined - S_{D1}^2 , S_{D2}^2 , S_{D3}^2 , S_{L1}^2 , S_{L2}^2 and S_{L3}^2 (table 3).

3. The hypothesis of equality of the variances of the controlled dimensions D and L was verified using the Fisher criterion, the empirical values of which were determined in accordance with the dependencies:

- when using two lubricating coolant:

$$\hat{F}_{D_{1-2}} = \frac{S_{D1}^2}{S_{D2}^2} = 0.397 ; \hat{F}_{L_{1-2}} = \frac{S_{L1}^2}{S_{L2}^2} = 0.889 ;$$

- when machining with different cutting speeds:

$$\hat{F}_{D_{2-3}} = \frac{S_{D2}^2}{S_{D3}^2} = 0.994 ; \hat{F}_{L_{2-3}} = \frac{S_{L2}^2}{S_{L3}^2} = 1.067 .$$

After comparing the determined empirical values of the Fisher criterion with the Fisher quantile $F_{\alpha=0.05,k_1=33,k_2=33} = 1.51$ [3] it has been established that $\hat{F} < F_{\alpha,k_1,k_2=33}$, that is, the dispersions of the diameter and linear size when using lubricating coolant ECOCOOL MACH 40 are smaller than when applying lubricating coolant VASCO 6000. Reducing the cutting speed when using lubricating coolant VASCO 6000 does not lead to a

reduction of the deviations from the set nominal values of the controlled dimensions.

4. The hypothesis of equality of mathematical expectations of the controlled dimensions was verified when using lubricating coolant, brands ECOCOOL MACH 40 and Vasco 6000 and at cutting speeds Vc = 150 m/min and Vc = 125 m/min and application of lubricating coolant Vasco 6000. To test the hypothesis, the Student's criterion was used, the empirical values of which were determined in accordance with the dependencies:

- when using two lubricating coolant:

$$\hat{t}_{D_{1-2}} = \frac{\left|\overline{D}_1 - \overline{D}_2\right|}{s_{D_{1-2}}} \cdot \sqrt{\frac{n_1 n_2}{n_1 + n_2}} = 0{,}4688 ;$$

$$\hat{t}_{L_{1-2}} = \frac{\left|\overline{L}_1 - \overline{L}_2\right|}{s_{L_{1-2}}} \cdot \sqrt{\frac{n_1 n_2}{n_1 + n_2}} = 2.975 ;$$

- when machining with different cutting speeds:

$$\hat{t}_{D_{2-3}} = \frac{\left|\overline{D}_2 - \overline{D}_3\right|}{s_{D_{2-3}}} \cdot \sqrt{\frac{n_1 n_2}{n_1 + n_2}} = 0.069 ;$$

$$\hat{t}_{L_{2-3}} = \frac{\left|\overline{L}_2 - \overline{L}_3\right|}{s_{L_{2-3}}} \cdot \sqrt{\frac{n_1 n_2}{n_1 + n_2}} = 0.1487 ,$$

where: $S_{D_{1-2}}, S_{L_{1-2}}, S_{D_{2-3}}, S_{L_{2-3}}$ - pooled estimates of the variances of the general populations in the conducted experiments (table 3); $n_1 = n_2 = n$.

After comparing the empirical values of Student's criterion with Student's quantile $t_{\alpha,k} = 1{,}999$ [3] ($\alpha = 0{,}05$; $k = n_1 + n_2 - 2$) it was found that the mean values of the controlled size *D*=11,8±0,2 mm do not differ when processed with lubricating coolant, brands ECOCOOL MACH 40 and Vasco 6000 ($\hat{t}_{D_{1-2}} < t_{\alpha,k}$). The values of the controlled dimensions do not differ significantly *D*=11,8±0,2 mm и *L*=11,6±0,2 mm, obtained by processing with speeds *Vc* = 150 m/min и *Vc* = 125 m/min and application of lubricating coolant Vasco 6000 ($\hat{t}_{D_{2-3}} < t_{\alpha,k}$; $\hat{t}_{L_{2-3}} < t_{\alpha,k}$). Significant difference in linear size means *L*=11,6±0,2 mm is observed when processing with lubricating coolant, marks ECOCOOL MACH 40 и Vasco 6000 ($\hat{t}_{L_{1-2}} > t_{\alpha,k}$).

TABLE 1. EXPERIMENTAL RESULTS IN TURNING USING LUBRICANT-COOLANT LIQUIDS, BRANDS ECOCOOL MACH 40 И VASCO 6000

Details, no.	ECOCOOL MACH 40		VASCO 6000	
	Diameter D_1, mm	length L_1, mm	Diameter D_2, mm	length L_2, mm
1	11,58	11,36	12,11	11,36
10	11,62	11,41	11,89	11,41
20	11,68	11,43	11,85	11,41
100	11,66	11,42	11,68	11,65
300	11,71	11,44	11,87	11,58
500	11,70	11,42	11,80	11,53
600	11,72	11,46	11,72	11,71
700	11,71	11,45	11,58	11,65
800	11,75	11,43	11,61	11,71
900	11,74	11,45	11,66	11,67
1000	11,81	11,47	11,65	11,47
1100	11,76	11,51	11,68	11,51
1200	11,78	11,53	11,81	11,71
1300	11,80	11,51	11,80	11,66
1400	11,78	11,54	11,72	11,60
1500	11,79	11,55	11,68	11,55
1600	11,83	11,56	11,75	11,45
1700	11,81	11,57	11,84	11,59
1800	11,87	11,53	11,85	11,53
1900	11,88	11,58	11,97	11,71
2000	11,85	11,60	11,85	11,67
2100	11,89	11,61	11,86	11,61
2200	11,86	11,59	11,88	11,59
2300	11,85	11,59	11,87	11,55
2400	11,89	11,62	11,23	11,62
2500	11,86	11,63	11,85	11,69
2600	11,91	11,64	11,96	11,61
2700	11,88	11,61	11,96	11,76
2800	11,87	11,70	11,94	11,65
2900	11,93	11,76	11,95	11,76
3000	11,90	11,81	11,90	11,82
3100	11,88	11,42	11,98	11,49
3200	11,91	11,44	12,01	11,66
3300	12,20	11,41	11,35	11,79

The statistical analysis carried out shows:

- In the experiments carried out with lubricating coolant, marks ECOCOOL MACH 40 and Vasco 6000, comparable average values are obtained for the dimension D=11.8±0.2 mm. Regarding the linear dimension L=11.6±0.2 mm, however, there is a significant difference in the measured average values, that is, there is a significant influence of the type of lubricating coolant on accuracy. The variances of the controlled dimensions D and L when turning using ECOCOOL MACH 40 are smaller than when applying Vasco 6000. This is evidence of greater stability of the technological process when using ECOCOOL MACH 40 and is a prerequisite for obtaining higher quality of processed surfaces.

TABLE 2. EXPERIMENTAL TURNING RESULTS USING LUBRICANT-COOLANT, VASCO BRAND 6000 AND TWO CUTTING SPEEDS

Details, no.	*Vc* = 150 m/min		*Vc* = 125 m/min	
	Diameter D_2, mm	length L_2, mm	Diameter D_3, mm	length L_3, mm
1	12,11	11,36	12,15	11,36
10	11,89	11,41	11,89	11,41
20	11,85	11,41	11,85	11,41
100	11,68	11,65	11,68	11,65
300	11,87	11,58	11,87	11,58
500	11,80	11,53	11,8	11,53
600	11,72	11,71	11,72	11,71
700	11,58	11,65	11,63	11,65
800	11,61	11,71	11,61	11,71
900	11,66	11,67	11,66	11,67
1000	11,65	11,47	11,65	11,47
1100	11,68	11,51	11,68	11,51
1200	11,81	11,71	11,81	11,71
1300	11,80	11,66	11,8	11,66
1400	11,72	11,60	11,72	11,6
1500	11,68	11,55	11,68	11,55
1600	11,75	11,45	11,75	11,58
1700	11,84	11,59	11,84	11,59
1800	11,85	11,53	11,85	11,53
1900	11,97	11,71	11,97	11,71
2000	11,85	11,67	11,85	11,67
2100	11,86	11,61	11,86	11,61
2200	11,88	11,59	11,88	11,59

2300	11,87	11,55	11,87	11,55
2400	11,23	11,62	11,23	11,62
2500	11,85	11,69	11,85	11,69
2600	11,96	11,61	11,96	11,61
2700	11,96	11,76	11,96	11,76
2800	11,94	11,65	11,94	11,65
2900	11,95	11,76	11,95	11,76
3000	11,90	11,82	11,9	11,82
3100	11,98	11,49	11,98	11,49
3200	12,01	11,66	12,01	11,66
3300	11,35	11,79	11,35	11,79

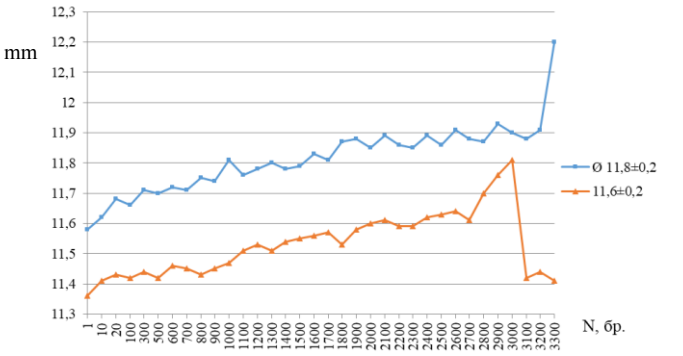

Fig.3. Measurements of controlled dimensions when machining with lubricating coolant, brand ECOCOOL MACH 40 and cutting speed Vc = 150 m/min

- When turning with speeds Vc = 150 m/min and Vc = 125 m/min and applying lubricating coolant

Vasco 6000, no significant difference is observed between the average values of the controlled dimensions. Furthermore, the variances of the controlled dimensions D and L when machining at the lower speed are larger, i.e. the stability of the technological process is not improved This, in combination with the fact that the reduction of the cutting speed leads to an increase in the processing time from 43÷46 s to 62÷65s and until the cost of the processed part increases, it is recommended to process the parts with the application of COT Vasco 6000 to be carried out at cutting speed Vc = 125 m/min.

TABLE 3. STATISTICAL ANALYSIS OF EXPERIMENTAL RESULTS

Statistical quantities	**Контролирани размери**					
	Диаметър D=11.8±0.2 mm			**Дължина L=11.6±0.2 mm**		
Average values	$\overline{D}_1$	$\overline{D}_2$	$\overline{D}_3$	$\overline{L}_1$	$\overline{L}_2$	$\overline{L}_3$
	11.814	11.797	11.800	11.531	11.610	11.614
Dispersion	S^2_{D1}	S^2_{D2}	S^2_{D3}	S^2_{L1}	S^2_{L2}	S^2_{L2}
	0.0127	0.0320	0.0322	0.0113	0.0127	0.0119
Mean Square Deviation	S_{D1}	S_{D2}	S_{D3}	S_{L1}	S_{L2}	S_{L3}
	0.1127	0.1789	0.1795	0.1063	0.1127	0.1092
Pooled variance estimates	$S_{D_{1-2}}$		$S_{D_{2-3}}$	$S_{L_{1-2}}$		$S_{L_{2-3}}$
	0.1495		0.1792	0.1095		0.1109

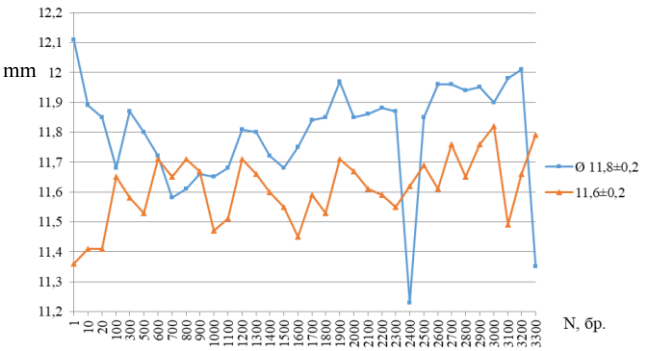

Fig.4. Measurements of controlled dimensions when machining with lubricating coolant, brand Vasco 6000 and cutting speed Vc = 150 m/min

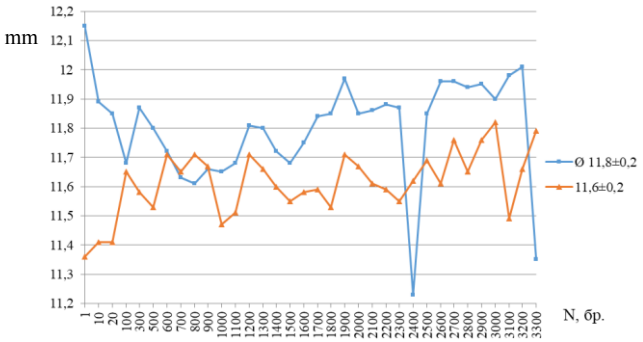

Fig.5. Measurements of controlled dimensions when machining with lubricating coolant, brand Vasco 6000 and cutting speed Vc = 125 m/min

III. CONCLUSIONS

The article presents the results of experimental studies and statistical analysis of the accuracy of machined surfaces of hardened steel 42CrMoS4 workpieces using a quick-change holder, different cooling media and cutting speeds, based on which the following conclusions can be drawn:

- Statistical testing of the parametric hypotheses of equality of mathematical expectations and variances proves that when machining with different cutting speeds, comparable values of the controlled diametral and linear dimensions are obtained, and the variances of these dimensions are smaller at higher cutting speeds , i.e. the stability of the technological process is greater.

- The type of lubricating coolant has a significant influence on the dispersions of the controlled diametral and linear dimensions, as when turning using ECOCOOL MACH 40 they are smaller than when applying Vasco 6000. This is proof of greater stability of the technological process at use of ECOCOOL MACH 40 and is a prerequisite for obtaining a higher quality of the treated surfaces. The type of lubricating coolant used has a significant influence on the accuracy of the linear dimension studied and a minor influence on the accuracy of the diametric dimension.

The proposed approach to the selection of the cooling medium and cutting speed creates conditions for optimizing the working conditions when turning parts made of hardened steel 42CrMoS4 using quick-change holders.

This work was supported by the European Regional Development Fund within the OP “Science and Education for Smart Growth 2014 - 2020”, Project CoC “Smart

Mechatronic, Eco- and Energy-saving Systems and Technologies“, No BG05M2OP001-1.002-0023

REFERENCES

[1] Chinchanikar S, S.K. Choudhury Machining ofhardenedsteel—Experimental investigations, performance modeling and cooling techniques: Areview. International Journal of Machine Tools&Manufacture, 89, 2015, 95–109.

[2] Karlovski G., K. Krumov, I. Aleksandrova, S. Tsenkulovski, I. Mitev. Selection of Instrumentation Based on Statistical Analysis. In: 32nd International Scientific Symposium Metrology and Metrology Assurance, MMA 2022, Conference Proceedings, Sozopol, 7-11 September 2022, Code 185634, DOI: 10.1109/MMA55579.2022.9992429, ISBN 978-166548569-2.

[3] Kuzmanov T., K. Krumov. Quality management. Exercise guide. Publishing house “EKS-PRESS” - Gabrovo, 2013, p. 97. ISBN 978-954-490-382-4.

[4] Kumar Sahoo A., B. Sahoo. Experimental investigations on machinability aspects in finish hard turning of AISI 4340 steel using uncoated and multilayer coated carbide inserts. Measurement, Vol. 45, 2012, 2153–2165.

[5] Nabil M., O. Taha, T. Elbitar, I. El Mahallawi. Thermomechanical processing of 42CrMoS4 steel. International heat Treatment and Surface Engineering IHSE 2010. Vol. 4 (2). DOI - 10.1179/174951410X12646901266726, pp. 87-92.

[6] [6] Samsonov I., A. Lyubomirov, A. Vinogradov, A. Platonov Research on the design features of block-module tooling used on CNC machine tools. Part 1 – Analysis of block-module tooling used on CNC lathes. Volga Scientific Journal, volume 52 (12-3), 2015, 74-80.

[7] Satheesh Kumar N., Ajay Shetty, Ashay Shetty, Ananth K, Harsha Shettyb. Effect of spindle speed and feed rate on surface roughness of CarbonSteels in CNC turning. Procedia Engineering, Vol. 38, 2012, 691 – 697.

[8] [8] Seregin A. Systems of instrumental equipment of basic technological equipment of machine-building plants. OGU, Orenburg, 2012.

[9] Saez-de-Buruaga M., L. Gainza, P. Aristimuno, D. Soler, G. Ortiz-de-Zarate, O. Aizpuru, R. Mielgo, P.J. Arrazola. FEM modeling of hard turning 42CrMoS4 steel. 17th CIRP Conference on Modelling of Machining Operations. 82 (2019), pp. 77–82. DOI 10.1016/j.procir.2019.04.059.

[10] Suresh R., S. Basavarajappa, V.N. Gaitonde, G.L. Samuel. Machinability investigations on hardened AISI 4340 steel using coated carbide insert. Int. Journal of Refractory Metals and Hard Materials, 33, 2012, 75–86.

[11] https://www.lastuamisnesteet.fi/wp-content/uploads/2019/12/Vasco-6000-Esite.pdf.

[12] https://avesta-sanat.com/wp-content/uploads/2021/12/Wmb_Nwmb_KSS_EN_SQ-1.pdf.

SECTION V
MEASUREMENTS IN THE ELECTRICAL POWER ENGINEERING

New Software System for Power Transformers Diagnosis Based on Partial Discharges Appearances

Nikolina Petkova
Dept. of Theoretical Electrical Engineering
Technical University of Sofia
Sofia, Bulgaria
e-mail: npetkova@tu-sofia.bg

***Abstract*— There are many methods to diagnose the power transformers current state. The electrical method of partial discharges measure in the volume of the power transformer gives the maximum information that can be desired. In this paper is presented a method with new software system. It is based on the determining algorithm for analyzing the signals measured as well as on preparing the necessary recommendations by the expert monitoring system, is suggested.**

Keywords—partial discharges, diagnosis, monitoring system

I. INTRODUCTION

This paper describes method using a new software system for determines the state of the power transformer based on the area of partial discharge (PD) appearance. The electrical partial discharge measurement is the most suitable method for assessing the condition of insulation systems in high voltage equipment. Conventional partial discharge measurement systems have proven to have some difficulties in the measurements, particularly in online conditions and noisy environments. In high voltage devices, such as transformers, PDs can be symptomatic of problems within the device such as floating components and insulation flaws. Over time, electrical and mechanical stress can damage the materials within the transformer, including the winding and the paper insulation lining the walls of the transformer tank. If the damage is not detected or corrected, the faults can cause the transformer to operate outside of its normal parameters and eventually a catastrophic failure may occur, causing potential damage to surrounding equipment and facilities, as well as lost revenue due to an unscheduled power outage. Power transformers are used to step up or step down voltage and are an integral component of any efficient power distribution network. A typical transformer incorporates coils of conducting wire wrapped around a core and covered with a paper-based insulator. Essential to the operation of these units are transformer oils that have two functions: electrical insulation and heat dissipation.

II. MAIN PARAMETERS THAT IS APPLY IN SOFTWARE SYSTEM

The most important parameters regarding the final software decision about the actual transformer state are the location of the partial discharge, the partial discharge case and the transformer oil conditions.

A. Location of partial discharges

The measurement signals and the type of oscillations can be classified depending on the following parameters:

- Location of discharge: most pulses in advance of the voltage peaks
- Variability of Response: random movement
- Relative Magnitude of discharge: different magnitude on two half cycles
- Test voltage: rises with test voltage
- Time of application: constant with time

The output data is the case of PD occurrence.

B. Cases of PD appearences though the voltige test

This new software system determines the state of the power transformer based on the area of partial discharge appearance. These depend on parameters such as location of discharges on test voltage, variability of response, relative magnitude of discharges on positive/negative half cycle and variation of discharge magnitude depending on test voltage and time of application.

The possible cases of partial discharge occurrence are A, B, C, D, E, F, G, H, J, K, L, M and N. The possible locations of partial discharges are in the tank, windings (wndg), leads, tap changer and other. Only two cases of oil conditions are considered- good and bad oil.

Failures are usually triggered by severe conditions, such as lightning strikes, switching transients, short-circuits, or other incidents. When the transformer is new, it has sufficient electrical and mechanical strength to withstand unusual system conditions. As transformers age, their insulation strength can degrade to the point that they cannot withstand system events such as short-circuit faults or transient overvoltage. [1, 2]

To prevent these failures and to maintain transformers in good operating condition is a very important issue for utility companies. Traditionally, preventive routine maintenance programs combined with regular testing are used. With deregulation, it has become increasingly necessary to reduce maintenance costs and equipment inventories. This has led to reductions in routine maintenance. The need to reduce costs has also resulted in reductions in spare transformer capacity and increases in average loading. There is also a trend in the industry to move from traditional time-based maintenance programs to condition-based maintenance. [1, 2]

These changes occur at a time when the average age of the transformers in service is increasing and approaching the end of nominal design life. The change to condition-based maintenance has resulted in the reduction, or even elimination, of routine time-based maintenance. Instead of doing maintenance at a regular interval, maintenance is only carried out if the condition of the equipment requires this. Hence, there is an increasing need for better nonintrusive diagnostic

The authors would like to thank the Research and Development Sector at the Technical University of Sofia for the financial support.

and monitoring tools to assess the internal condition of the transformers. If there is a problem, the transformer can then be repaired or replaced before it fails. [1, 2]

C. *Dissolved Gas Analysis*

In a substation, the condition of the oil can be examined using Dissolved Gas Analysis (DGA). It has only been performed in a lab, where at first the oil sample is degassed followed by a gas-chromatographic analysis of the extracted gas sample. Then, the composition of the gas mixture and the total amount of extracted gases is analyzed. This method gives precise and reproducible results, thus reliable results are achieved. The result of such a transformer examination is nevertheless influenced by the quality of the oil sample that is used for DGA [3].

The gasses that are dissolved in the insulating oil are energy generated due to a fault, thus resulting in the partial or complete destruction of the Hydrocarbon molecular chains of the insulating oil. The fractions consist of:

- Hydrogen H2
- Methane CH4
- Ethane C2H6
- Ethene C2H4
- Ethyne C2H2
- Propane C3H8
- Propene C3H6.

Due to the de-polymerization of the solid paper insulation additionally:

- Carbon Dioxide CO2 and
- Carbon Monoxide CO are generated.

The atmospheric gases:

- Oxygen O2 and
- Nitrogen N2

are dissolved in the insulating liquid as well if the transformer is of breathing type and is exposed to the environment [3].

As long as the concentrations of the dissolved gasses do not exceed certain limits or changes in oil solubility, the composition of the dissolved gases can be used for analysis if the ratio of their content is evaluated.

This relation is dominated by the form and amount of energy that has been applied in the transformer failure, thus thermal faults and electrical faults can be distinguished. A more precise distinction between the sizes of the failures and the level of concentration of gases is also specified in the standard IEC 60599.

In our case, the results from the chemical conditions of the oil could be summarized as GOOD OIL (if the concentrations of the gases are in compliance to standard IEC 60599) or BAD OIL (if the concentrations of the gases are not in compliance to standard IEC 60599). These results are used when the operator takes the final decision regarding the emergency of the partial discharge that is detected. In substations, information for the condition of the oil is provided by technical labs in six month intervals.

III. Software System Running

The software program responsible for the decision regarding the status of the transformer is developed in Visual Studio.

It has to be set the settings for the next parameters: case of PD occurrence, partial discharge location and oil condition. The software determines the level of criticality of the power transformer state.

- Step 1– Start the program and the following window will appear:

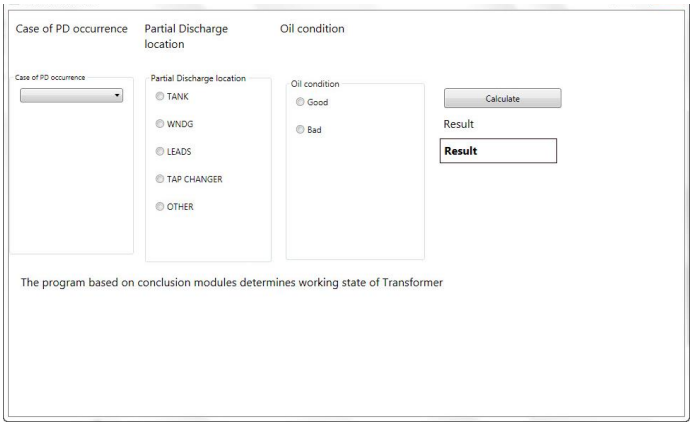

Fig. 1. Screenshot of software system

Step 1 is common for all tests. Screenshot of program is shown in Fig. 1.

- Step 2: Depending on the input data, the following situations are done:

*1) Status **WORK***

In this state the input data is given in Fig. 2:

Case of PD occurrence: **A**
Partial discharge location: **TANK**
Oil condition: **GOOD**

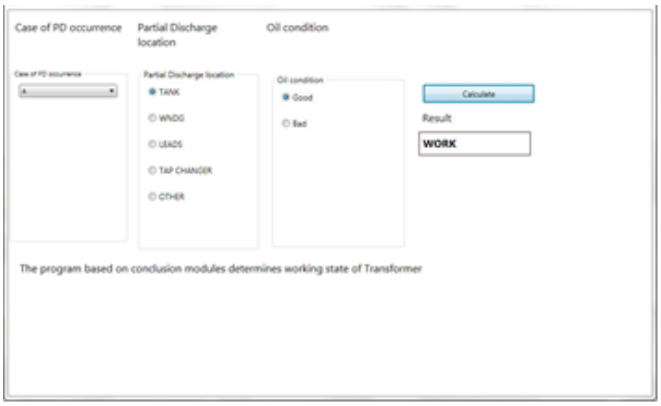

Fig. 2. Screenshot - case A (work state-TANK)

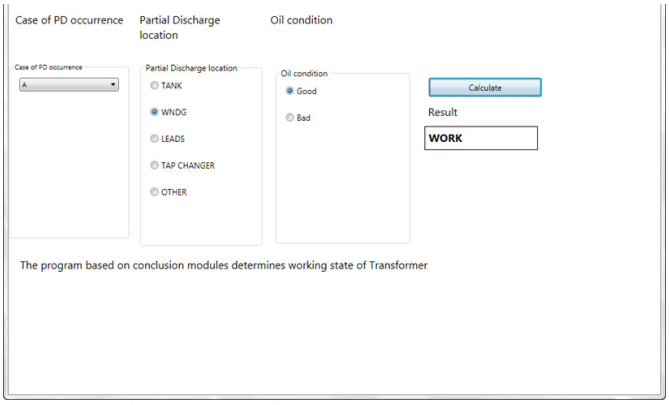

Fig. 3. Screenshot - case A (work state-WNDG)

Input data that is given in Fig. 3:
Case of PD occurrence: **A**
Partial discharge location: **TANK**
Oil condition: **GOOD**

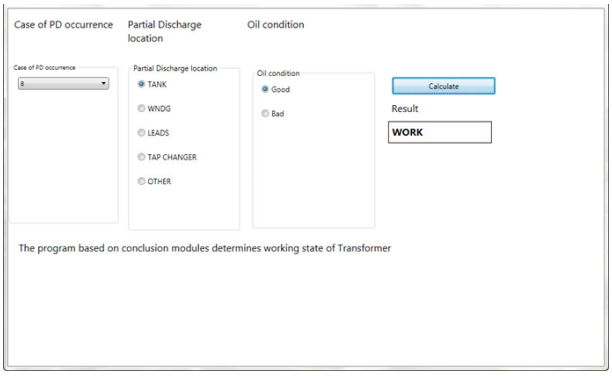

Fig. 4. Screenshot - case B (danger state - TANK)

Input data that is given in Fig. 4:
Case of PD occurrence: **B**
Partial discharge location: **TANK**
Oil condition: **GOOD**
Output data:
Status message: **WORK.**

*2) Status **ATTENTION***
For this disition the input data is shown in Fig. 5:
Case of PD occurrence: **A**
Partial discharge location: **TANK**
Oil condition: **BAD**

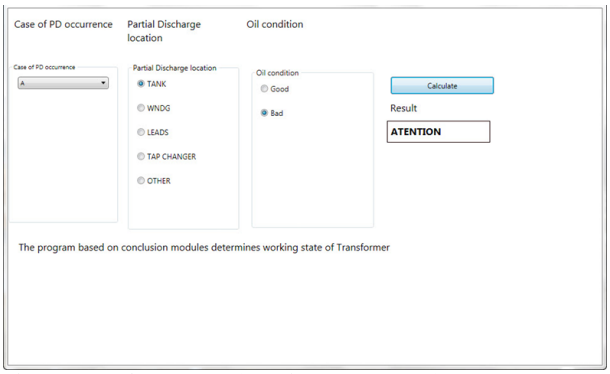

Fig. 5. Screenshot - case A (attention state - TANK)

For this disition the input data is shown in Fig. 6:
Case of PD occurrence: **C**
Partial discharge location: **WNDG**
Oil condition: **GOOD**

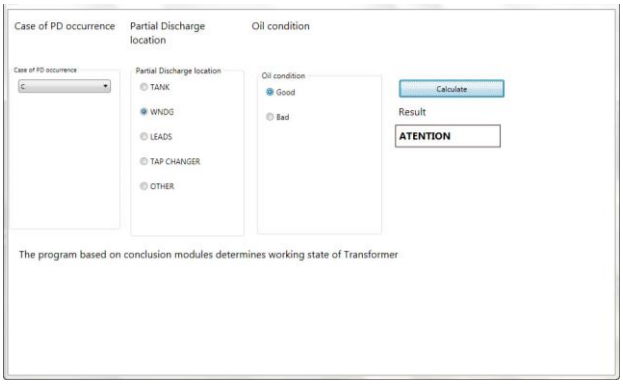

Fig. 6. Screenshot - case C (attention state - WNDG)

Input data that is shown in Fig. 7:
Case of PD occurrence: **D**
Partial discharge location: **LEADS**
Oil condition : **GOOD**

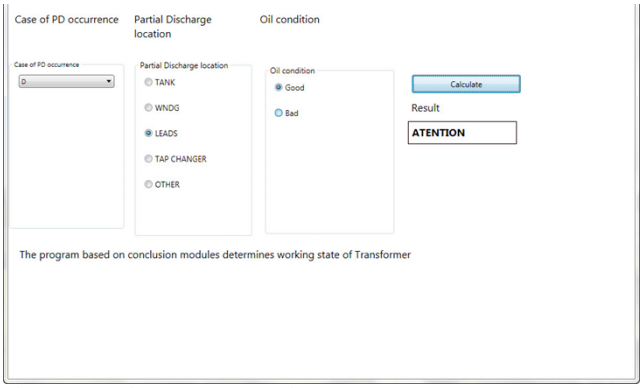

Fig. 7. Screenshot - case D (attention state - LEADS)

Output data:
Status message: **ATTENTION**.

*3) Status **DANGER***
The input data in this status is given in Fig. 8*:*
Case of PD occurrence: **C**
Partial discharge location: **WNDG**
Oil condition : **BAD**

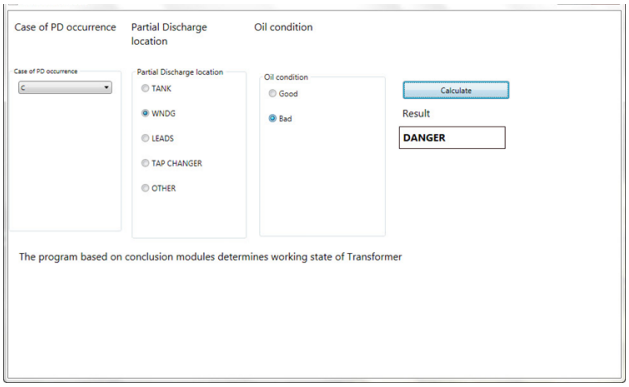

Fig. 8. Screenshot - case C (danger state - WNGS)

Input data is shown in Fig. 9*:*
Case of PD occurrence: **C**
Partial discharge location: **LEADS**
Oil condition: **BAD**

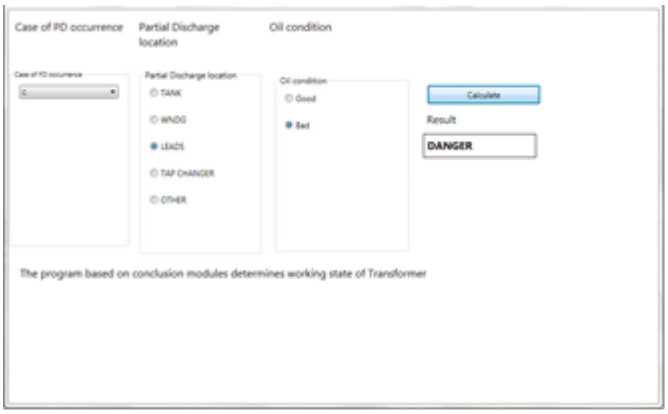

Fig. 9. Screenshot - case C (danger state - LEADS)

Input data is done in Fig. 10:

Case of PD occurrence: **D**

Partial discharge location: **LEADS**

Oil condition: **BAD**

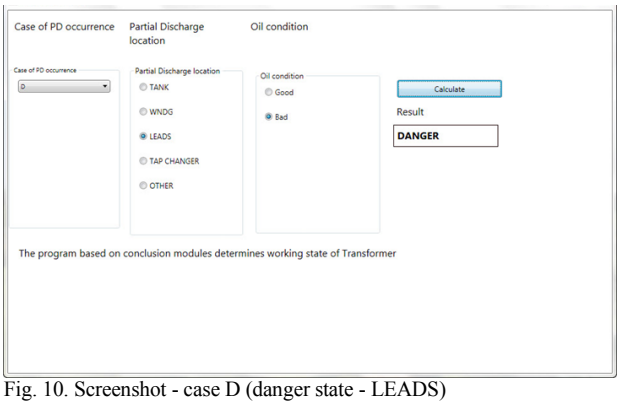

Fig. 10. Screenshot - case D (danger state - LEADS)

Output data:

Status message: DANGER.

IV. Conclusion

In this paper a new PD methodology were described. This kind of logic is approximately new and in progress. This new way provides meaningful and additional information for PD analysis. The software based on the prescribed algorithm for analyzing the signals measured as well as on preparing the necessary recommendations by the expert monitoring system.

References

[1] IEC 60270:2000 - High-voltage test techniques - Partial discharge measurements.

[2] IEC 60076-3:2000-03 - Power transformers – Insulation levels, dielectric tests and external clearances in air.

[3] Online gas analysis of transformers, Energy Support, http://energy-support.de/3_trafo/analytik-schadgas.php

Energy and Environment Monitoring Online Controller for Renewable Energy Systems

Valentin Mateev
Department of Electrical Apparatus
Technical University of Sofia
Sofia, Bulgaria
vmateev@tu-sofia.bg

Onur Çam
Department of Electrical Apparatus
Technical University of Sofia
Sofia, Bulgaria

Iliana Marinova
Department of Electrical Apparatus
Technical University of Sofia
Sofia, Bulgaria
iliana@tu-sofia.bg

***Abstract*— In this paper is presented energy monitoring device controller which is optimized for small renewable energy systems. It is based on PIC18F series microcontroller with six channels for current and voltage measurements. Also it can collect data of environmental conditions as CO_2 concentration and temperature. With the energy monitoring device, voltage, current and power information can be monitored and controlled in time of operation. It is an optimal and reliable solution for small scale house microgrids with distributed dynamic energy sources.**

Keywords*— *electric energy monitoring, controller, renewables, power and energy measurements

I. INTRODUCTION

Modern design and optimization of electrical equipment benefit from computer technology and advance of modern algorithms. Energy monitoring becomes of paramount importance fir many industrial and household power supply systems. As reliable are these systems, as useful for users they are. This is of major importance for systems of renewable sources, where significant variations of power parameters must be continuously observed in many distributed sensing nodes [1-3]. Here is presented energy monitoring device controller which is optimized for small renewable energy systems. It is based on PIC18F series microcontroller with six channels for current and voltage measurements. [4-5]

The energy monitoring device measures the voltage and current of the system it is connected to. It can be set upper and lower limits for voltage measurements from the device or from computer software. The main control of this device is designed with PIC18F series smd microcontroller of microchip company. The microcontroller is programmed in C language. 6 analog inputs are used for volt and current measurement. 4 digital inputs are used for menu control. 11 digital outputs are used for warning and controller. In addition, 1 uart communication unit is used for computer communication.

The project generally consists of two different control and monitoring units. The first of these is the grid-connected energy monitoring device. The technical operator can instantly control the desired values on the device. If desired, upper and lower measurement limits can be adjusted on the device. The second unit is the computer recording system where data is recorded and monitored. Thanks to this system, the data received from the energy monitoring device can be monitored instantly and reporting can be made. If desired, lower and upper limit values can be observed on the program. and adjustable.

The basis of the project is designed with a pic microcontroller. In addition, a monitoring and reporting interface was designed with C# for data monitoring and reporting. The energy monitoring device provides data transmission and reception to the computer interface wirelessly with the RF module. Electronic Simulation and Hardware Design; The interface program, which has been made ready for use, has been simulated by using the ISIS program virtually in computer environment, communicating with electronic equipment via serial port, and performing all software and hardware tests.

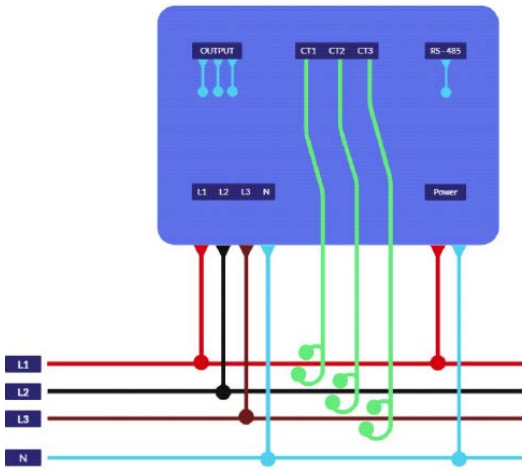

Fig. 1. Monitoring device main connection diagram.

CT1, CT2, CT3 Current sensor connection terminal. L1, L2, L3 Connection terminal for voltage measurement. POWER Main power supply of the device. RF Communication with interface. OUTPUT Relay output for use in alarm condition.

II. ENERGY MONITORING DEVICE HARDWARE

In this section, information about the basic hardware of the PIC18F45K22 microcontroller used in the project is given. The details of the hardware specifications are examined in other hardware components. Microcontroller is the most important unit that enables the hardware units in the project to communicate with each other and to analyze and process. The total number of pins in the TQFP case of the PIC18F45K22 microcontroller is 44. In the project, a total of 35 pins were used for input, output and communication.

The RF Module HC-12 is used to transparently transmit the data coming from the Uart between the receiver and the transmitter. 433.4 - 473.0 MHz has a transmit power of 100 mW. It provides a communication within an average of 1,000 meters distance.

979-8-3503-3810-2/23/$31.00 ©2023 IEEE

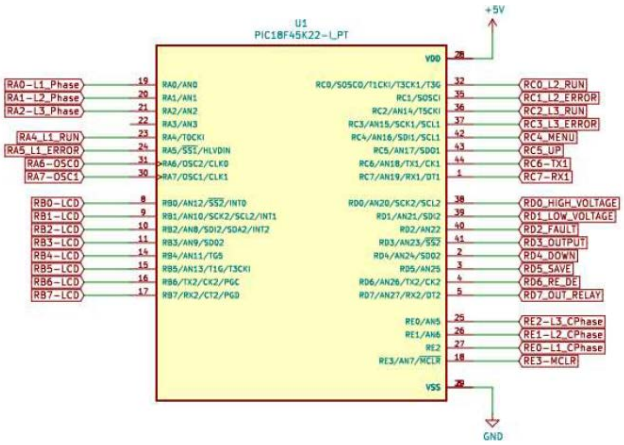

Fig. 2. Schematic of 18F45K22.

The cooler must fit in a space with dimensions: Width: 60mm; Height: 100mm; Thickness: 10mm.

III. Device Inputs

Current Sensor is an important device in power calculation and management applications. It measures the current through a device or circuit and produces an appropriate signal proportional to the measured current. SCT-013 Current Sensor, this product, which can measure AC current up to 100 Amperes with the current transformer on it, so it is a non-contact inductive sensor.

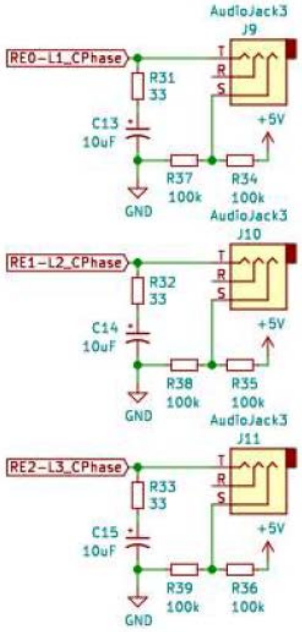

Fig. 3. SCT-013 Current Sensor pin out.

For voltage measurements. The microcontroller we use can also measure analog value. Since the maximum operating voltage of our microcontroller is 5 VDC, our analog measurement range is between 0 VDC and 5 VDC. Since we cannot directly connect the 230 VAC mains voltage to our microcontroller, we need a converter and voltage divider circuit. It helps us to make analog measurements by converting the 230 VAC that we will measure over the Mains for each phase to the 0 VDC and 5 VDC range, which is the measurement range of the microcontroller, thanks to this part.

IV. Instrument Panel

In general, it is the instrument panel where it can besee the necessary measurements during the operation of the system. Thanks to the LCD screen on the instrument panel, it can be instantly seen the voltage information, current information and power information in the system to which it is connected. In addition to the measurement values, we can observe whether the phases are connected via the instrument panel or the fault conditions in the system and whether the output that we can use as an alarm is active. In addition, it can be made adjustments such as lower and upper limits to the measurements that have been made, thanks to the buttons on the instrument panel without being connected to any device or computer interface.

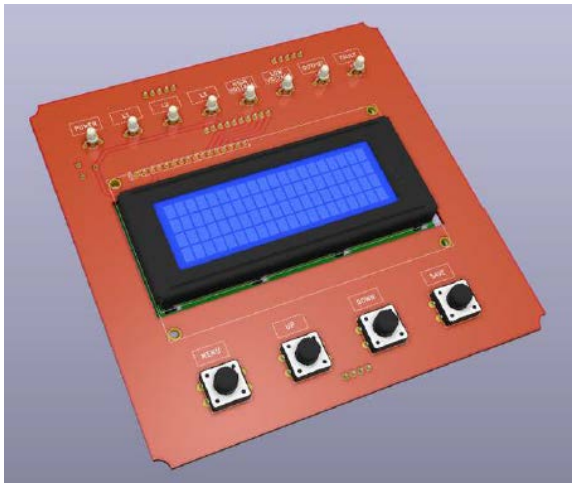

Fig. 4. 3D design of Front PCB and Top Side.

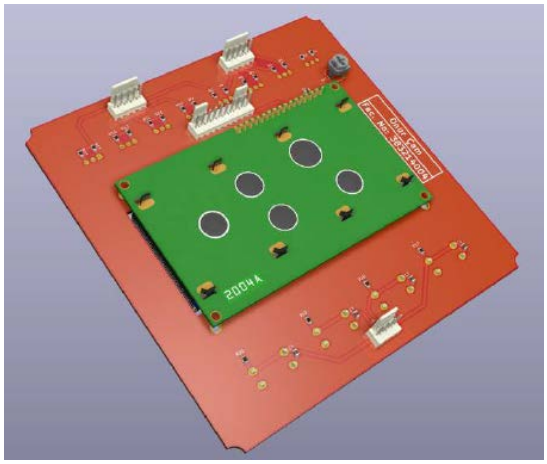

Fig. 5. 3D design of Front PCB and Bottom Side.

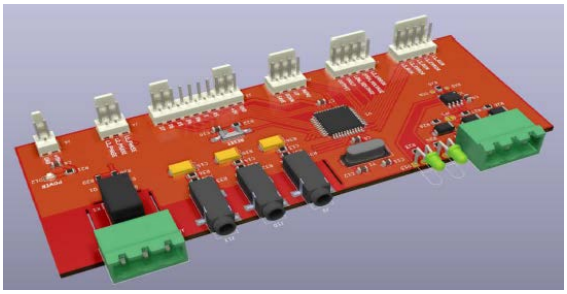

Fig. 6. 3D design of Main PCB and Top Side.

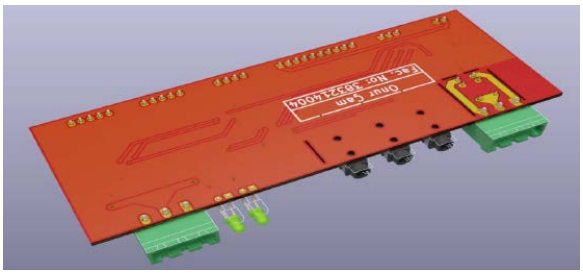

Fig. 7. 3D design of Main PCB and Bottom Side.

Main controller board, it is the part where all the data coming from the instrument panel and measurement part are read by the microcontroller and the scenarios are realized according to the written program. There are RS-485 communication port on the main board, current sensors connection ports, connection ports from the instrument panel, connection ports from the power floor and 1 relay output that allows the user to get information by connecting with different devices. Fig. 8 and Fig. 9 shows the connection diagram of the Main Controller Board.

Fig. 8. Actual device front view.

Actual outlook of prototyped controller is presented in operational conditions in Fig. 8 and Fig. 9. These are working pictures and menu pictures of Energy Monitoring Device. Power supply module and measuring transducers are not shown in Fig. 9.

Fig. 9. Actual main PCB and Bottom Side.

V. ONLINE MONITORING SYSTEM

The computer interface was developed in Microsoft Visual Studio in C#. With this interface, we can monitor the measurement values, report in excel format and make limit settings. There are 5 menus in the interface program. In the first menu, connection settings are made with the device. Measurements can be monitored and set in the second menu. The measurements can be monitored with date and time information and reports can be recorded in excel format in the third menu. Users can be added to the system by the admin to access the interface in the fourth menu, Measurements can be viewed graphically in the fifth menu.

Fig. 10. Online Graphical User interface.

When the user runs our interface program for the first time, it is the first form that opens after entering our user name and password to access the system (Fig. 10). There are menus on the main form that we can access with 4 different buttons. These are the main ones; Connection, Measurements, Reports, Add User menus.

Fig. 11. Data Report Form outlook.

The computer interface was developed in C# language in Microsoft Visual Studio 2012 compiler. In general, the program consists of 6 different forms. Information regarding the operation to be performed in each form can be monitored and adjusted. The lines starting with // contain explanations about the codes.

Login Form. With this form, it is aimed to prevent the access of our interface by unauthorized persons. In order to use the program by logging into the main interface, user accounts must be defined by the system administrator Admin. You can log in to the system with a user name and password.

Main Form. With this form, the main menu of the interface was created. We can make the necessary connections and settings by accessing the forms related to the menu buttons on the left.

Connection Form. With this form, necessary connection settings are made for our interface to connect with our Energy Meter device. After making the necessary settings, we can connect or terminate our connection with our device.

Measurement Form. With this form, we can instantly observe the values such as volts, currents and watts that I have measured on our Energy Meter device via our interface. In addition, if there is a setting set on our device, we can see these settings instantly.

Reports Form. With this form, it is aimed to be able to see all the volt, current, watt information that we have measured from the Energy Meter device as a date, time and second report. The system administrator using my interface can export the reported data in Excel file format whenever he wants.

CONCLUSION

In this paper is presented energy monitoring device controller which is optimized for small renewable energy systems. It is based on PIC18F series microcontroller with six channels for current and voltage measurements. Also it can collect data of environmental conditions as CO_2 concentration and temperature. With the energy monitoring device, voltage, current and power information can be monitored and controlled in time of operation. It is an optimal and reliable solution for small scale house microgrids with distributed dynamic energy sources.

ACKNOWLEDGMENT

This work was partially supported by the National Science Fund of the Ministry of Education and Science of the Republic of Bulgaria under contract KP-06-N47/2.

REFERENCES

[1] K. Kgopana and O. Popoola, "An Intelligent Fuzzy Rule-Based Load Monitoring for Improving Energy Utilization of Energy Storage Systems," 13th International Renewable Energy Congress (IREC), Hammamet, Tunisia, 2022, pp. 1-6.

[2] J. C. Lorenzana-Gerardo, J. L. Díaz-Reséndiz and E. A. Rivas-Araiza, "IoT based robust electrical energy monitoring system with Programmable Logic Controller," IEEE International Conference on Automation/XXIII Congress of the Chilean Association of Automatic Control (ICA-ACCA), Concepcion, Chile, 2018, pp. 1-6.

[3] L. Prasetyani, M. J. F. Arifianto, D. Subagio, W. Sarfat and Aprilyanto, "Experimental Analysis Design of Solar Panel Energy Monitoring Prototype," 7th International Conference on Information Technology, Computer, and Electrical Engineering (ICITACEE), Semarang, Indonesia, 2020, pp. 236-240.

[4] E. Irmak, H. I. Bülbül, A. Kose and A. Calpbinici, "A web-based real-time industrial energy monitoring system," 4th International Conference on Power Engineering, Energy and Electrical Drives, Istanbul, Turkey, 2013, pp. 1713-1716.

[5] M. P. Kokare and S. H. Pawar, "Energy Monitoring System In Electric Grids: The Role Of Advanced Intelligent And Iot For Future Electric Grid," International Conference on Emerging Trends in Information Technology and Engineering (ic-ETITE), Vellore, India, 2020, pp. 1-4.

[6] V. Mateev and I. Marinova, "Distributed Internet of Things System for CO2 Monitoring with LoRaWAN," 2021 12th National Conference with International Participation (ELECTRONICA), Sofia, Bulgaria, 2021, pp. 1-5.

SECTION VII
MEASUREMENTS IN THE ECOLOGY, BIOTECHNOLOGY, MEDICINE, AND SPORT

Development of a Wireless Sensor Node for Early Fire Detection

Ilian Georgiev
Department of "Electrical Measurement Systems"
Technical University of Sofia
Sofia, Bulgaria
ilian_1308@abv.bg

Antonia Pandelova
Department of "Electrical Measurement Systems"
Technical University of Sofia
Sofia, Bulgaria
apandelova@tu-sofia.bg

***Abstract*—In the recent years, there has been a growing interest in the planting and growing of large arrays of fruit trees in Bulgaria. One of the dangers that threaten farmers is the occurrence of fire, especially during the hot summer months. Very often the fire occurs at a time when there is no human presence on site and alternative methods of monitoring the relevant territory are needed.**

In the article, a wireless sensor node for early warning of fire is developed. It includes three sensors - to measure temperature and humidity, to measure carbon monoxide and to measure the concentration of particulate matter. Each sensor has been adjusted individually as well as whether they are functioning properly. Exemplary experiments were conducted with the configured sensor node to verify operability and timely response in the presence of a fire hazard. The measurement information collected by the sensors is transmitted wirelessly to a base station where it can be further processed for measurement purposes. The proposed sensor node will be used to build a wireless sensor network for early detection of fires in large tracts of agricultural crops and open pastures in rural areas of the country.

Keywords—wireless, temperature, CO, particulate matter, fire detection

I. INTRODUCTION

In recent years, there has been a growing interest in the planting and growing of large arrays of fruit trees in Bulgaria. The initial investment is large and this requires taking preventive measures to protect the plantations. One of the dangers that threatens farmers is the occurrence of fire. This danger is especially strong during the so-called fire season - the period of the year when fires develop in nature, especially forest fires. Because wildfires are predisposed to dry and hot weather, much of the fire season coincides with the summer months.

In the last decade, fires of high intensity affecting large areas were observed in the country. According to the General Directorate "Fire Safety and Protection of the Population" for the period 2015-2019, there was an increase in the number of fires from 30,009 to 42,141 fires [1]. One of the main reasons for this result is high temperatures, prolonged drought and strong winds. Other causes of the frequent fires in recent years include lightning, re-occurrence of a previous fire, human negligence and unknown causes, as well as deliberate arson.

Timely signaling of the occurrence or danger of fire is extremely important. There are different fire detection methods - satellite-based [2, 3], using artificial neural networks [4, 5], various mathematical models have also been developed [6, 7, 8, 9]. One alternative for detecting and preventing fires in forest and rural areas using new technologies are wireless sensor networks [10, 11, 12]. The different types of sensors involved in the sensor nodes of wireless sensor networks can measure different variables, which helps determine the direction and development of the flame [13, 14, 15].

The aim of this paper is to develop a low-cost wireless sensor node for early detection of fires in orchards. The sensor node includes three sensors – a sensor for measuring temperature and humidity, a sensor for measuring carbon monoxide and smoke (CO) and a sensor for measuring particulate matter (PM). The choice of the latter sensor is due to the fact that smoke from forest fires contains high levels of fine particulate matter. Subsequently, this sensor node will be part of a wireless sensor network for early detection of fires located along the borders of the fruit plantations.

II. MATERIAL AND METHODS

A wireless sensor node is part of a sensor network. The sensor node has the ability to process the collected sensor information and communicate with other nodes of the wireless sensor network. A sensor node includes several main components, as a microcontroller, a transceiver, an external memory, a power source, and a sensor or sensors. Thanks to the wireless communication and the small size of the sensor node, large areas such as forests, pastures, buildings can be monitored.

A. Microcontroller Espressif ESP32 DevKitC

Espressif ESP32 DevKitC is a microcontroller board. It has Bluetooth and WiFi communication, built with ESP-WROOM-32 wireless module working with ESP32 microcontroller. There is also a micro USB connector and a built-in PCB antenna. Supports SPI, I2C, UART, I2S, DAC, analog inputs, PWM outputs. Since the ESP 32 microcontroller is equipped with a wireless communication chip, it will upload measurement data online via an HTML web server. The microcontroller is preferred as the main core for the wireless sensor nodes due to its characteristics - energy-efficient computing unit, its ability to connect easily with other devices and the built-in memory.

B. Sensors

The sensors used for the project were purchased commercially as modules providing power supply and interface.

- DHT11 Temperature and humidity sensor. The temperature range of measurement is from 0° to 50°

The authors would like to thank the Research and Development Sector at the Technical University of Sofia for the financial support under contract №231ИХЪБ0002-08.

C, and the relative humidity range is 20% - 90%. The temperature and humidity sensor uses a digital input of the controller where it provides a data signal, powered by 5 V. Since it has a pre-calibrated digital output, it does not need calibration.

- MQ-7 gas sensor. It measures the concentration of carbon monoxide CO. The sensor interface provides two types of output signal, analog and digital. The analog output is related to the reported CO concentration, while the digital output is related to the sensitivity of the sensor. It is characterized by low consumption of the order of 170 - 220 mA.
- Sharp GP2Y1010AU0F particulate sensor. It measures fine dust particles with a diameter greater than 0.8 μm. The sensor is mounted on a board that provides the power supply. The interface consists of an analog output and an ILED trigger pin. Measuring range of the sensor - 500μg/m^3.

C. *Connection diagram*

Fig. 1 shows the connection diagram of the sensor node. To implement the scheme, in addition to the elements mentioned above, a breadboard, a 150 Ω resistor and a capacitor with a capacity of 220 μF were also used.

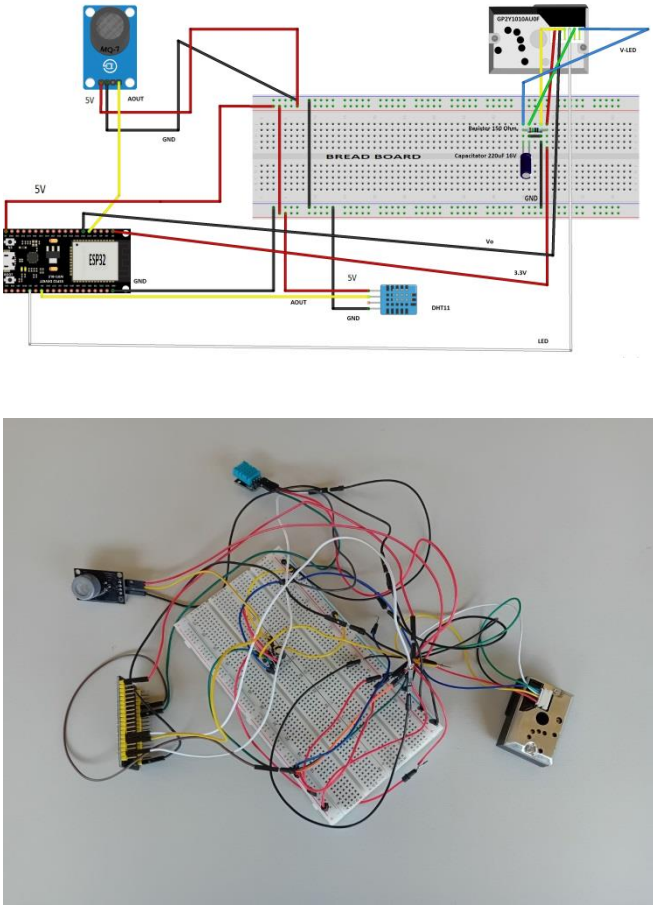

Fig. 1. Connection diagram of the sensor node

The ESP32 microcontroller is used to collect data from the sensors, transmit the data and control the power supply. The microcontroller supports 5 V input power supply and has 5 V and 3.3 V output power supply.

The MQ-7 carbon monoxide sensor uses an analog input of the microcontroller to provide data, its power supply is 5 V. The calibration of the sensor is programmatic and is based on standardized coefficients taken from an Internet source. A mathematical formula is used to convert the measurement units from ppm to mg/m^3. The correction is applied at 1 bar atmospheric pressure, nominal temperature and humidity. The MQ-7 operates with a 10-bit binary code format. Before starting the measurements, it is recommended to pre-warm the MQ-7 and after the warm-up period to start the actual measurements.

The Sharp GP2Y1010AU0F particulate matter sensor uses a 12-bit analog input of the controller and operates at a nominal voltage of 3.3 V. The calibration is done programmatically, taking into account the nominal value of particulate matter in mg/m^3 in the Sofia Region in the raw form. A conversion from ppm to mg/m^3 via a mathematical formula is included. The manufacturers of all three sensors give them a 5-year period of use.

III. Results and Discusion

After assembling the sensor node, it is necessary to program the microcontroller, set up the sensors and establish communication between all components.

The ESP32 can be programmed using a variety of firmware and programming languages, and for the purposes of this study we chose the Arduino IDE software, which is open-source. Although it is not the best IDE, it works well, is simple and intuitive and easy to use from beginners. Multiple case libraries as well as solved examples are also available.

The microcontroller should be able to read the data from the three sensors. The relevant libraries need to be installed. After the successful installation, a code is written through which the microcontroller will be able to read the information from each sensor. The code for the HTML server, where the data is sent and stored, is written in a text document or in Visual studio.

Simulated experiments were conducted with the constructed sensor node to verify the correctness of the configuration. The sensors are set to take data every 10 s. The measurement time can be changed at any time depending on the specific situation. Fig. 2 shows values for measured temperature and humidity, and fig. 3 shows values for CO and particulate matter. It can be seen that all four parameters were measured simultaneously, with no delay in data recording.

In order to be used in the field, the sensor node must be placed in a suitable box. Fig. 4 shows the assembled box with the sensor node attached. The box is quite bulky, but this is due to the peculiarities of the particulate matter sensor - enough space must be provided for the measured atmospheric air. Fig. 5 shows the contents of the box. The location of the microcontroller 1 and the particulate sensor 2 can be seen. At the bottom of the box, the breadboard auxiliary board is immovably fixed. With longer wires, the connection to the CO sensor and temperature and humidity sensor mounted on the outside of the box is made. The actual placement of these two sensors is shown in fig. 6.

The logical question is whether the sensor node placed in this box will be able to perform measurements. New measurements were made and the results of the measurements carried out are shown in figures 7 and 8.

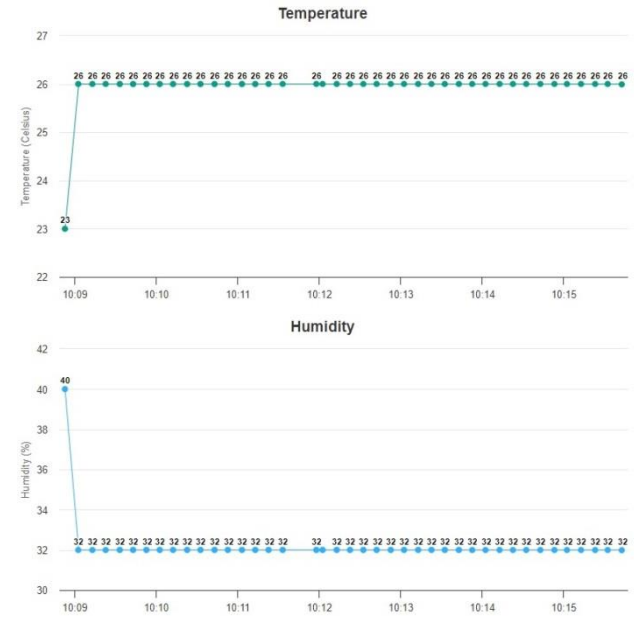

Fig. 2. Obtained results for measured values of temperature and humidity

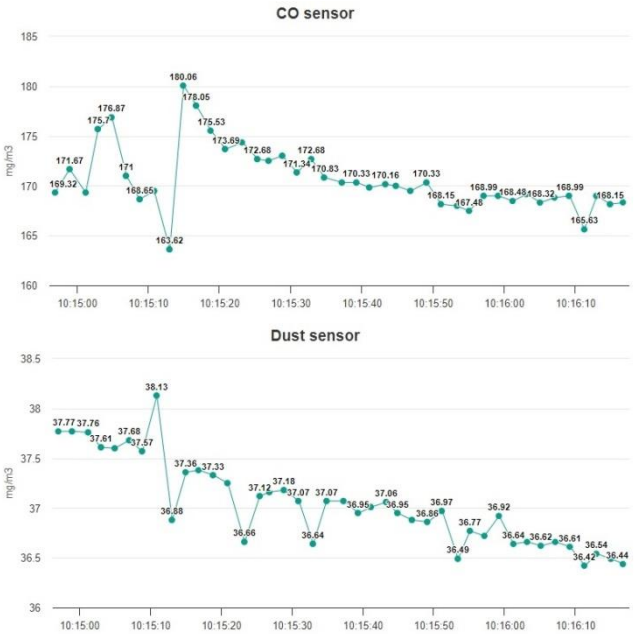

Fig. 3. Obtained results for measured values of carbon monoxide CO and particulate matter

Fig. 4. Appearance of the sensor box

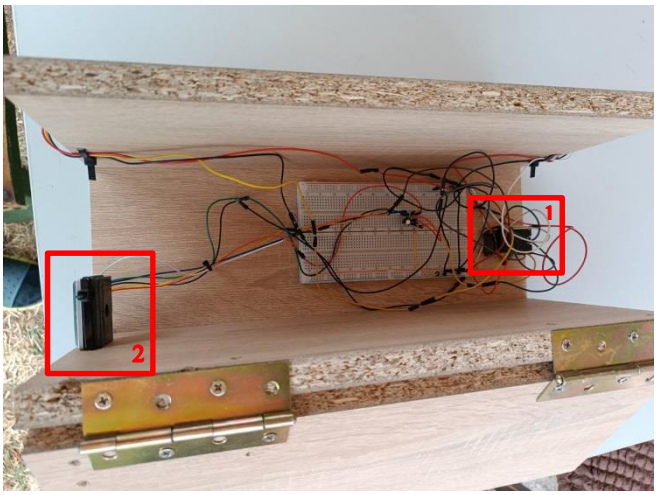

Fig. 5. The contents of the box after opening the lid. 1 – microcontroller, 2 – sensor for particulate matter

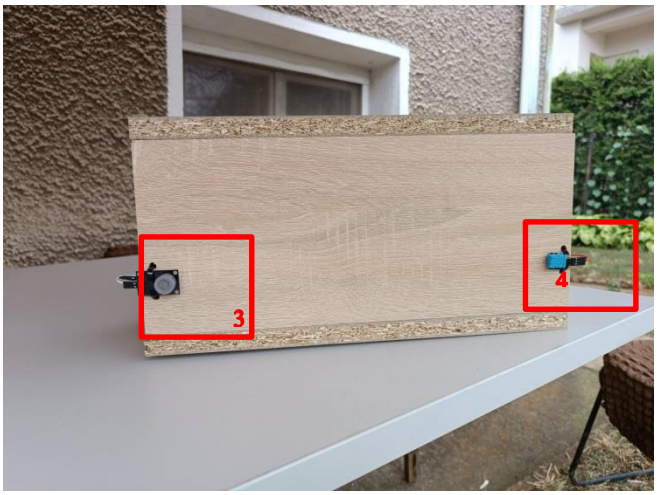

Fig. 6. Sensor box with externally attached sensors. 3 - carbon monoxide sensor, 4 - temperature and humidity sensor

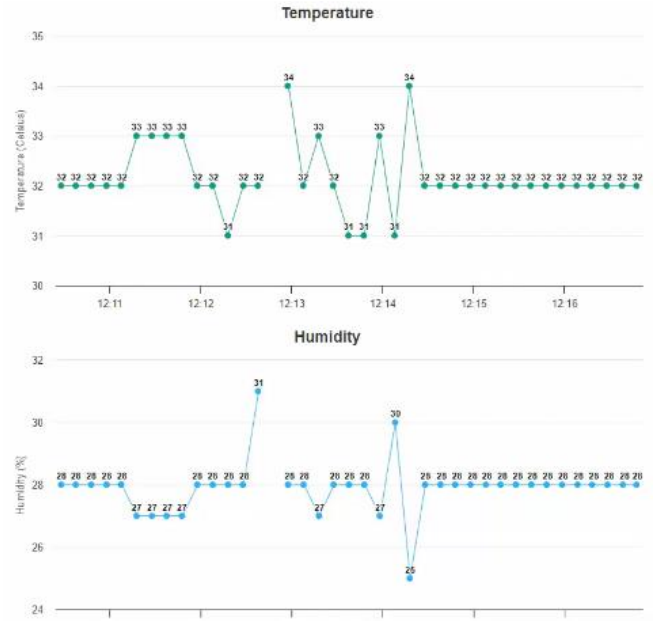

Fig. 7. Measured values of temperature and humidity after installing the sensor node in the box

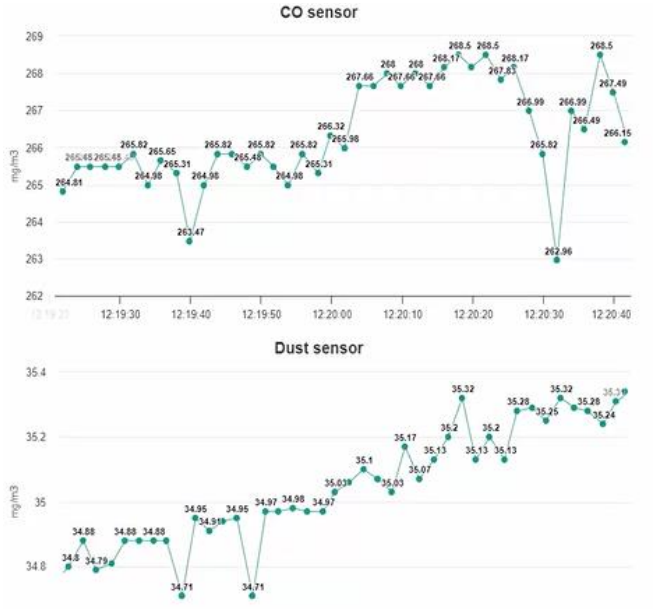

Fig. 8. Measured values of CO and particulate matter after installing the sensor unit in the box

Fig. 7 shows the measured values for temperature and humidity after installation in the sensor box. The values of these two parameters hardly change. This is due to the nature of the simulated experiment – burning papers near the sensor box. However, at the expense of this, the carbon monoxide sensor detects an increased concentration of the measured gas, as can be seen in fig. 8. The dust sensor also registers an increase in the level of particulate matter, no matter how little it is.

CONCLUSION

In this study we presented a low-cost wireless sensor node for early fire detection in fruit plantations. The sensor node is consist of three sensors – a sensor for measuring temperature and humidity; sensor for measuring carbon monoxide; sensor for measuring particulate matter. The measurement of temperature and humidity are key indicators when there is a risk of fire - high temperature and dry air are prerequisites for this. Fire smoke is saturated with carbon monoxide and contains high levels of fine particulate matter. These are the reasons for choosing these sensors to construct the sensor node. The information from the sensors is read by an ESP32 microcontroller. Through a communication module, the measurement information is transmitted to the computer, where it is recorded, visualized and stored.

The sensor node is housed in a specially made box with holes at both ends. All movable elements are properly secured so that they do not interfere with the measurement process. Simulated measurements were taken with the sensor node before it was placed in the box and repeated after it was secured in the box. From the obtained results, it can be seen that the measurement information from the three sensors is received simultaneously, without delay in recording the data. The proposed sensor node will be used to build a wireless sensor network for early detection of fires large arrays of fruit plantations and open pastures in the country's rural areas.

At the next stage, it is planned to attach the explored sensor node to a drone. In this way, along with the data from the sensors, there will also be a visual picture of the terrain that the drone is crawling and the credibility of the information collected by the sensor node will be added. The presence or absence of fire will be confirmed. Also, unlike a static sensor node, the drone is mobile and can go around inconvenient places, where it would otherwise be difficult to get timely information.

REFERENCES

[1] https://www.mvr.bg/gdpbzn

[2] V. Cuomo, R. Lasaponara,V. Tramutoli, “Evaluation of a new satellite-based method for forest fire detection” International Journal of Remote Sensing, vol. 22, p. 1799-1826, 2001.

[3] Z. Li, A. Khananian, R.H. Fraser, J. Cihlar, “Automatic detection of fire smoke using artificial neural networks and threshold approaches applied to AVHRR imagery” IEEE Trans. Geosci. Remote Sens., vol. 39, p. 1859–1870, 2001.

[4] D. Zhang, Y. Cao, G. Zhang, X. Lu, “An Attention Convolutional Neural Network for Forest Fire Smoke Recognition” in: 2019 6th International Conference on Systems and Informatics (ICSAI), p. 1207–1211, 2019.

[5] F. M. A. Hossain, Y. Zhang, C. Yuan, C. Su, “Wildfire Flame and Smoke Detection Using Static Image Features and Artificial Neural Network” in: 2019 1st International Conference on Industrial Artificial Intelligence (IAI), p. 1–6, 2019.

[6] Xuemei Guan, Yanxiu Wei, Kai Liu, Sheldon Q. Shi, “Research on solving differential equations of forest fire monitor based on Runge-Kutta” Alexandria Engineering Journal, vol. 59, p. 2233-2238, 2020.

[7] Song Wang, Yanzhu Hu, “A forest fire rescue strategy based on variable extinguishing rate” Alexandria Engineering Journal, vol. 60, p. 1271-1289, 2021.

[8] Z. Wang, S. Zlatanova, A. Moreno, P. Van Oosterom, C. Toro, “A data model for route planning in the case of forest fires” Comput. Geosci., vol. 68, p. 1-10, 2014.

[9] H. Nikova, R. Deliyski, “Binary Regresion Model for Automated Wildfire Early Prediction and Prevention”, ICARAI’2023, 16-18.06.2023, Sozopol, Bulgaria, 2023.

[10] J. Lloret, M. Garcia, D. Bri, S. Sendra, “A Wireless Sensor Network Deployment for Rural and Forest Fire Detection and Verification” Sensors, vol 9, p. 8722-8747, 2009.

[11] C. Gomathi, K. Vennila, M. Sathyananth, B. Shriaarthi, S. Selvarasu, “Forest Fire Detection using Wireless Sensor Network” IJERT, vol. 3, p. 1-4, 2015.

[12] U. Dampage, L. Bandaranayake, R. Wanasinghe, K. Kottahachchi, B. Jayasanka, “Forest fire detection system using wireless sensor networks and machine learning” Sci Rep, vol. 12, 2022.

[13] A. Molina-Pico, D. Cuesta-Frau, A. Araujo, J. Alejandre, A. Rozas, “Forest Monitoring and Wildland Early Fire Detection by a Hierarchical Wireless Sensor Network” Journal of Sensors, vol. 2016, 8 pages, 2016.

[14] E. Abdul Kadir, S. Listia Rosa, A. Syukur, M. Othman, H. Daud, “Forest fire spreading and carbon concentration identification in tropical region Indonesia” Alexandria Engineering Journal, vol. 61, p. 1551-1561, 2022.

[15] W. Benzekri, , A. El Moussati, O. Moussaoui, M. Berrajaa, “Early Forest Fire Detection System using Wireless Sensor Network and Deep Learning” IJACSA, vol. 11, p. 496-503, 2020.

SECTION VIII
METROLOGY PRACTICE

NATIONAL INTERLABORATORY COMPARISON OF CALIBRATION LABORATORIES IN THE FIELD OF PRESSURE MEASUREMENT, BIM-MM-P-2022-01

1st Lyuboslav Hristov
Metrology Assurance
Kozloduy NPP EAD
Kozloduy, Bulgaria
lhhristov@npp.bg

2nd Momchil Lazarov
Metrology Assurance
Kozloduy NPP EAD
Kozloduy, Bulgaria
mglazarov@npp.bg

3rd Ivan Ivanov
Metrology Assurance
Kozloduy NPP EAD
Kozloduy, Bulgaria
ipivanov1@npp.bg

4th Petya Vasileva
Metrology Assurance
Kozloduy NPP EAD
Kozloduy, Bulgaria
plvasileva@npp.bg

Summary: **This report presents the results of the participation of Pressure, Flow Rate and Level Measurement (PFRLM) Laboratory, Metrology Assurance Department, Kozloduy NPP EAD, in the BIM-MM-R-2022-01 national interlaboratory comparison for pressure transmitter calibration in the 0 bar-60 bar range, which took place between 24 October 2022 and 1 January 2023.**

Keywords: Interlaboratory comparison, subject of comparison, reference laboratory, reference value.

I. Introduction

The interlaboratory comparison was organised by the Bulgarian Institute of Metrology (BIM), General Directorate National Centre of Metrology (DG NCM), Mechanical Measurements Department.

The main objective of our participation in the interlaboratory comparison was to demonstrate the laboratory's calibration competences in the field of pressure measurement by comparing the results of our measurements to the results of the reference laboratory measurements. An analysis was made thereafter, identifying measures to improve performance quality, where necessary (the laboratory announced calibration and measurement capabilities for the respective values).

The interlaboratory comparison involved four accredited and three non-accredited laboratories equipped with the necessary technical capacities and competences to calibrate pressure transmitters.

II. Subject of Comparison

The subject of comparison was an S-20 pressure transmitter made by Wika, No. A00NAV642D, range 0 - 60 bar, accuracy 0.25% FC, a DI35 digital indicator made by Wika, No. 18020166.

The reference laboratory tested the stability of the subject of comparison and found it was sufficient to meet the objectives of the comparison. A method of direct measurement comparison was used.

The measurement points were 0 bar, 10 bar, 20 bar, 30 bar, 40 bar, 50 bar, 60 bar.

III. Reference Laboratory

- The X_{REF} reference value with the respective uncertainty level were

assigned via calibration of the subject performed by the organiser in line with instruction МИ-И-404РТ-03-01. The calibration was performed using a piston unit by a methodology of the reference laboratory for calibration of digital pressure measuring devices. Three series of measurements were made.

- The uncertainty of the reference value was determined using the following formula:

$$u_{\text{REF}} = \sqrt{u^2(X_{\text{REF}}) + u^2(X_{\text{STAB}})} \qquad (1)$$

where:
$u(X_{\text{REF}})$ - uncertainty of the reference laboratory measurement;
$u(X_{\text{STAB}})$ - contribution of the instability of the subject of comparison for the period of the performance of the comparison.

IV. Measurement and Result Processing

The calibration of the pressure transmitter in the 0 bar - 60 bar range at the PFRLM Laboratory was performed based on a routine method of comparison, taking into account all measurement instructions set out in the technical protocol [1] and the requirements set out in the subject of comparison's technical specifications.

A 580DX piston unit set, No. 580/27286, 882G piston cylinder, DH-Budenberg, accuracy 0.015%, including piston unit weights, No. A 7004/1, DH-Budenberg was used as a reference gauge.

The calibration was performed at seven points: 0 bar, 10 bar, 20 bar, 30 bar, 40 bar, 50 bar, 60 bar. Six series of measurements were made.

The uncertainty budgets at all calibration points demonstrated clearly that the contributions of uncertainty, used by the reference gauge to measure the actual value of pressure, and the uncertainty resulting from the calibration method, were negligibly low compared to the contributions of uncertainty used to measure the pressure values. Therefore, these can be neglected.

The expanded uncertainty from the measurement was calculated as the product of the combined average square uncertainty and the coverage factor, K=2, which, in case of normal distribution, corresponds to a confidence coefficient of approximately 95%.

The assessments of the results obtained by the participating laboratories were based on the normalised deviation En criterion, calculated in line with БДС ISO/IEC 17043.

The criterion represents the normalised deviation of the result of each laboratory from the reference value.

En is calculated using the formula:

$$E_n = \frac{X_{\text{LAB}} - X_{\text{REF}}}{\sqrt{U_{\text{LAB}}^2 + U_{\text{REF}}^2}} \qquad (2)$$

where:

X_{LAB} - the value of the error of the transmitter reading obtained by the participating laboratory for the respective point;

X_{REF} -the reference value of the transmitter reading error obtained by the reference laboratory for the respective point;

U_{LAB} - the expanded uncertainty of the participating laboratory result for the relevant point;

U_{REF} - the expanded uncertainty of the reference value result for the relevant point.

If condition $|\text{En}| \leq 1.0$ is met, then the the comparison result for the relevant participating laboratory is considered satisfactory.

If $|\text{En}| > 1.0$ – the comparison result is considered unsatisfactory.

V. Comparison Results

Participants in the comparison were assigned individual codes. Code 22P1 was assigned to PFRLM Laboratory.

Based on the reports presented by the participants, the results were published in a FINAL REPORT dated 13 February 2023 on operability testing via BIM-MM-P-2022-01 interlaboratory comparison for calibration of a pressure transmitter with a range of up to 60 bar [2]. The differences between the results of the participating laboratories were presented

graphically in groups in comparison to the reference laboratory X_{LAB}-X_{REF} for each measurement point. The dashed lines represent the limits of the U_{REF} reference value expanded uncertainty.

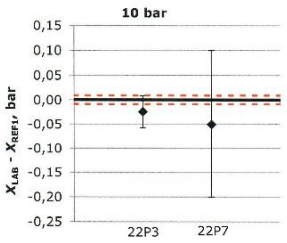

Figure 1. Group 1 results

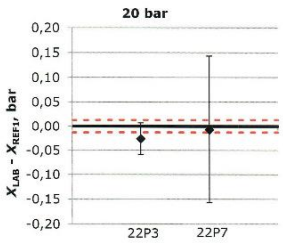

Figure 2. Group 1 results

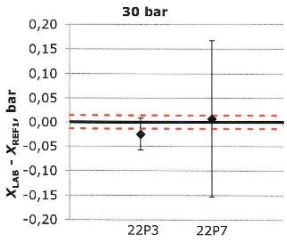

Figure 3. Group 1 results

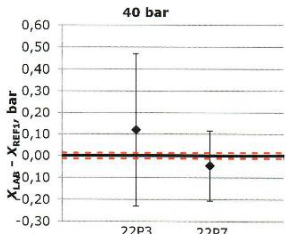

Figure 4. Group 1 results

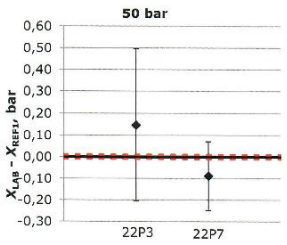

Figure 5. Group 1 results

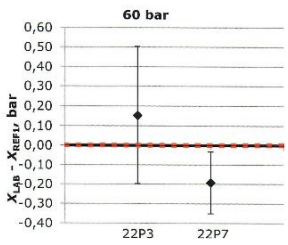

Figure 6. Group 1 results

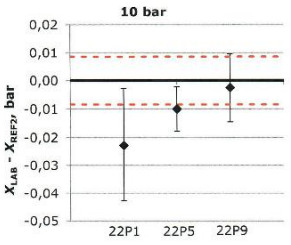

Figure 7. Group 2 results

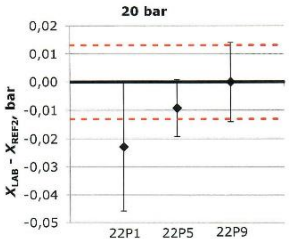

Figure 8. Group 2 results

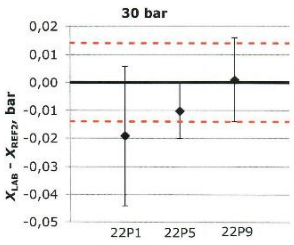

Figure 9. Group 2 results

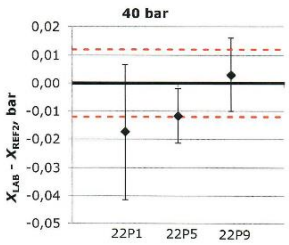

Figure 10. Group 2 results

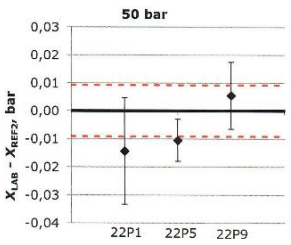

Figure 11. Group 2 results

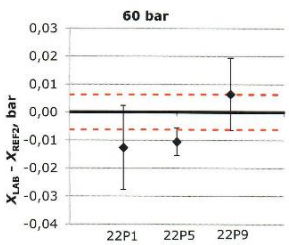

Фигура 12. Резултати на група 2

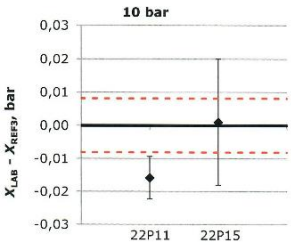

Figure 13. Group 3 results

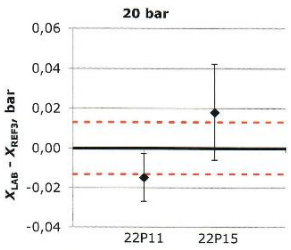

Figure 14. Group 3 results

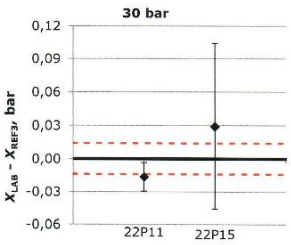

Figure 15. Group 3 results

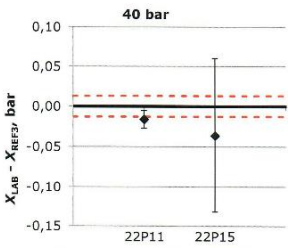

Figure 16. Group 3 results

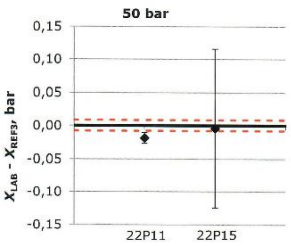

Figure 17. Group 3 results

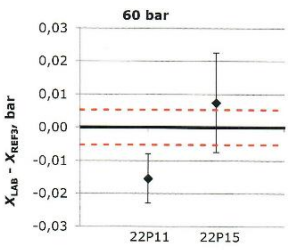

Figure 18. Group 3 results

For each measured value of each laboratory, the obtained results of the normalised deviation (criteria En) were presented graphically as follows:

Figure 12. Group 2 results

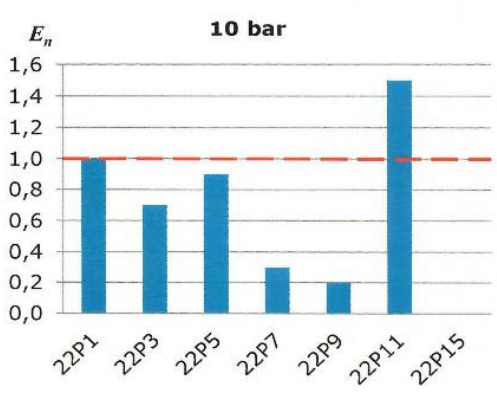

Figure 19. Normalised deviation at 10 bar

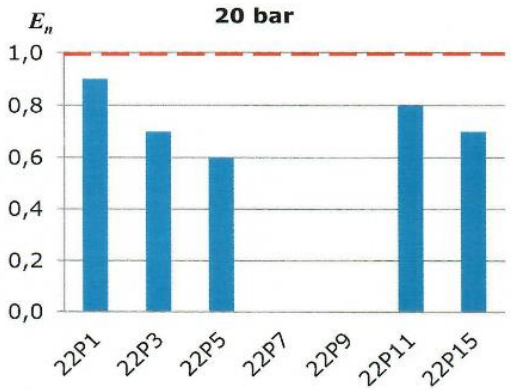

Figure 20. Normalised deviation at 20 bar

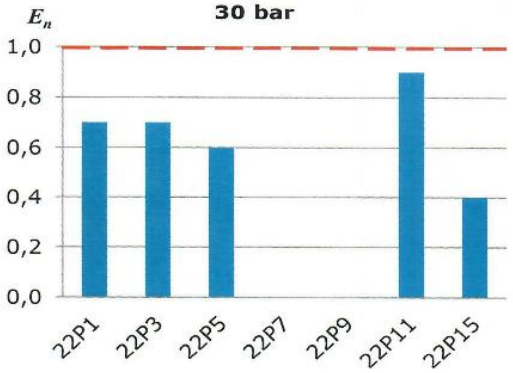

Figure 21. Normalised deviation at 30 bar

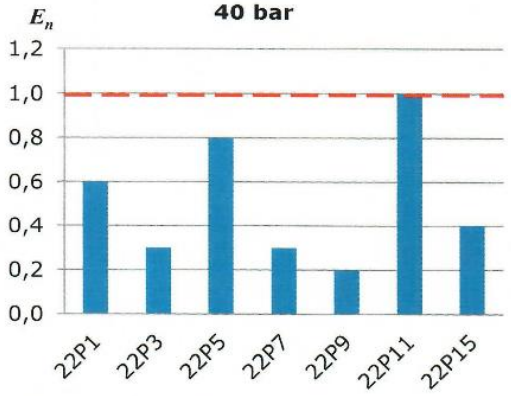

Figure 22. Normalised deviation at 40 bar

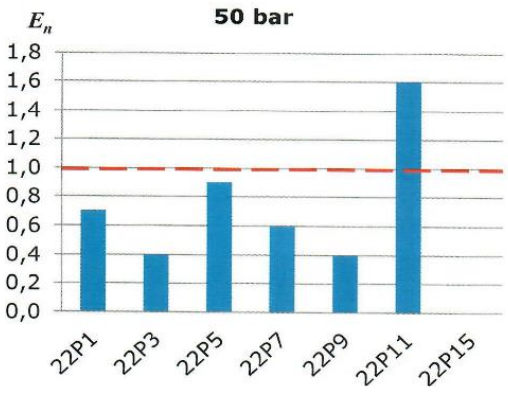

Figure 23. Normalised deviation at 50 bar

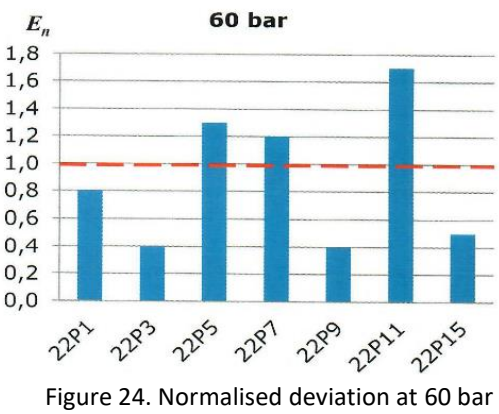

Figure 24. Normalised deviation at 60 bar

VI. Conclusion

The results of the PFRLM Laboratory in the BIM-MM-P-2022-01 interlaboratory comparison for calibration of a pressure transmitter with a range of up to 60 bar meet the satisfactory result criterion $|En| \leq 1$ at all measurement points.

The obtained expanded uncertainty values are equal to the announced calibration and measurement capabilities (CMC).

For the laboratory, the comparison result is satisfactory.

References:

[1] Technical operability protocol BIM-MM-P-2022-01 on the calibration of a pressure transmitter (range up to 60 bar)

[2] FINAL REPORT dated 13 February 2023 on the operability testing via interlaboratory comparison BIM-MM-P-2022-01 on the calibration of a pressure transmitter (range up to 60 bar).

TECHNICAL UNIVERSITY OF SOFIA

RESEARCH AND DEVELOPMENT SECTOR OF TECHNICAL UNIVERSITY OF SOFIA

The Technical University of Sofia is a modern educational and research institution, with highly qualified lecturers, researchers, engineers and technicians. The laboratory facilities with advanced equipment and qualified research staff provide high-quality scientific and experimental research.

The main goal of the Technical University of Sofia is its establishment as the leading European scientific and research center. Through its infrastructure, research potential and network of contacts, the University supports the solution of many scientific and engineering problems related to the needs of society.

Technical University of Sofia conducts a variety of applied research activities and provides opportunities for technology transfer at national and international level through the following units:

- Research and development sector
- "Technical University of Sofia – Technologies" Ltd.
- Small enterprises
- Educational-experimental enterprise
- The publishing house of the Technical University of Sofia

An important role for the establishment of TU-Sofia as a leading educational and research engineer center in the country and the region has the numerous annual scientific forums, united in the unique format "Science Days of TU-Sofia".

The strong international character, the high scientific level of the presented research findings and papers, included in proceedings, referenced and indexed in leading international science databases, and the significant support of the industrial partners make this forum an efficient environment for the transfer of knowledge, ideas and technologies from science to industry and business.

The introduced e-learning system E-SCIENCE provides the opportunity to obtain unified, complete and comprehensive information on scientific activities, projects and the scientists' career development. The system provides ways and methods for finding optimal management decisions and improves the effectiveness of research and applied work. Thanks to the publications module, updated daily, bibliographic data and summaries of scientific papers, publications, and posters are available on the web.

Training and Sport Wellness base "LAZUR" is the host of the annual international scientific conferences "Science Days of TU-Sofia" in the town of Sozopol, where the scientific elite of Bulgaria and the world is held.

The forums organized by the TU-Sofia are a meeting place for scientists from different research fields, challenged to transform innovative ideas into products and services that create sustainable partnerships between science and business, build high-skilled human potential, giving new skills that provides prepared researchers and specialists.

Technical University of Sofia

8 Blvd. Kl. Ohridski, 1797, Sofia, Bulgaria

Phone: (+359) 2 96 25 72, (+359) 2 868 51 83, Fax: (+359) 2 96 25 72

www. tu-sofia.bg

СЪЮЗ НА МЕТРОЛОЗИТЕ В БЪЛГАРИЯ

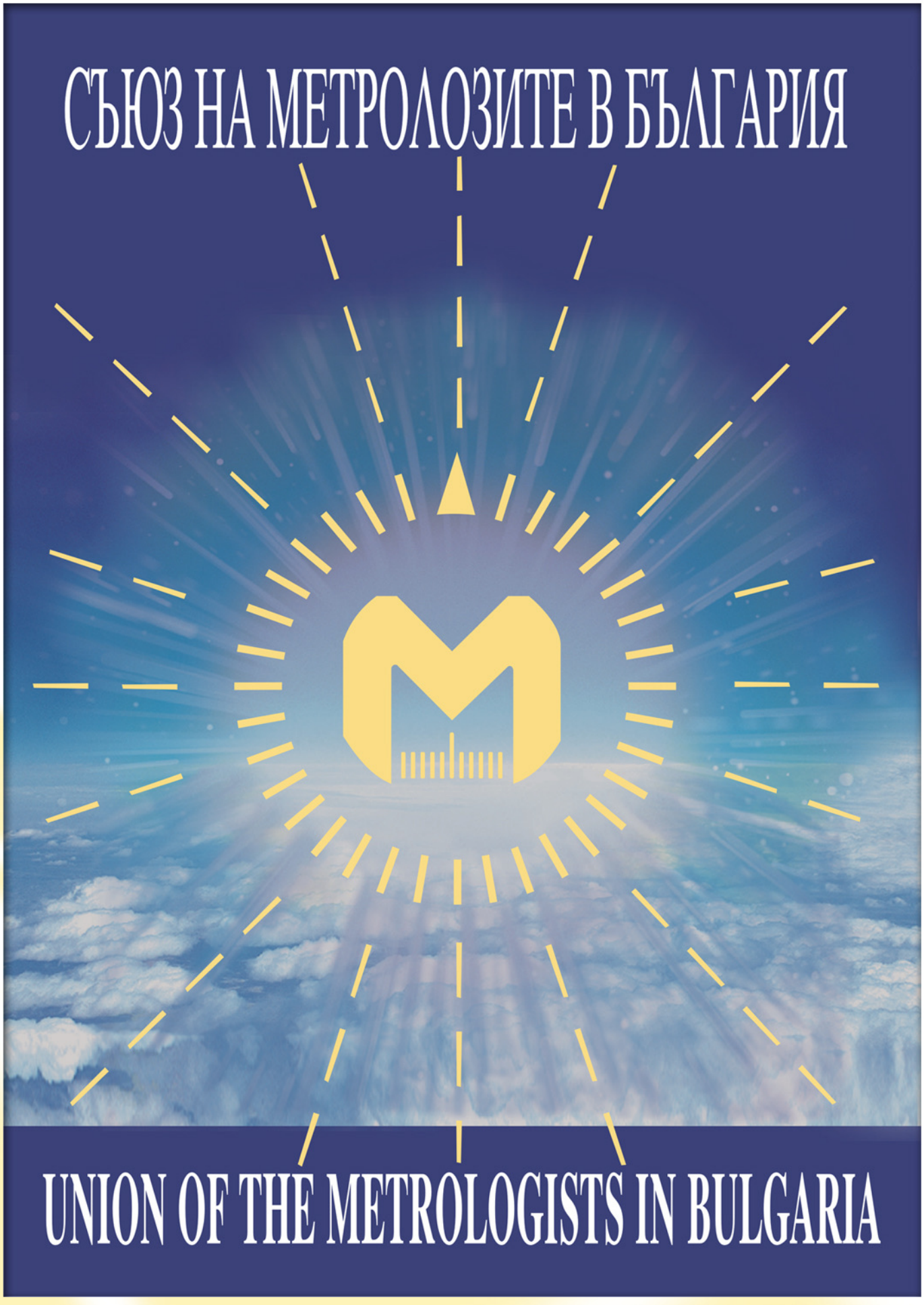

UNION OF THE METROLOGISTS IN BULGARIA